2022

Distinct VIP interneurons in the cingulate cortex encode anxiogenic and social stimuli

BOSTON UNIVERSITY

SCHOOL OF MEDICINE

Dissertation

DISTINCT VIP INTERNEURONS IN THE CINGULATE CORTEX ENCODE ANXIOGENIC AND SOCIAL STIMULI

by

LISA NICOLE KRETSGE

B.A., Vassar College, 2014

Submitted in partial fulfillment of the

requirements for the degree of

Doctor of Philosophy

2022

Approved by

First Reader

Alberto Cruz-Martín, Ph.D.
Assistant Professor of Biology

Second Reader

Mark Howe, Ph.D.
Assistant Professor of Psychological & Brain Sciences

Third Reader

Michael E. Hasselmo, D.Phil.
William Fairfield Warren Distinguished Professor
Professor of Psychological & Brain Sciences
Professor of Biomedical Engineering

ACKNOWLEDGMENTS

I'd like to give an enormous thank you to everyone who has supported me throughout graduate school. This experience has been really challenging and I can't imagine making it through without my labmates, the Boston University neuroscience community, my friends, and my family.

First, thank you to my advisor, Alberto Cruz-Martín. I'm grateful that you allowed me to follow the scientific questions I was most interested in and that you always brought such enthusiasm to our work. Thank you for encouraging me to take risks and pursue opportunities and collaborations that have made me a more well-rounded scientist. And lastly, thank you for building an amazing team!

Thank you to the other members of my dissertation advisory committee: Camron Bryant, Michael Hasselmo, Mark Howe, and Renata Batista-Brito. Thank you all for your incredibly valuable feedback on this work and for your support and guidance throughout this process. Our discussions have shaped the work presented here and made this story much stronger.

I'd also like to thank all of the current and former members of the Cruz-Martín lab for their contributions to these data, their feedback throughout the writing process, and for creating a collaborative and fun environment, where I knew I always had teammates that I could count on to help with experiments and bounce ideas off of. First, I'd like to thank our current lab manager, Connor Johnson. Connor, your contributions to this work cannot be overstated. I feel so fortunate to have had you as my partner in this work for the past few years. I can't wait to see what you do with the rest of your career

because you are such a gifted scientist and admirably devoted to this work. I'd also like to thank Will Yen, our former lab manager, for getting miniscopes working in our lab, building the framework that made so much of this research possible, and running the initial experiments. You were an excellent teacher as I got my start working with these techniques and you've always been a great listener and friend. Thank you to my fellow graduate students, Ashley Comer, Kelly Wingfield, Rhush Phadke, Ali Brack, and Luke Fournier. Ashley, you were the perfect model of the student I wanted to become, and I still regularly ask myself "What would Ashley do?" (Though sometimes the answer is "consume more Gatorade powder" or "ruin a backpack"). I seriously don't know where I would be without you. Kelly, I'm so excited to see where you take this project and I'm really proud of how much you've already achieved. There's no one I'd rather have continue my work. Thanks for having great taste in your recommendations for sci-fi movies, thrift shops, and take out that delivers to lab. Rhush, thanks for being calm when I'm stressed about computers and cords not working and enthusiastic even when you're moving a giant, heavy couch. I'll miss hearing all your jokes that take me 5 minutes to understand. Ali and Luke, I'm so glad you both joined the lab and that we got some overlapping time. You're both going to do amazing work and I can't wait to see it!

I'd also like to thank all the other members of the lab that have contributed to the data presented here. Alex O'Connor was an incredibly talented undergraduate student who wrote the code that became an integral part of our analysis pipeline. Eun Cho worked with me for years on a number of projects and always maintained a positive attitude and an incredible focus. Charlotte Yeung was an undergrad turned master's

student who brought such an enthusiastic and genuine interest in learning to lab every day. Thank you also to Tushare Jinadasa, Ruichen Sky Liu, Thanh Nguyen, Erelle Fuchs, Eli Spevack, Berta Escude Velasco, Frances Hausmann for your contributions to this work. Building this story took the strength of a big team and I'm so lucky to have had you all involved. I was also lucky enough to work with many other brilliant undergraduates, including Carly Rose Willing, Chloe Ketchmark, Meaghan Connolly, Shirley Mai, Emma Odom, Michelle Chuckwu, Katherine Baharona, and Dani Torres.

I was also fortunate to have amazing collaborators in other labs. Balaji Sriram provided essential feedback on our analyses and helped me learn how to analyze our behavioral data. Jessica Jimenez was instrumental in our start to using miniscopes and analyzing calcium imaging data. Thank you to Sarah Melzer for teaching me how to perform in situ hybridization and helping acquire electrophysiological data. I'm grateful to the Gardner, Davison, and Chen laboratories at Boston University for their shared supplies and guidance. Thanks especially to Margaret Minnig, Timothy Otchy, Nathan Perkins, and Daniel Leman for optimization of miniscope imaging and lens implant placement, Tim Gardner for providing access to 3D printers and sharing video acquisition software, Peyman Golshani, Daniel Aharoni, and Federico Sangiuliano for donating the camera sensor and data acquisition boards for miniscope experiments. Ashely Comer, Nancy Padilla, Mark Howe, William A. Liberti III and members of the Cruz-Martín lab helped critically by reading my co-first author manuscript and engaging in helpful discussions. I'd also like to thank Alex Harris and Josh Gordon for taking a chance on me when I didn't have much experience and giving me my first job in neuroscience.

Working with you both stoked an enthusiasm for research that is responsible for my interest to go to graduate school in the first place. Thank you to Todd Blute, Pete Castellano, and Dennis Batista for the many, many times you've all helped me out over the years. In addition, Todd Blute and the Boston University Biology Imaging Core provided use of the epifluorescence microscope and we used the Boston University Shared Computing Cluster to analyze our data. This work was supported by a NARSAD Young Investigator Grant, the NSF NRT UtB: Neurophotonics National Research Fellowship, the Dr. Marion R. Kramer Scholarship, and the Boston University Undergraduate Research Opportunities.

I have also received a lot of support from the Boston University neuroscience community, including the Graduate Program for Neuroscience (GPN), the Biology department, the Neurophotonics program, and the Center for Systems Neuroscience. Thank you to Shelley Russek, Sandi Grasso, and Nazifa Haque for running GPN so smoothly and with such compassion for the students. I'd also like to thank my fellow GPN students - Shelley did an amazing job selecting a group of scientists that I'm lucky to have as friends. I'd especially like to shout out Kristyn Borrelli, Ashley Comer, Margaret Minnig, Scott Knudstrup, Greg Wirak, Emily Schlafly, Jenny Klein, Stuart Babcock, and Ali Al Abdullatif (even though you aren't a GPN student, technically). Thank you to the Neurophotonics program, especially Helen Fawcett, David Boas, and Tom Bifano. Thank you to Michael Hasselmo and Kim McCall for running the Center for Systems Neuroscience and Biology department, respectively. Thank you to Jerome Mertz for giving me the opportunity to collaborate with your lab.

Next I'd like to thank my parents, Pam Knight and Harris Kretsge, for their unwavering support. Thanks for always believing I could do anything and giving me the education that made all of this possible. And thanks to my mom for being my first model of a woman in STEM and for making me believe that was the norm. I'd also like to thank Mike Arsham and Caroline Kalkut, as well as my aunts, uncles, and cousins.

I'd like to thank all the current and former 121 residents for being my pandemic pod so I didn't totally lose it from lack of social interaction. One trillion thank yous to my favorite member of my cohort, Kristyn Borrelli. Can you believe we've lived together for 5 years? Thanks for putting up with me for this long even though it takes me so long to take the recycling out and I can't stop making that "annoyed even though we're at a wine tasting in Porto" face at you. Thanks for encouraging me even when its undeserved, indulging in luxury even when we can't afford it, and taking me to see Katya. Thanks to Surya Rajan for spending more hours chatting with me than anyone else in the world?! Even though we've been talking to each other since we were basically babies, you're still the most captivated listener I know (even when I'm telling you something that objectively isn't interesting). Also, thanks for watching Lost with me while I made all my figures – I'm so happy that I'll forever associate you and that masterpiece with this work. Thanks to Katie Kolodziej for (somewhat) forgiving me for my messiness and choosing to like me anyway. Thank you for managing our landlord, getting riled up with me about feminist issues, and providing the educational audio commentary on Free Willy. Thanks to Tag (Tom) Tagliaferro for the million little things you've done over the past few years to make my life easier and better. Without your willingness to chauffeur me to work, who

knows how much less I would've accomplished? And it's unclear if I would've finished writing this dissertation without the fuel of the frosted sugar cookies/ cheese and crackers/ sweatshirt combo. Thanks to Ellis Andrews for believing in me (specifically my ability to do the crossword) even when I didn't believe in myself. Thanks to Peter Wilke simply for taking me to Chili's, it's such an honor to make the cut twice.

Thanks to Elly Schoenburg for psychoanalyzing us and for being the blunt voice of reason we all constantly need. I can't wait to get back to our joint birthday celebrations and overly-complicated cooking projects. Thanks to Molly Kornfeld for visiting me 100 times, leaving me riveting voice memos, and for being my favorite celebrity. Remember this acknowledgement when you make it big. Thanks to Jay Louik for cracking me up for the past decade, commiserating about how hard school is, and curating exactly which media you recommend to me because it's all good (e.g., The Craft). Thanks to all three of you for responding to 5 years of my dumb texts and for always being down to watch a revenge-based thriller from the 80s-90s. Thanks to Dana Kessler for letting me be your maid of honor and for being patient when I treat you like my personal physician even though you're literally busy saving lives during a global pandemic. Thanks to you and Dan for humoring me when I make myself the focal point of your marriage. Thanks to Cambria Jensen, Sema Quadir, Gavin Lagani, and Anna Berenson for your friendship, life stories, and dedication to personally keeping Cornwall's in business. Thanks to Cammy for being my outdoor lunch buddy even when it's completely inappropriate weather and for being someone I can talk to at length about abosultely anything. Thanks to Sema for always matching my outrage and to Gavin for bringing us all back to

(relative) calmness. Thanks to Claire Marsden, Firsker, and Becca Rosen for (along with Surya) being my oldest friends and sticking with me. Every friend and family member I have has played a part in keeping me sane and functional over the course of this Ph.D. and I'll be forever grateful for you all.

DISTINCT VIP INTERNEURONS IN THE CINGULATE CORTEX ENCODE ANXIOGENIC AND SOCIAL STIMULI

LISA NICOLE KRETSGE

Boston University School of Medicine, 2022

Major Professor: Alberto Cruz-Martín, Ph.D., Assistant Professor of Biology

ABSTRACT

A hallmark of higher-order cortical regions is their functional heterogeneity, but it is not well understood how these areas are able to encode diverse behavioral information. The anterior cingulate cortex (ACC), for example, is known to be important in a large range of behaviors, including, decision making, emotional regulation and social cognition. In support of this, previous work shows activation of the ACC to anxiety-related and social stimuli but does not use cellular resolution or cell-type specific techniques to elucidate the possible heterogeneity of its subcircuits. In this work, I investigate how subpopulations of neurons or microcircuits within the ACC encode these different kinds of stimuli. One type of inhibitory interneuron, which is positive for vasoactive intestinal peptide (VIP), is known to alter the activity of clusters of pyramidal excitatory neurons, often by inhibiting other types of inhibitory cells. Prior to this research, it was unknown whether the activity of VIP cells in the ACC (VIP^{ACC}) encodes anxiety-related or social information and whether all VIP^{ACC} activate similarly to the same behavioral stimuli. Using in vivo Ca^{2+} imaging and 3D-printed miniscopes in freely

behaving mice to monitor VIP^{ACC} activity, I have identified distinct subpopulations of VIP^{ACC} that preferentially activate to either anxiogenic, anxiolytic, social, or non-social stimuli. I also demonstrate that these stimulus-selective subpopulations are largely non-overlapping and that clusters of cells may co-activate, improving their encoding. Finally, I used trans-synaptic tracing to map monosynaptic inputs to VIP and other interneuron subtypes in the ACC. I found that VIP^{ACC} receive widespread inputs from regions implicated in emotional regulation and social cognition and that some inputs differ between types of ACC interneurons. Overall, these data demonstrate that the ACC is not homogeneous – there is marked functional heterogeneity within one interneuron population in the ACC and connective heterogeneity across ACC cell types. This work contributes to our broader understanding of how the cortex encodes information across diverse contexts and provides insight into the complexity of neural processes involved in anxiety and social behavior.

TABLE OF CONTENTS

LIST OF TABLES

LIST OF FIGURES

LIST OF ABBREVIATIONS

ΔG……...……Glycoprotein Gene-deleted

5-HT……...……Serotonin

5-HT3R……...……..Serotonin Receptor 3

AAV……...……..Adeno-associated Virus

AAV-TVA-Glyco……...AAV2/1-synP-Flex-split-TVA-EGFP-B19G

ACC……..……Anterior Cingulate Cortex

ACh……..……Acetylcholine

AD……..…….Anterodorsal Thalamic Nucleus

AD……..……...Alzheimer's Disease

AM……...Anteromedial Thalamus

Am Thal……...Anteromedial Thalamus

Amyg…….Amygdala

ANOVA……Analysis of Variance

AP…….……Anterior/Posterior

ASD……..……...Autism Spectrum Disorder

AuROC…….Area Under the Receiver Operating Characteristic Curve

AV……..……Anteroventral Thalamic Nucleus

C……..Closed

CA……...Cornu Ammonis

Ca^{2+}……Calcium

CaImAn…….Calcium Imaging Analysis (Software)

CCK…….……Cholecystokinin

Cen…….…….Center

ChAT…….……...Choline Acetyltransferase

Cl…….……..Contralateral

CL……..…….…Centrolateral Thalamic Nucleus

CMOS……..……Complementary Metal-oxide-semiconductor

CPu…….……Caudate Putamen

CR…….....Calretinin

Ctx……...Cortex

DAPI……4′,6-Diamidino-2-Phenylindole

DAQ……Data Acquisition

Df/f……Delta Fluorescence/Fluorescence

Diag Band……Diagonal Band of Broca

DS……..Dorsal Subiculum

DV……..Dorsal/Ventral

E……..Empty

EGFP…….……...Enhanced Green Fluorescent Protein

EnvA……...Avian Sarcoma Leucosis Virus Glycoprotein

EZM……...Elevated Zero Maze

fMRI…….……Functional Magnetic Resonance Imaging

FP…….…….……...False Positive

FPR…….…….False Positive Rate

GABA…….……...Gamma Aminobutyric Acid

GAD……..……..Generalized Anxiety Disorder

GECI……...Genetically Encoded Calcium Indicator

Glyco……..……...Glycoprotein

GRIN……..……Gradient-index

HDB……..Nucleus of the Horizontal Limb of the Diagonal Band

HPC……..……Hippocampus

Hypo……..…….Hypothalamus

IL……..Infralimbic Cortex

L……Layer

LC……Locus Coeruleus

LED……..Light-emitting Diode

LDVL…….Laterodorsal Thalamic Nucleus Ventrolateral Part

Lit……..……Littermate

LO…..…….Lateral Orbital Cortex

LPMR……..Lateral Posterior Thalamic Nucleus Medio Rostral Part

M1……...Primary Motor Cortex

M2……...Secondary Motor Cortex

MD……Mediodorsal Thalamus

MDD……...Major Depressive Disorder

MDL…….Mediodorsal Thalamic Nucleus Lateral Part

M-FISH…….Multiplex Fluorescent *In Situ* Hybridization

ML..……..……..Medial/Lateral

MO……..……Medial Orbital Cortex

mPFC…….…….Medial Prefrontal Cortex

MPtA……..Medial Parietal Association Cortex

MSC…….……Medial Septal Cortex

Nov……...……Novel Mouse

O……..Open (Chapter 3) or Object (Chapter 4)

OF……...…..Open Field

Orb…….…….Orbital

P……...…Postnatal Day

PBS……..…....Phosphate Buffered Saline

PF……...Parafascicular Thalamic Nucleus

Per……...……Periphery

Peri……..……...……Periphery

PFA……...Paraformaldehyde

PFC…….……...…….Prefrontal Cortex

Pop…….……...Population

Pref…….…….Preferred

Prim/asso…….……...Primary And Association Cortex

PrL……...……...Prelimbic Cortex

PTSD……....Post-Traumatic Stress Disorder

PV……..Parvalbumin

PV^{ACC}……Parvalbumin Cells in the Anterior Cingulate Cortex

Pyr……..…….Excitatory Pyramidal Cells

Q……Quartile

ROC…….……Receiver Operating Characteristic

RS……...…….…….Retrosplenial

RSD……..Retrosplenial Dysgranular Cortex

RSG……...….Retrosplenial Granular Cortex

RV…….……Rabies Virus

RV*dG*……...ΔG EnvA Pseudotyped RV with mCherry

S1……...……..Primary Somatosensory

S1BF…….Primary Somatosensory Cortex Barrel Field

S1FL…….Primary Somatosensory Cortex Forelimb Region

SAD…….…….……...Social Anxiety Disorder

SC……...…….……Subcutaneous

SCZ……...……..Schizophrenia

SD……...…….Standard Deviation

Sel……Selective

SEM……..……..Standard Error of the Mean

Social nov……..Social Novelty

SOM……...……...Somatostatin

SOM^{ACC}……...Somatostatin Cells in the Anterior Cingulate Cortex

TP……...……...True Positive

TPR …….…….True Positive Rate

TVA…….……..……..Avian Sarcoma/Leukosis Virus Subtype A Receptor

UTR……...Untranslated Region

V1…..…….Primary Visual Cortex

V2ML...……Secondary Visual Cortex Mediolateral Area

V2MM…….Secondary Visual Cortex Mediomedial Area

VA…….…….Ventral Anterior Thalamic Nucleus

VDB……..Nucleus of the Vertical Limb of the Diagonal Band

VIP……...…….……...Vasoactive Intestinal Peptide

VIP^{ACC}...……..Vasoactive Intestinal Peptide Cells in the Anterior Cingulate Cortex

VM…….……Ventromedial Thalamic Nucleus

VO……..……Ventral Orbital Cortex

Wks……..…….……...……...Weeks

CHAPTER ONE

Introduction to Inhibitory Circuits of the Anterior Cingulate Cortex

1.1 Diverse Functions of the Anterior Cingulate Cortex in Health and Disease

1.1.1 Introduction

A given region of cerebral cortex, or just cortex, is often involved in a wide array of behaviors, but it is not well understood how the cortex is able to encode such diverse information. The anterior cingulate cortex, or ACC, is a frontal cortical area that has been implicated in a variety of functions including socialization, anxiety-related behaviors, learning, and pain (Kim et al., 2011; Weible et al., 2017; Di Martino et al., 2009; Rudebeck et al., 2006; Guo et al., 2019; Fuchs et al., 2014; Weible et al., 2012; Weible et al., 2009). Not only is the ACC important for these behaviors in healthy animals and humans, but dysfunction in this region is also implicated in multiple psychiatric disorders (Nitschke et al., 2009; Kitayama, Quinn, & Bremner, 2006; Kasai et al., 2008; Di Martino et al., 2009; Nelson et al., 2015).

1.1.2 The ACC in Anxiety, Stress, and Emotional Regulation

Anxiety disorders are highly prevalent and can have pervasive effects on patients' lives. In fact, almost one third of adults in the United States are diagnosed with an anxiety disorder over the course of their lifetimes and about one third of those patients experience severe symptoms (Harvard Medical School, 2007). Conditions including generalized anxiety disorder (GAD), social anxiety disorder (SAD), and post-traumatic stress disorder

(PTSD) are often grouped together under the broader title of anxiety disorders (Harvard Medical School, 2007).

ACC morphology and activity have been linked to stress, anxiety, and emotional regulation in both human subjects and animal models. On average, individuals who have experienced early life stress (ELS) or have been diagnosed with PTSD have smaller ACC volumes than their healthy counterparts (Kitayama, Quinn, & Bremner, 2006; Kasai et al., 2008; Cohen et al., 2006). This volumetric difference was even seen in stress-exposed individuals with no psychiatric or neurological conditions, which suggests there is a connection between stress and the ACC, even in healthy subjects (Cohen et al., 2006).

Studies investigating stress exposure in both humans and animal models show increased activity throughout the frontal cortex, as well. In patients with untreated GAD, ACC activity levels correlate with symptom severity and, interestingly, with treatment efficacy once it is provided (Nitschke et al., 2009). ELS-exposed women demonstrate increased prefrontal cortex (PFC) activity during a facial expression identification task and rodent models show ACC-specific increases in the immediate early gene *C-fos*, which is a marker of recent neuronal activity (Colich et al., 2017; Chung et al., 2007; Horii-Hayashi et al., 2013).

Although these data are correlational, manipulating the ACC in animal models is sufficient to alter anxiety-related behaviors. Inhibiting the ACC using the muscimol (an agonist for gamma aminobutyric acid (GABA) A receptors) is sufficient to diminish anxiety-like behaviors in rodents (Kim et al., 2011). Selective inhibition of the cytoskeletal protein NEURABIN in the ACC also decreases anxiety-like behaviors (Kim

et al., 2011). Conversely, another group chronically and rhythmically stimulated the ACC by optogenetically inhibiting GABAergic neurons (Weible et al., 2017). Although this manipulation is functionally the opposite of the muscimol experiment (Kim et al., 2011), it also results in decreased anxiety-like behaviors (Weible et al., 2017).

The conflicting results of these studies may be due to differences in the techniques used to manipulate neural populations or in the behavioral tests used to quantify anxiety-like behavior. Importantly, these studies either chronically or acutely inhibited the ACC (Kim et al., 2011; Weible et al., 2017), so that difference in timing may also explain their outcomes. Despite the dissimilarity in results across experiments, these data all suggest a causal relationship between ACC activity and anxiety-related behaviors. Cell type specific manipulations and in vivo data demonstrating real time changes in ACC activity during behavior would further clarify the nuanced relationship between the ACC, anxiety, and stress.

1.1.3 The ACC in Social Behaviors and Impairments

Social deficits are a feature of many prevalent psychiatric disorders, including schizophrenia (SCZ), autism spectrum disorder (ASD), major depressive disorder (MDD), and Alzheimer's disease (AD) (Yizhar et al., 2011; Nelson et al., 2015; Porcelli et al., 2019). Recent work has highlighted the possibility that the neurobiology of social behavior and social impairments may explain some commonalities between these different disorders (Porcelli et al., 2019). A comparison of SCZ, MDD, and AD revealed networks of brain regions that are involved in social behavior and are impaired in all

three disorders (Porcelli et al., 2019). For example, many brain regions involved in reward processing (like the nucleus accumbens and ventral tegmental area) are impacted in these disorders, leading to one hypothesis that social dysfunction may result from social interactions feeling less rewarding across multiple disorders (Porcelli et al., 2019). Abnormalities of the ACC were also tied to all three disorders (Porcelli et al., 2019). Similarly, shared neural pathology may link some anxiety disorders and social dysfunction, as social deficits are a common feature across several anxiety disorders (Yizhar et al., 2011; Nelson et al., 2015; Porcelli et al., 2019). Fitting with this idea, evidence suggests that the ACC is important in both healthy and irregular social behaviors. However, many questions remain about the mechanisms that underlie social dysfunction, especially at the level of the neural circuit (Chen & Hong, 2018). Even the detailed neural mechanisms involved in normal social behavior remain poorly understood (Chen & Hong, 2018).

ACC abnormalities have been found in patients with conditions that involved both social deficits and anxiety. Similar to the data in patients with GAD, individuals with social phobia show more dramatically increased ACC activity during a task that involves identifying negative facial expressions, as compared to healthy controls (Amir et al., 2009). In individuals with SAD, ACC volume is negatively correlated with symptom severity (Frick et al., 2013). Because social anxiety disorders encompass aspects of both anxiety and social dysfunction, in the context of the anxiety-related data presented above, these results could simply reflect the relationship between the ACC and anxiety. This

seems unlikely, however, because of the wealth of data linking social cognition to the ACC.

In a meta-analysis of human fMRI studies, increased cingulate activity was found more often in studies monitoring social tasks than non-social tasks (Di Martino et al., 2009). When neurotypical controls are compared to individuals with ASD, ACC activation is more pronounced amongst the controls across a variety of tasks (Di Martino et al., 2009). Diminished gray matter in the ACC is also linked to SCZ (Job et al., 2003; Wiithaus et al., 2009). Within SCZ patients, more severe social dysfunction is correlated with abnormally low ACC activation in a task with positive-valence visual stimuli (Nelson et al., 2015). No relationship was found between ACC activity and the severity of positive symptoms, like hallucinations (Nelson et al., 2015). Taken together, these data make a convincing case for the involvement of the ACC in both normal social behavior and in psychiatric diseases that often coincide with social deficits.

In addition to altering anxiety-related behaviors, ACC manipulation can cause social impairments. In non-human primates, ACC lesions cause abnormally decreased socialization (Rudebeck et al., 2006). In rodents, excitatory pyramidal cells (Pyr) in the ACC preferentially activate during social behavior and optogenetic inhibition of these cells decreases sociability, which points to a causal relationship between ACC activity and normal social behavior (Guo et al., 2019). Increasing ACC activity was also sufficient to partially rescue social deficits in a mouse model of ASD, which suggests that manipulation of this brain region can be therapeutic for social impairments (Guo et al., 2019). Although this research demonstrates a clear relationship between the ACC and

social behavior, existing work has focused either on global ACC activity or that of Pyr alone. Additionally, information about the roles of inhibitory circuits in the ACC during social behavior is still lacking. Better understanding this local circuit and differences across cell types would improve our ability to develop superior therapeutic interventions.

1.1.4 The ACC in Novelty, Learning, and Cognition

The ACC has a wide range of functions and has also been implicated in cognitive tasks, such as those assaying learning and memory, interactions with objects and environments, and novelty (Weible et al., 2012; Weible et al., 2009; Tanimizu et al., 2017; Rudebeck et al., 2006; Rudebeck et al., 2014). ACC lesions in primates have been shown to impair appropriate arousal responses during learning, demonstrating the importance of this brain region in the learning process (Rudebeck et al., 2014). Additionally, memory formation (including social memory formation) has been linked to significant increases in multiple immediate-early genes in ACC neurons (Tanimizu et al., 2017).

Single unit recordings from in vivo electrophysiology have shown that about 50% of ACC cells show significantly different activity during interactions with objects (Weible et al., 2012). Interestingly, some ACC neurons preferentially higher activity near the object, whereas others showed significantly less activity near the object (Weible et al., 2012). After multiple exposures to an object, some neurons that fired preferentially to that object sustained the same patterns of activity even when the object was removed, suggesting a possible relationship between these cells and object memory (Weible et al.,

2012). Similarly, introduction of a novel object or movement of an object to a new location was shown to alter firing patterns of many ACC cells (Weible et al., 2009). These data demonstrate that many ACC cells are recruited during interactions with novel and familiar objects, but not all ACC cells respond to them similarly (Weible et al., 2012; Weible et al., 2009).

Combining the knowledge that the ACC is involved in cognition and in social behavior, it is unsurprising that the ACC seems to be involved specifically in social learning and memory. One study knocked out an ASD-related gene (*Shank3*) in the ACC only and found abnormal behavior in a task assaying social novelty (Guo et al., 2019). This phenotype was recapitulated when Pyr in the ACC were optogenetically inhibited and stimulation showed the opposite effect (Guo et al., 2019). In this study, none of these manipulations induced deficits in a novel object recognition task, suggesting this effect was specific to social novelty (Guo et al., 2019). It remains unclear whether ACC manipulation alters an animal's ability to detect social novelty or alters the animal's level of interest or motivation to investigate the novel social stimulus. Another study pharmacologically inhibited protein synthesis in the ACC and found that was sufficient to impair long term social memory formation but had no impact on a social interaction assay that did not depend on long term memory formation (Tanimizu et al., 2017).

1.1.5 Investigating How the ACC Encodes Diverse Behaviors

The ACC is necessary for emotional processing and social cognition, but a circuit-level understanding of how this region encodes stimuli relevant to both processes

is unknown (Chen & Hong, 2018; Rudebeck et al., 2006; Guo et al., 2019; Kim et al., 2011; Weible et al., 2017). Recent studies in both humans and animal models have provided insight into the ACC's importance for these functions by monitoring bulk activity of this region (Amir et al., 2009; Colich et al., 2017; Di Martino et al., 2009; Guo et al., 2019; Nelson et al., 2015; Nitschke et al., 2009). However, these data do not parse out the roles of different neural subtypes or microcircuits within the ACC, which may have different functions across relevant behaviors. It remains unknown how neuronal representations of diverse stimuli are embedded within ACC subcircuits.

Functional diversity within the ACC as described throughout this section of the Introduction (1.1) is summarized in Table 1.1. A wide range of diseases and behaviors have been linked to ACC function in humans or animal models. This summary table highlights some established functions of the ACC, but is not a comprehensive list of all known functions.

Table 1.1: Diversity of function and connectivity in the ACC

Disease Relevance	Behaviors	Connectivity	Subregions linked to tasks
Generalized anxiety disorder	Anxiety-related behaviors	Prefrontal cortex	Social tasks: rostral/ perigenual ACC
Post-traumatic stress disorder	Socialization and social memory	Motor cortex	Non-social cognitive tasks: caudal ACC
Schizophrenia	Object/ environment interactions	Retrosplenial cortex	Pain-related learning: rostral ACC
Social phobia	Learning and memory	Anteromedial thalamus	
Social anxiety disorder	Novelty	Mediodorsal thalamus	
Alzheimer's disease	Pain		
Major depressive disorder			
Stress; early life stress			

1.2 Understanding the Differences Between the Anterior Cingulate Cortex and the Prefrontal Cortex

The PFC is often described as a large cortical structure composed of several subregions, including the prelimbic cortex (PrL) and infralimbic cortex (IL) (Allen Institute for Brain Science, 2004). In previous research studying the frontal cortex, some work has grouped ACC and PFC together (Shang et al., 2014; Becht et al., 2020), whereas others have differentiated the two areas from each other (Milham et al., 2001; De Pisapia & Braver, 2006; Womelsdorf et al., 2014; Scheinost et al., 2018). Much like the ACC, the PFC has been implicated in social behavior, anxiety-related behavior, and related psychiatric disorders (Comer et al., 2020; Porcelli et al., 2019; Shang et al., 2014; Bishop et al., 2004; Venkatasubramanian et al., 2008; Perlstein et al., 2003). However, a thorough investigation of the differences between these areas and their functions may provide a clearer understanding of their respective roles in both health and disease.

Although the ACC and PFC are both involved in cognition and attention, some groups have found that minor changes to the tasks used in their studies are sufficient to skew neural activation towards either the PFC or the ACC (Milham et al., 2001). Even when both areas are recruited during the same task, they may perform slightly different functions. For example, in cognitive tasks with visual stimuli where subjects need to focus on task-relevant information, it has been hypothesized that ACC and PFC activity are both involved, but on different time scales (Milham et al., 2001; De Pisapia & Braver, 2006). This suggests that although the PFC and ACC are often involved in similar processes, their patterns of activity are not completely identical. Grouping data from both

areas together could obscure nuanced differences in how they activate during different behavioral tasks. Differences between these two brain regions are often subtle, perhaps because they are highly connected and may work cooperatively in certain tasks (Milham et al., 2001; Sun et al., 2019). Human imaging studies demonstrate that distinct ACC-PFC networks are involved in diverse aspects of emotional processing (Etkin et al., 2011, Milad et al., 2007, Critchley et al., 2003, Critchley et al., 2004, Mobbs et al., 2009, Johnstone et al., 2007, Bush et al., 2000, Mechias et al., 2010, Lavin et al., 2013). The differences between these areas are not insignificant; human imaging data suggest clinically relevant differences between the PFC and the ACC. A meta-analysis of resting state functional connectivity data also shows amygdala-ACC connectivity is more aberrant than amygdala-PFC connectivity in individuals with mood disorders (Marusak et al., 2016).

Not only do the PFC and ACC differ from each other, but areas within these regions show functional and connective heterogeneity, as well. Within the ACC, for example, fMRI data in human subjects shows increased perigenual ACC and rostral ACC activity during social tasks and increased dorsal ACC activity in non-social cognitive tasks (Di Martino et al., 2009). In addition, rostral and caudal ACC are known to have different involvement in pain processing (Johansen, Fields & Manning, 2001; Qu et al., 2011). Lesioning rostral ACC impairs behavior in a pain-related learning task, but lesioning caudal ACC had no effect on this behavior (Johansen, Fields & Manning, 2001). Some differences in ACC subregion function, as described here, as summarized in Table 1.1. Similarly, neural mapping has revealed differences in the brain regions that

project to medial PFC subregions IL and PrL (Sun et al., 2019). In the following work, we were interested in better understanding the functional heterogeneity within the ACC. Thus, if we focused broadly on the PFC, any heterogeneity we found may have resulted from this inclusion of diverse subareas of the PFC. The ACC was of particular interest because of its described roles in anxiety-related and social behaviors and the lack of in vivo, cell type specific information about this brain region. Because data specific to the ACC is limited, information about inhibitory cells and functional heterogeneity in the PFC still provide context to more broadly understand frontal cortical circuits.

1.3 Local Cortical Inhibitory Circuits

1.3.1 Introduction to Cortical Inhibition

A circuit-level understanding of the brain hinges on the idea that there are long-range connections (between cells in different brain regions) and local connections (between cells within one brain region), that both impact neural activity in a given area (Fornito & Bullmore, 2015; Karnani et al., 2016; Pi et al., 2013; Cichon et al., 2017; Marusak et al., 2016). The cortex is comprised of excitatory and inhibitory cells that synapse onto one another, forming a local microcircuit (Figure 1.1) (Cichon et al., 2017; Karnani et al., 2016; Pi et al., 2013). When excitatory neurons fire, they release glutamate and increase the likelihood that the cells they project onto also fire. Inhibitory cells, often referred to as interneurons, release GABA and suppress the activity of the cells they synapse onto; through this mechanism, they are able to exert powerful control over large

populations of neurons (Karnani et al., 2016; Pi et al., 2013). In vivo studies of inhibitory circuits within the ACC, specifically, are limited.

Some previous studies that broadly manipulate all GABAergic ACC cells show conflicting results, linking increased ACC activity to different phenotypes (Weible et al., 2017; Kim et al., 2011). For example, different studies have shown that either pharmacological stimulation or optogenetic inhibition of GABAergic ACC cells both lead to decreased anxiety-like behaviors (Kim et al., 2011; Weible et al., 2017). One possible explanation to reconcile these findings is that although these studies used either inhibition or stimulation, both interfered with the normal activity patterns of GABAergic ACC cells, which could therefore lead to abnormal anxiety-related behaviors in both cases. Alternatively, the same cell types and circuits may be recruited by different neuromodulators across diverse tasks. Another possible explanation involves thinking of the ACC not as one uniform area that is either more or less active, but as a brain region made up of cell types that respond differently to diverse stimuli such as stressors and social interactions. Different cell types within the cortex may have opposite roles in behavior because many of them inhibit each other (Figure 1.1). If the activity of different cell types has opposite effects on sociability or anxiety, ideal therapeutics may target only some of these subpopulations.

Previous research in the PFC shows that manipulation of either excitatory or inhibitory neurons can have profoundly different effects on social behavior. In the medial PFC (mPFC), manipulating either excitatory or inhibitory cells is sufficient to alter social behaviors (Yizhar et al., 2011). While animals normally spend more time investigating a

novel social stimulus, this effect is blunted in mice who receive optogenetic stimulation of Pyr cells in the mPFC (Yizhar et al., 2011). In addition, these animals showed impairments in fear learning, but no changes in locomotion, novel object recognition, or anxiety-like behavior (Yizhar et al., 2011). There was no effect on social behavior or fear learning when one type of interneuron was stimulated in these animals (Yizhar et al., 2011).

In fact, a manipulation of mPFC GABAergic cells has been proposed as a means to rescue abnormal social behaviors. One study addressed this by transplanting interneuron precursors from healthy mouse embryos to the brains of ASD model mice (Southwell et al., 2020). This manipulation targeted the mPFC but also transplanted cells into the ACC and some motor, sensory, and insular cortices (Southwell et al., 2020). This potentially therapeutic technique was sufficient to rescue normal social behaviors in the ASD model animals but did not impact their behavior in anxiety-related, locomotor, or novel object recognition tasks (Southwell et al., 2020).

1.3.2 Cortical Interneuron Subtypes

Inhibitory neurons are subdivided into more specific cell types based on their activity patterns, morphology, and their roles within the neural circuit. They are commonly referred to by specific proteins they express as way to categorize and identify them. Some of the most prevalent interneuron subtypes include parvalbumin (PV), somatostatin (SOM), and vasoactive intestinal peptide (VIP) positive cells (Rudy et al.,

2011; Xu, Roby, & Callaway, 2010; Tasic et al., 2016; Tasic et al., 2018; Pfeffer et al., 2013).

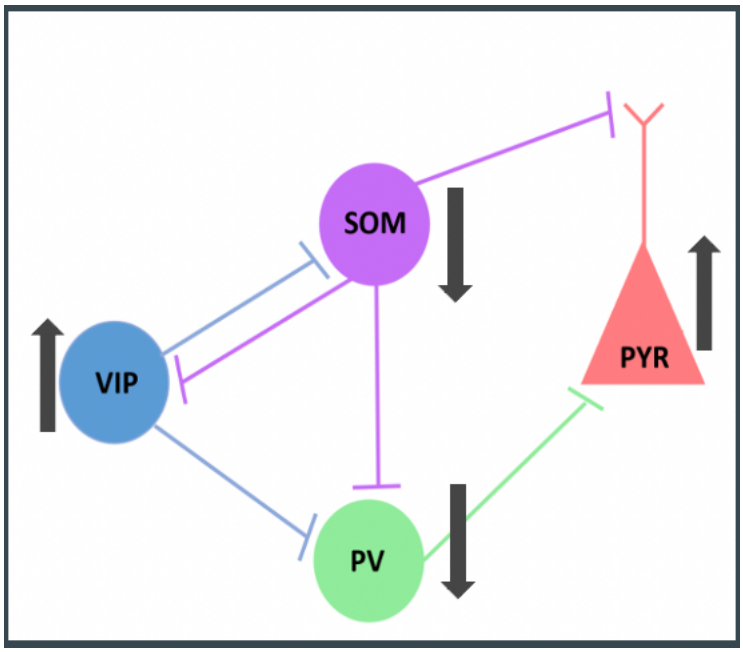

Figure 1.1: Schematic of a typical disinhibitory cortical microcircuit. Based on data from (Pi et al., 2013; Karnani et al., 2016; Cichon et al., 2017) demonstrating common patterns of connectivity between the three most prevalent cortical interneuron subtypes and excitatory cells. Black arrows represent typical impact on activity when VIP activity is increased. This is one example of a typical disinhibition of Pyr by VIP, but is not the only way these cell types can be connected. Other work has shown direct connections from VIP to Pyr (Lee et al., 2013; Obermayer et al., 2019). VIP: vasoactive intestinal polypeptide interneuron, SOM: somatostatin interneuron, PV: parvalbumin interneuron, PYR: excitatory pyramidal neuron. Note: Figure preparation by Lisa Kretsge. Figure not previously published.

While PV and SOM cells directly inhibit Pyr, VIP cells often inhibit these other types of interneurons (Figure 1.1). (Cichon et al., 2017; Karnani et al., 2016; Pi et al., 2013; Cauli et al., 1997). In rodent primary somatosensory cortex (S1), about 30% of interneurons are SOM, 40% are PV, and 12% are VIP (Rudy et al., 2011). This

breakdown varies dramatically by cortical layer and by brain region; deeper layers often have more PV and SOM neurons, while VIP cells are more highly prevalent in superficial layers (Rudy et al., 2011; Xu, Roby, & Callaway, 2010). In frontal cortex, PV cells are dispersed similarly across layer (L) 2/3 and 5 but are not found in L1, SOM cells are most highly prevalent in L4-6, and VIP cells are most dense in L2/3 (Xu, Roby, & Callaway, 2010).

Currently, there is very little information about these distinct interneuron subtypes in the ACC. Previous work demonstrates that the ACC is involved in social and anxiety-related behaviors, but this has either centered around global ACC activity or Pyr activity. It remains unknown whether ACC interneurons are involved in these behaviors and how VIP, PV, and SOM contribute to behavior in this higher-order cortical region.

1.4 Deciphering the Connectivity Patterns of the ACC and its Inhibitory Circuits

In addition to further understanding the roles of local ACC microcircuits in various behavioral functions, I have investigated the long-range connectivity to interneurons in the ACC. While it is fairly well understood which brain regions send projections to the ACC, there is minimal data available that is specific both to this brain region and to different interneuron subtypes. Mapping with classic neural tracers in rodents has revealed that the ACC receives extensive local projections as well as long-range connections from areas including motor cortex, nearby frontal cortical subregions, retrosplenial cortex, and anteromedial and mediodorsal thalamus (AM and MD,

respectively) (Allen Institute for Brain Science, 2011; Shibata & Naito, 2005; Shibata, 1993; Shibata, Kondo, & Naito, 2004; Jones, Groenewegen, & Witter, 2005).

Some recent studies have used viral strategies to identify inputs to the mPFC (Sun et al., 2019; DeNardo et al., 2015). These studies often rely on rabies trans-synaptic tracing, which is a method that allows for specific labelling of mono-synaptic inputs to a given population of virally infected neurons (DeNardo et al., 2015; Sun et al., 2019). Rabies tracing uses multiple viral constructs to fluorescently tag neurons throughout the brain that synapse onto cells in a given neural subpopulation (Callaway & Luo, 2015). For example, to identify which cells send projections to the ACC, researchers could inject a helper adeno-associated virus (AAV) and a rabies virus into the mPFC. Each virus would express a different fluorophore to allow for identification of starter cells (cells in the area of interest that are infected by both viruses) and input cells (retrogradely labeled cells that send projections to the starter cells and express only the fluorophore associated with the rabies virus) (Callaway & Luo, 2015). This technique can be combined with other genetic approaches, like the Cre/lox system, to limit infection of starter cells to specific cortical layers or cell types (Callaway & Luo, 2015). This approach allows researchers to visualize a connective map of all projections to a given brain region with detailed information, like cell-type specificity.

Across brain regions and even within one brain region, different cell types may receive vastly different inputs and may therefore be implicated in different functions. When comparing inputs to PV or SOM interneurons across cortical regions, rabies trans-synaptic mapping revealed different patterns of connectivity to each cell type in visual,

somatosensory, and motor cortices (Pouchelon et al., 2020). Not only did PV and SOM cells demonstrate different connectivity, but the ways they differed varied by cortical region studied (Pouchelon et al., 2020). This variability highlights the need for neural mapping studies for any given brain region and cell type of interest, because we cannot assume patterns are similar for different interneuron subtypes or that patterns will be comparable across different cortical areas.

L5 cells in the mPFC (including IL and PrL) receive inputs predominantly from local connections, the dorsal thalamus, and ACC (DeNardo et al., 2015). They also receive many inputs from motor and sensory cortex, as well as the hippocampus and amygdala (DeNardo et al., 2015). Cell-type specific tracing in the mPFC shows large groups of neurons that synapse onto VIP cells from local mPFC, nearby frontal cortical regions, the ACC, motor cortex, and higher-order thalamic structures like AM and MD (Sun et al., 2019). Although this study focused on the mPFC, they also quantified differences between the PrL and the IL and found that, although these regions are often grouped together, their connectivity patterns differ (Sun et al., 2019). Not only did they find differences across PV, SOM, and VIP cells within IL or PrL, but they also discovered differences for each interneuron subtype between IL and PrL (Sun et al., 2019).

As described above, the ACC and mPFC are not interchangeable, but these data may provide some insight into how frontal cortical circuits are organized. These datasets show high connectivity between ACC, IL, and PrL, but connectivity to interneuron subtypes in the ACC has not yet been fully explored. VIP cells in other cortical areas are

known to receive long-range inputs from other brain regions, which may allow them to coordinate the activity of the ACC with other brain regions to respond to diverse stimuli (Lee et al., 2013; Melzer et al., 2020; Karnani et al., 2016).

Connectivity to the ACC from other brain regions, as described throughout this section of the Introduction (1.4), is summarized in Table 1.1. Many brain regions are connected to this area and may be important for different ACC functions. Table 1.1 inlcudes some areas of interest that send inputs to the ACC, but is not a comprehensive list of all known connections.

1.5 Vasoactive Intestinal Peptide-Positive Interneurons

VIP interneurons are named for their expression of vasoactive intestinal peptide, which is involved in normal social behavior. Global pharmacological inhibition of VIP in early postnatal development causes social deficits and VIP is expressed at abnormal levels in the blood of children with ASD and in the cortex of a mouse model of Down syndrome (Hill et al., 2003; Hill, Cuasay, & Abede, 2007; Lim et al., 2008; Nelson et al., 2001). These studies show that VIP itself can be involved in long-lasting social impairments, but they provide no information about the role of VIP interneurons in the ACC (VIP^{ACC}) or their activity in vivo.

VIP cells are able to inhibit other inhibitory cells, thereby driving excitatory pyramidal cell activity (Askew et al., 2019; Lee et al., 2013; Pi et al., 2013; Karnani et al., 2016; Melzer et al., 2020). On the other hand, a small population of VIP cells has been shown to synapse onto Pyr or other interneurons and release acetylcholine (ACh)

(Obermayer et al., 2019; Lee et al., 2013). This would allow VIP cells to either directly excite Pyr (rather than disinhibiting) or to excite (rather than inhibit) other interneurons (Obermayer et al., 2019, Lee et al., 2013). In either case, VIP interneurons are in a unique position to modulate the activity of local microcircuits (Karnani et al., 2016). In other cortical areas, VIP cells interrupt widespread inhibition by other interneurons, which may allow for increased activity of different clusters of excitatory neurons (Karnani et al., 2016; Pi et al., 2013). Developmental manipulations that alter VIP neuron activity can lead to abnormal Pyr and SOM activity and behavioral abnormalities that persist into adulthood (Batista-Brito et al., 2017; Mossner et al., 2020).

In vivo data from VIP cells in different brain regions may inform our understanding of diverse VIP^{ACC} functions. In the CA1 subregion of the hippocampus, VIP interneurons form functional clusters that are differently modulated by behavioral states, but this has not been studied in higher-order frontal cortical regions like the ACC (Turi et al., 2019). In the auditory cortex, VIP cells respond to both reward and punishment in an auditory discrimination task (Pi et al., 2013). In other cortical areas, VIP cells activate preferentially to novel or unexpected stimuli, so within the ACC they may be able to integrate information about social and novel stimuli, making them especially important in social interactions with novel animals and social learning (Garrett et al., 2020; Krabbe et al., 2019). In vivo data from the medial PFC (mPFC) demonstrates different behavioral relevance of PV, SOM, VIP, and Pyr cells using calcium (Ca^{2+}) imaging (Pinto & Dan, 2015). The activity of these neural populations was monitored during a learning and memory task in mice (Pinto & Dan, 2015). While almost all PV and

SOM cells are modulated by a learned behavior, only about 80% of VIP and Pyr cells are task-modulated (Pinto & Dan, 2015). Additionally, VIP cells are the only group that do not activate to the auditory cues that signaled reward (Pinto & Dan, 2015). Similar discrepancies across cell types are found in the activity associated with the cue designating the start of a trial, the licking response to receive the water reward and the task's outcome (Pinto & Dan, 2015). Importantly, these data show that frontal cortical interneuron subtypes and Pyr can preferentially activate to completely different stimuli. This highlights the importance of investigating the neural activity of these distinct cell types separately to decipher the complexities of cortical encoding of diverse behaviors.

Manipulation of specific cell types also leads to vastly different behavioral outcomes (Kamigaki & Dan, 2017). Optogenetic activation of SOM, PV, or Pyr neurons is sufficient to impair learned behaviors, but activation of VIP cells improves the animals' performance (Kamigaki & Dan, 2017). Conversely, inhibition of VIP cells impairs task performance (Kamigaki & Dan, 2017). The opposite effects of VIP versus PV or SOM activation may be expected, as they play exhibit different connectivity patterns and dissimilar roles in the local circuit (Sun et al., 2019; Cauli et al., 1997; Cohen et al., 2006; Karnani et al., 2016; Pi et al., 2013). However, VIP cells largely disinhibit Pyr, so this discrepancy underscores the importance of studying the relationship between cortical activity and behavior with cell-type specific data. In the ACC, however, the functions of VIP cells remain poorly understood.

1.6 Heterogeneity in Cortical Function and VIP Interneurons

1.6.1 Evidence of Functional Heterogeneity in the Frontal Cortex

Within various cortical areas, evidence suggests different groups of cells activate preferentially to diverse stimuli, potentially playing different functional roles in animal behavior (Frost, Haggart, & Sohal, 2021; See et al., 2021; Liang et al., 2018). This has not been thoroughly investigated in the ACC, but some recent studies have identified functional heterogeneity in the PFC. For example, it was recently shown that some, but not all, neurons preferentially activate during social interactions and that different ensembles of cells may encode nuanced differences across types of social stimuli (Frost, Haggart, & Sohal, 2021; Liang et al., 2018). Two recent studies have used miniaturized microscopes (miniscopes) for in vivo Ca^{2+} imaging in the PFC with cellular resolution during social behaviors (Liang et al., 2018; Frost, Haggart, & Sohal, 2021).

In the first, GCaMP (a genetically encoded calcium indicator) under a synapsin promoter was used to visualize neural activity across all PFC neurons in wild type or ASD model animals (Frost, Haggart, & Sohal, 2021). PFC cells demonstrate an overall increase in activity during social interactions (Frost, Haggart, & Sohal, 2021). However, when looking at the level of the individual neuron, some cells activate to social stimuli while others preferentially activate during non-social behavioral epochs (Frost, Haggart, & Sohal, 2021). In addition, these PFC cells normally activate as ensembles, which show different activation patterns in an ASD mouse model (Frost, Haggart, & Sohal, 2021). Crucially, these data show functional heterogeneity in the PFC during social behavior,

but because the PFC is a broad area and GCaMP was driven by a synaptic promoter, this work included many subtypes of neurons (Frost et al., 2020).

This type of heterogeneity is not simply a facet of the PFC being comprised of various subareas, because similar findings were revealed when only monitoring the activity in the PrL (Southwell et al., 2020). Again, some neural ensembles activated to social stimuli and others showed diminished activity during social interactions (Southwell et al., 2020). Some social-selective cells even showed selectively increased activity to either novel or familiar social stimuli (Southwell et al., 2020). The activity of these ensembles was also altered in a SCZ mouse model with abnormal social behaviors (Southwell et al., 2020).

One remaining question is whether cortical ensembles with opposite activity profiles correspond to different molecularly identifiable cell types. The heterogeneity described above relies on datasets without cell type specificity. Because many interneurons directly inhibit Pyr, cortical heterogeneity like this may reflect the fact that a given stimulus could be associated with activation of VIP and Pyr as well as inhibition of PV and SOM (or vice versa). Alternatively, cortical heterogeneity may reflect diverse responses within each of these cell types, where a given stimulus elicits increased activity from subclusters of VIP, PV, SOM, and Pyr.

These existing studies provide critical insight into the functional heterogeneity of prefrontal cortical neurons. Nonetheless, the field still lacks information specific to the ACC and to VIP interneurons. While these prior studies have found cells that encode social stimuli and social novelty, it remains unknown whether these same cells activate to

other stimuli the ACC and PFC are thought to encode, like anxiety-related stimuli. Additionally, because VIP cells are poised to alter the activity of Pyr clusters, functional heterogeneity of these cells could lead to downstream Pyr heterogeneity, as well.

1.6.2 Heterogeneity Amongst VIP Interneurons

Although specific profiles of VIP interneurons in the ACC are lacking, previous work shows that VIP cells in other cortical regions exhibit diverse molecular, morphological, and electrophysiological properties (Ferezou et al., 2002; Cauli et al., 1997; Gonchar, Wang, & Burkhalter, 2008; Kawaguchi & Kubota, 1997; Ketchesin, Huang, & Seasholtz, 2017; Obermayer et al., 2019; Porter et al., 1999; Tasic et al., 2016; Tasic et al., 2018). Morphologically, VIP cells have been described as bipolar, multipolar, basket-type, or bouquet cells (Tasic et al., 2018; Cauli et al., 1997; Kawaguchi & Kubota, 1997). In vitro electrophysiology has identified some VIP cells as regular-spiking, burst-spiking, irregular-spiking, or switching between burst and tonic firing (Kawaguchi & Kubota, 1997; Cauli et al., 1997; Rudy et al., 2011; Pronneke et al., 2020). In addition, VIP cells have a large range of molecular and genetic markers that vary across the population, including a range of proteins involved in neuromodulation (Tasic et al., 2016; Tasic et al., 2018; Hodge et al., 2019; Obermayer et al., 2019; Gonchar, Wang, & Burkhalter, 2008).

Data from human temporal cortex shows a wide variety of transcriptomic profiles across VIP interneurons – one recent study divided VIP cells into 21 distinct subclusters (Hodge et al., 2019). Similar sequencing data pinpoints VIP interneuron transcriptomic

subtypes in mouse visual and motor cortices (Tasic et al., 2016; Tasic et al., 2018). Groups of VIP cells varied largely and showed different profiles across cortical layers (Tasic et al., 2016; Tasic et al., 2018). One noteworthy feature was the diversity of genes related to neuromodulation, the physiological process by which a given neuron uses one or more chemicals to regulate diverse populations of neurons (Tasic et al., 2016; Tasic et al., 2018). This included groups of VIP neurons that were positive for genes involved in either ACh or oxytocin (Oxt) signaling (Tasic et al., 2016; Tasic et al., 2018). VIP cells have also been linked to opioid singalling in other brain regions; some VIP cells are positive for mu opioid receptors and/or enkephalin (an endogenous mu opioid agonist) (Drake & Milner, 2002; Ferezou et al., 2007; Leroy et al., 2021). Differences in neuromodulation among VIP cells may be especially important in the context of behavior. ACh is known to be involved in attention, memory, and cognition, whereas Oxt is important in social behavior and bonding, and enkephalin in hippocampal VIP cells is linked to social memory (Hasselmo, 2006; Hasselmo & McGaughy, 2004; Sarter & Bruno, 1997; Heinrichs, von Dawans, & Domes, 2009; Feldman, 2012; Leroy et al., 2021).

In addition, neuromodulators like ACh and serotonin (5-HT) can modulate functionally distinct groups of VIP interneurons (Ferezou et al., 2002; Poorthuis, Enke, & Letzkus, 2014; Pronneke et al., 2020). It follows logically that these VIP cells with different neuromodulatory profiles may be recruited during different behaviors and contribute to cortical functional heterogeneity. VIPs that are positive for choline acetyltransferase (ChAT+), are primarily located in L2/3 of mouse cortex and comprise

about 1% of cortical neurons in rats, while about 15% of VIP in the PFC are ChAT+ (Obermayer et al., 2019; Bayraktar et al., 1997; Tasic et al., 2018; Gonchar, Wang, & Burkhalter, 2008). ChAT+ VIP cells may play a different role in the local microcircuit than disinhibition of Pyr (Obermayer et al., 2019). Some ChAT+ VIP cells synapse onto other interneurons or Pyr and release ACh, which can directly excite these neurons (Obermayer et al., 2019). Some of these VIP cells can release both GABA and ACh (Obermayer et al., 2019). Still other VIP cells (about 30%) are positive for 5-HT receptors, often serotonin receptor 3 (5-HT3R) (Ferezou et al., 2002). There is some overlap between VIP cells expressing 5-HT3R and those expressing ChAT, but many VIP cells express neither (Ferezou et al., 2002).

Attempts to categorize VIP cells by protein expression, morphology, or electrophysiology have frequently relied on markers like ChAT, 5-HT3R, cholecystokinin (CCK), calretinin (CR), or calbindin 2 (Gonchar, Wang, & Burkhalter, 2008; Obermayer et al., 2019; Kawaguchi & Kubota, 1997; Tasic et al., 2016). Out of all GABAergic cells in the mouse visual cortex, about 12% are VIP+/CR+, 3% are VIP+/ChAT+, and less than 1% are CCK+/VIP+ (Gonchar, Wang, & Burkhalter, 2008). Often, one of these markers will align with a particular morphological or electrophysiological phenotype (Obermayer et al., 2019; Kawaguchi & Kubota, 1997). For example, CCK+/VIP+ cells exhibit distinctive morphology (small, bipolar) and some are positive for nicotinic ACh receptors or for 5-HTRs (Obermayer et al., 2019; Porter et al., 1999; Ketchesin, Huang, & Seasholtz, 2017; Cauli et al., 1997). Even more specifically, VIP+/CCK+/5-HTR3+ cells display regular spiking electrophysiological

patterns (Ferezou et al., 2002), whereas some VIP+/CCK+/CR+ cells are irregularly spiking neurons (Cauli et al., 1997).

However, these classifications remain complex, in large part because many of these marker-based identities are not mutually exclusive and can vary across brain regions or cortical layers. When identifying CR+ and CCK+ VIP cells in rat frontal cortex, for example, CR and CCK co-localize in VIP cells much more often in the deeper cortical layers V and VI than in the more superficial layer II/III (Kawaguchi & Kubota, 1997). Thus, VIP cells have many heterogeneous properties, but whether these differences correspond to functional heterogeneity in the ACC is not known.

VIP heterogeneity as described in two sections of the Introduction (1.5 and 1.6) is summarized in Table 1.2. This table includes information about molecular markers, electrophysiology, morphology, neuromodulators, and receptors in VIP cells, but is not a comprehensive list of all differences VIP cells can exhibit.

Table 1.2: Heterogeneity of VIP interneurons

Molecular/ Genetic	Electrophysiology	Morphology	Neuromodulators	Receptors
Calretinin	Regular spiking	Bipolar	GABA	Serotonin (ionotropic and metabotrophic; 5-HT2R, 5-HT3aR)
Cholecystokinin	Burst spiking	Double bouquet	Acetylcholine	Nicotonic (4, 5, 2 subunits; non alpha-7)
Choline acetyltransferase	Burst-tonic switching	Small basket	Enkephalin	Mu opioid
Calbindin 2	Irregular spiking	Multipolar		Oxytocin

1.7 Investigating the Functional and Connective Heterogeneity of Inhibitory Neuron Subtypes in the ACC

It is unknown whether VIP cells have heterogeneous functions in the ACC and whether disinhibitory circuits are involved in ACC processing of diverse stimuli. Despite prior evidence that cortical VIP cells exhibit diverse molecular, morphological, and electrophysiological properties, there are no existing data using in vivo Ca^{2+} imaging of VIP^{ACC} activity with single-cell resolution. This technique also makes it possible for us to determine whether VIP^{ACC} cells function cooperatively. In addition to functional heterogeneity within VIP^{ACC}, we aimed to illuminate connective heterogeneity across interneuron subtypes in the ACC.

We hypothesized that some subpopulations of VIP^{ACC} would encode anxiety-related and social behavioral information, but that not all VIP^{ACC} would activate to the same stimuli as one cohesive population. To investigate this possible functional heterogeneity, we used in vivo single-cell resolution Ca^{2+} imaging of VIP^{ACC} during animal behavior. We injected AAV9-flex-GCaMP6f into the ACC of VIP-IRES-Cre mice to express this fluorescent calcium indicator in VIP^{ACC}. We then implanted gradient-index (GRIN) lenses and miniaturized microscopes, or miniscopes, into the ACC to image VIP^{ACC} Ca^{2+} dynamics during behavioral assays.

We identified distinct VIP^{ACC} subgroups that reliably encoded behavioral states by preferentially activating to anxiety-related, social, or non-social stimuli despite a lack of stimulus-dependent changes in activity at the population level. In addition, we found that averaging selective cell activity made this coding more reliable. When the same neurons were monitored across anxiety-related and social tasks, we determined that the majority of VIP^{ACC} that were engaged during these tasks were highly selective, activating

to only one stimulus. Lastly, using rabies trans-synaptic mapping, we showed that VIP^{ACC} receive inputs from brain regions implicated in emotional regulation and social behavior and their inputs differ from PV and SOM cells in the ACC. Our data show that VIP^{ACC} are functionally heterogeneous and that non-overlapping subgroups of VIP^{ACC} activate preferentially, providing a cellular substrate for encoding different types of stimuli.

CHAPTER TWO

Materials and Methods

2.1 Ethics Statement

All procedures were approved by the Institutional Animal Care and Use Committee (IACUC; protocol #17–031) at Boston University and practices were consistent with the Guide for the Care and Use of Laboratory Animals (Committee for the Update of the Guide for the Care and Use of Laboratory Animals, 2010) and the Animal Welfare Act.

2.2 Animals

Animals were grouped housed in a 12-hr light/dark schedule vivarium with food and water ad libitum. Experimental mice for Ca^{2+} imaging and behavioral experiments were male postnatal day (P) 60-120 VIP-Cre mice (Vip-IRES-Cre, #010908, The Jackson Laboratory, Bar Harbor, Maine) (Taniguchi et al., 2011). Stimulus mice for social interaction were littermates (male VIP-Cre) or novel (age matched male CD-1 IGS, strain code: 022, Charles River Laboratories, Wilmington, Massachusetts). For rabies trans-synaptic tracing experiments, the animals used were either VIP-Cre, SOM-Cre (Sst-IRES-Cre, #028864, The Jackson Laboratory, Bar Harbor, Maine), or PV-Cre (B6 PV^{cre}, #017320, The Jackson Laboratory, Bar Harbor, Maine). Wild type mice (C57BL/6J, #000664, The Jackson Laboratory, Bar Harbor, Maine) were used for control virus injections. Interneuron-Cre mice were made by inserting the Cre recombinase gene into

the 3' untranslated region (UTR) of the locus for VIP, SOM, or PV (Vip, Sst, or Pvalb, respectively), which allows for Cre expression wherever a given interneuron marker peptide would normally be expressed (Taniguchi et al., 2011). On caveat in our work with Cre animals is that our mouse colonies were maintained using a homozygous-homozygous breeding scheme, which can lead to mutations and abnormalities in behavior over generations. We performed control viral injections to ensure expression was Cre-dependent (Figures 3.3 and 6.2) and unimplanted behavioral controls were all the same genetic background (VIP-Cre) as experimental animals.

2.3 Viruses

To monitor VIP^{ACC} activity, we injected AAV9-CAG-Flex-GCaMP6f.SV40, titer: 5.23 x 10^{13} GC/ml, packaged by the University of Pennsylvania Vector Core, Philadelphia, Pennsylvania.

For trans-synaptic tracing of monosynaptic inputs to VIP^{ACC}, $SOM^{ACC,}$ or PV^{ACC} we first injected AAV2/1-synP-Flex-split-TVA-EGFP-B19G (AAV-TVA-Glyco) (Kohara et al., 2014) (titer: 0.98 x 10^{12} GC/ml, University of North Carolina Viral Core, Chapel Hill, North Carolina). We later injected ΔG EnvA pseudotyped RV with mCherry (RV*dG*, titer: 1.5 x 10^{9} GC/ml, Boston's Children Hospital Viral Core, Boston, Massachusetts).

For control experiments to determine if these viruses leaked into Cre negative cells, viral injections were performed as described above, but in wild type C57BL6/J mice.

2.4 Surgeries

Surgeries were performed using aseptic surgical techniques with autoclaved instruments. Animals were weighed and anesthesia was induced in a chamber with an isoflurane–oxygen mixture (4% [v/v]). Anesthesia was maintained throughout the procedure via mask inhalation of an isoflurane–oxygen mixture (Henry Schein, Melville, New York, 1-1.5% [v/v]). Animals were kept on a heating pad (T Pump, Gaymar Industries Inc., Orchard Park, New York) for the duration of the surgeries and for 30-min recovery periods before being returned to their home cages. Animals were injected with buprenorphine (3.25 mg/kg; SC, Patterson Veterinary, Greeley, Colorado), meloxicam (5 mg/kg; SC, Covetrus, Dublin, Ohio), and dexamethasone (Henry Schein, 2.5 mg/kg; SC) and the fur on the top of the head was removed with a trimmer. Animals were head-fixed using a stereotax (Kopf Instruments, Tujunga, California). The surgical area was sterilized with 3 alternating washes of 10% povidone-iodine and 70% isopropyl alcohol (CVS, Woonsocket, Rhode Island) and local anesthetic was applied (lidocaine 1% and epinephrine 1:100,000; SC, Henry Schein). After surgeries, post-operative analgesics were administered for 2 days, twice per day (buprenorphine 0.01 mg/kg; SC and meloxicam 5 mg/kg; SC). After each surgery, mice were allowed to recover in an empty chamber with a heating pad (T Pump, Gaymar) before being returned to the home cage.

2.4.1 Viral Injections

After the preparations above, an incision was made in the skin along the midline of the skull. A craniotomy was made over the injection site using a pneumatic dental drill (eBay, Inc., San Jose, California). Using a stereotax and the Nanoject II (Drummond Scientific, Broomall, Pennsylvania), a pulled-glass pipette (BF150-117-10; tip size approximately 3-15 μm, Sutter Instrument Co., Novato, California) was lowered into the ACC (AP: +0.90 mm, ML: -0.30 mm, DV: -1.00 mm) and virus was injected. After this injection was completed and the pipette was removed, the skin was sutured with non-absorbable sutures (AD Surgical, Sunnyvale, California).

2.4.1.1 For Ca^{2+} Imaging with Genetically-encoded GCaMP6f

To monitor VIP^{ACC} activity, we injected 460 nl of an adeno-associated virus (AAV) that expresses GCaMP6f, a fluorescent Ca^{2+} indicator, in a Cre-dependent manner (AAV9-CAG-Flex-GCaMP6f.SV40, see 2.3, Viruses). GCaMP6f was chosen due to its increased brightness and kinetics as compared to prior versions of GCaMP and GCaMP6s, respectively (Chen et al., 2013).

2.4.1.2 For Rabies Trans-synaptic Tracing

For trans-synaptic tracing of monosynaptic inputs to VIP^{ACC}, SOM^{ACC}, or PV^{ACC} we injected two different viruses into Cre driver mouse lines. We targeted different types of interneurons by using a different Cre line mouse for each cell type (VIP-Cre, SOM-Cre, or PV-Cre). For each, we first injected 128 nl of a Cre-dependent helper AAV that expresses target proteins under the human synapsin-1 promoter: (AAV-TVA-Glyco, see

2.3, Viruses). This AAV contained genes to express enhanced green fluorescent protein (EGFP), the avian sarcoma/leukosis virus subtype A receptor (TVA, which confers infection capability to rabies virus pseudotyped with the avian sarcoma leucosis virus glycoprotein (EnvA)), and the rabies virus glycoprotein (G) (Kohara et al., 2014; Haubensak et al., 2010; Callaway & Luo, 2015) (which is necessary for trans-synaptic transport of glycoprotein gene-deleted (ΔG) rabies virus (RV)) (Wall et al., 2016). These three genes were in frame and separated by porcine teschovirus self-cleaving 2A elements (Kohara et al., 2014).

After allowing this first virus to express for one month (Cruz-Martin et al., 2014), the skin was re-incised, a new craniotomy was drilled, and 128 nl RV*dG* (see 2.3, Viruses) was injected. It was crucial to inject the AAV before RV*dG* because AAVs require more time for expression to occur (Cruz-Martín et al., 2014). There is no cognate receptor for EnvA in the mouse, so RV*dG* only infects TVA-expressing cells. Together, Glyco, TVA, and RV*dG* allow for retrograde monosynaptic tracing only from Cre-expressing cells. In Cre-negative wild type mice (C57BL6/J, N = 3), we performed these injections and saw very few labeled cells outside of the injection site, suggesting a lack of leaky expression outside of the ACC (Figure 6.2). As part of the analysis, we did not include RVdG inputs at the site of the ACC injection since leakage in viral expression could lead to Cre-independent labeling locally (Callaway & Luo, 2015).

2.4.2 Gradient Index Lens Implants

To image neuronal activity with a miniaturized microscope (miniscope), a gradient-index (GRIN) lens was implanted in the ACC. This surgery was performed at least 2 weeks after viral injection surgery to allow for expression of the AAV containing GCaMP6f. After the preparations described above, the scalp was re-incised and a 1 mm diameter craniotomy was drilled, centered around the viral injection. Three screws (Fine Science Tools Inc., North Vancouver, Canada) were inserted into the skull and a layer of super glue (cyanoacrylate, Krazy glue, High Point, North Carolina) was applied to the screws and skull to ensure the lens and dental cement adhered strongly. Dura over the ACC and a small region of the secondary motor cortex were aspirated using a blunted 18G needle (BD, Franklin Lakes, NJ) coupled to a vacuum line. A GRIN lens (Table 2.1) attached to a stereotax via custom 3D-printed implant assembly (Figure 3.4, C-D) was lowered into the ACC at a 20° angle (AP: +0.90 mm, ML: -0.12 mm, DV: -0.13 mm), to improve access to the ACC and minimize the risk of puncturing the midline vasculature. Once the GRIN lens was in place, it was adhered to the skull with optical glue (Norland Products Inc., Cranbury, NJ) and dental cement (Ortho-Jet™ Liquid, Black, Lang Dental, Wheeling, Illinois). An antibiotic was administered via the water supply (Biomox, 0.75mgl/ml, Henry Schein) for 10 days after surgery.

2.5 Miniscope Parts

Miniscope models are available at https://github.com/CruzMartinLab. Commercially available parts are listed in Table 2.1, which lists names of products, suppliers, and websites with detailed information for each purchased miniscope part.

Custom parts were 3D printed (Form 3 Printer, Black Resin FLGPBK03, Formlabs, Somerville, Massachusetts) and assembled in-house (Figure 3.4).

Table 2.1: Miniscope Parts Table		
Part Name	**Supplier**	**URL**
UCLA Miniscope CMOS	LabMaker GmbH, Berlin, Germany	https://www.labmaker.org/products/cmos-pcb-miniscope
Custom filters: 470/40 EM (4mm x 4mm) (excitation), 535/50 EM (4mm x 4mm) (emission), 495nm BS (4mm x 4.8mm) (dichroic)	Chroma Technology, Cambridge, Massachusetts	
LUXEON Rebel Blue LED (470nm, 70 lm @ 700mA) (#LXML-PB01-0040)	Lumileds, San Jose, California	http://www.lumileds.com/products/color-leds/luxeon-rebel-color
Achromat lens (5mm diameter x 15mm FL, MgF2 Coated, Achromatic Doublet Lens) (#45-206)	Edmund optics, Barrington, New Jersey	http://www.edmundoptics.com/optics/optical-lenses/achromatic-lenses/mgf2-coated-achromatic-lenses/45207/
Drum lens (2.4mmx3.0mm) (#45-549)	Edmund optics, Barrington, New Jersey	http://www.edmundoptics.com/optics/optical-lenses/ball-condenser-lenses/drum-lenses/45549/
Objective GRIN lens (objective 2.0mm Dia, 0.25 pitch) (#GT-IFRL-200-inf-50-NC)	GRINtech, Jena, Germany	http://www.grintech.de/
Objective GRIN lens (objective 1.8mm Dia, 0.25 pitch) (#64-519)	Edmund optics, Barrington, New Jersey	http://www.edmundoptics.com/optics/optical-lenses/aspheric-lenses/gradient-index-grin-rod-lenses/64519/
Implanted GRIN lens (Relay Lens, 1 mm diameter, 4 mm length, 0.44 pitch length, 0.47 NA) (#GT-IFRL-100)	GRINtech, Jena, Germany	
UCLA DAQ board	LabMaker GmbH, Berlin, Germany	https://www.labmaker.org/products/daq-pcb
50 ohm coax silicone rubber jacketed cable (#CW2040-3650SR)	Cooner Wire, Chatsworth, California	https://www.coonerwire.com/mini-coax/
SMA Coax Connector (for connectorizing the coax cable above) (#901-9867-RFX)	Digikey Electronics, Thief River Falls, Minnesota	http://www.digikey.com/product-search/en?vendor=0&keywords=901-9867-RFX
UCLA Miniscope Acquisition Software	University of Cailfornia at Los Angeles, Los Angeles, California	http://miniscope.org/index.php?title=Main_Page

2.6 Miniscope Modification and Construction

The miniscopes used were modified from two existing designs previously used in zebra finches and rodents (Ghosh et al., 2011; Liberti, et al., 2017) to allow them to detach from the baseplate (Figure 3.4), which made it possible to co-house the animals without risking miniscope damage. This modification was essential to this work because singly housing mice can alter their behavior (Koike et al., 2009; Liu et al., 2020; Voikar et al., 2005). Miniscopes were attached to baseplates at a 15-20 degree angle relative to the midline to align with the GRIN lenses (Figure 3.4). Miniscope angle needed to be adjusted slightly on the stereotax because the animals's skin was not removed, so the skull could not be leveled as precisely as it was during surgeries. Miniscope implant angle (between 15-20 degrees) was chosen to best align with the lens implant and maximize the number of visible cells in the field of view. Miniscopes weighed approximately 3.5g and the wire attaching them to the acquisition board rested in a plastic loop hanging from the ceiling to minimize the weight on the animal's head. This allowed animals to freely move and behave normally (Figure 3.5).

2.7 Baseplating

After the GRIN lens implant surgeries, animals were given 3 weeks to fully recover and to ensure the GCaMP6f expression would be optimal. Animals were then anaesthetized, as described above (2.4, Surgeries), and GCaMP6f expression was assessed by imaging the fluorescent signal using miniscopes. Miniscopes were lowered towards the GRIN lens at a 20 degree angle using a stereotax and a custom 3D printed

baseplating assembly (Figure 3.4, E-F). When GCaMP6f-positive neurons were visible and in focus, baseplates were attached to the skulls with dental cement. After allowing cement to dry, miniscopes were detached and animals were allowed to recover.

2.8 In Vivo Ca^{2+} Imaging During Behavioral Assays

Before any behavioral testing, mice were handled for 10 minutes for 3 days to acclimate them to the experimenter. For anxiety-related assays, mice were not exposed to the arenas prior to testing, but for the social task, implanted mice were acclimated to the arena with empty cups for 10 minutes per day for 2 days prior to the task. This ensured that, during the social behavioral tasks, mice were familiar with the empty cups. In addition, stimulus mice were acclimated to being housed in cups for 10 minutes on each of these days. Arenas were custom made from acrylic and HDPE (McMaster-Carr, Elmhurst, Illinois) and were cleaned with 70% ethanol between trials and animals. Behavior was recorded (C270 Webcam, Logitech, Lausanne, Switzerland) at 30 frames/s under overhead lighting (200 lux). For Ca^{2+} imaging, miniscopes were attached and then animals were given 10 minutes to rest in an empty chamber before we started the experiments. Ca^{2+} imaging videos were acquired at 20 frames/s using a Miniscope Data Acquisition PCB and Data Acquisition Software (Aharoni et al., 2019) (Table 2.1). Acquisition software simultaneously recorded behavioral and neural videos. Although 20 Hz acquisition allowed for less temporal precision than a higher frame rate would (30 Hz is often chosen for Ca^{2+} imaging studies), it improved our ability to reliably see and capture Ca^{2+} fluorescence without applying high LED intensity to our samples. Other

recent work has used Ca^{2+} data acquired at similar frame rates for analysis linking the activity of individual neurons to behavioral data (Liang et al., 2018; Bollimunta et al., 2021; Zhang et al., 2019). We acquired images with a field of view of 720 x 480 pixels (approximately 800 μm × 600 μm). Excitation LED power was adjusted to optimize imaging for each animal with a maximum output of 1 mW. To avoid bleaching GCaMP6f, no trials were longer than 10 min and different behavioral assays were carried out on separate days.

2.8.1 Elevated Zero Maze (EZM)

To assay anxiety-like behavior, we used the elevated zero maze, or EZM, named as such because it is an elevated arena with a circular track. It is made up of two open arms and two closed arms (track diameter = 50 cm, track width = 5 cm, wall height for closed arms = 40 cm, height of track = 61 cm). Open arms are considered anxiogenic and closed are anxiolytic. Mice were initially placed in the closed arm and recorded for 10 minutes.

2.8.2 Open Field (OF)

To assay anxiety-like behavior and locomotion, the OF was used. The center of the arena is considered anxiogenic and the periphery is anxiolytic. Mice were placed in the center of a custom-made acrylic arena (50 × 50 × 30 cm length-width-height) and allowed to explore for 10 min.

2.8.3 Sociability and Social Novelty

The arena contained two mesh wire cups – one on each end of the arena (50 x 25 x 30.5 cm length-width-height). On Day 1 (Sociability), one mesh wire cup housed a littermate and the other was empty. On Days 2 and 3 (Social Novelty), one cup housed a littermate and the other housed an entirely novel male CD-1. Each day the experimental mouse was placed in the center of the arena and given 10 minutes to explore the arena and cups. The side of the arena with each stimulus was randomized.

2.8.4 Novel Object Task

In Novel Object, mice were allowed to freely explore a rectangular arena (50 x 25 x 30.5 cm length-width-height). One object was placed at one end of the arena and the animal was given 5 minutes to explore the arena and object. All objects were small, plastic toys of various shapes. The side where the object was placed was randomized between animals.

2.9 Perfusions, Histology, and Immunohistochemistry

Animals used in Ca^{2+} imaging experiments were perfused to determine the locations of the viral injections and lens placements. Animals used in trans-synaptic tracing experiments were perfused to visualize both starter and input neurons. Mice were injected with an overdose of sodium pentobarbital (250 mg/kg; IP, Vortech Pharmaceuticals Ltd., Dearborn, Michigan) and transcardially perfused with 1X phosphate buffered saline (PBS) followed by 4% paraformaldehyde in PBS (PFA).

Brains were extracted, stored in PFA for 24 hours at 4°C, and then transferred to a 30% (w/v) sucrose solution for 48 hours at 4°C. Tissue was sectioned at 50-100 μm using a freezing sliding microtome (SM2000, Leica Biosystems, Buffalo Grove, Illinois). Sections were mounted onto slides (Globe Scientific Inc., Mahwah, New Jersey) using Fluoromount-G mounting medium with DAPI (4′,6-diamidino-2-phenylindole, Thermo Fisher Scientific, Waltham, Massachusetts) to visualize nuclei and identify brain regions.

2.10 Tissue Imaging

Sections were imaged using an upright wide-field microscope (Nikon Eclipse Ni, Nikon Instruments Inc. Melville, New York) controlled by NisElements (Nikon Instruments Inc., 4.20). Images were acquired using a Plan Fluor 4X (NA 0.13) or 10X (NA 0.3) objective with standard Nikon HQ filter cubes for DAPI, EGFP/GCaMP, and mCherry. Images were viewed and analyzed using TIFF format in ImageJ (NIH). Whole slice images were compared to the Allen Mouse Brain Atlas (Lein et al., 2007) (brain-map.org/api/index.html) to identify brain regions where labelled neurons or lenses were present.

2.11 Behavioral Analysis

Behavioral videos from each task were analyzed to determine each animal's location, quantify its behavior in each task, and match its behavior with its neural activity. Behavior was analyzed using DeepLabCut (Mathis et al., 2018; Nath et al., 2019), an open-source program that uses machine learning to track the coordinates of an

animal's body parts in each frame of a behavioral video. Behavioral analyses were performed as described by Comer et al. (2020). To assess the program's accuracy, videos labeled by the software were inspected by a trained observer and custom MATLAB (MathWorks, Natick, Massachusetts) scripts were used to verify that DeepLabCut located each body part at least 95% of the total time the animal was tracked. For EZM and OF, we tracked the centroid of the mouse's body to determine velocity, distance traveled, and when the mouse was in each zone of the arenas. For the OF, we divided the arena into 25 squares (10 cm x 10 cm each) and defined the outermost 16 the periphery and the remaining inner 9 squares as the center (Seibenhener & Wooten, 2015). For the social and object tasks, we tracked the head to determine close proximity to cups or objects. Binary behavior matrices (vectorized behavior) indicating the location of the animal were created from DeepLabCut using custom MATLAB scripts.

2.12 Ca^{2+} Imaging Analysis

Ca^{2+} imaging data were processed using CaImAn (short for Calcium Imaging Analysis, Giovannucci et al., 2019) written in Python (https://www.python.org/). Using this program, we put Ca^{2+} imaging videos through piecewise rigid motion correction using patches of 48 x 48 pixels with 24 x 24 pixel overlap. After motion correction was completed, ROI detection was performed to detect neurons in the field of view with a merging threshold of activity correlation greater than 0.7 between nearby cells and a 2.5 minimum threshold for the signal to noise ratio. For each neuron, deltaf/f (df/f) traces and

spatial information were extracted, exported, and saved in .mat format using SciPy (Virtanen et al., 2020).

All subsequent analyses were performed using custom MATLAB and Python functions. Raw Ca^{2+} traces were z-scored using the mean baseline df/f and sigma from the entire time series for each trial. When we report df/f values, they are z-scored df/f values in units of standard deviation (SD). To identify cells with highly noisy signals, a binary filter was applied to all cells based on peaks of Ca^{2+} transients (Jimenez et al., 2018). Cells were excluded for excessive noise if they exceeded a threshold of 0.4 peaks/second.

Behavioral videos were acquired at 20 frames/s, while Ca^{2+} imaging was acquired at 30 frames/s. Due to these different acquisition frequencies, data needed to be aligned to match behavioral and neural data in time. These data were aligned using timestamps from the Miniscope Data Acquisition PCB and Data Acquisition Software (Aharoni et al., 2019) (Table 2.1) and custom MATLAB scripts. Starts and ends of behavioral epochs were matched to Ca^{2+} data timestamps to isolate neural activity during select behaviors. Fewer than 1% of the total frames of neural data were dropped, but any values for dropped frames were extrapolated by filling these gaps with averaged z-scored df/f values from surrounding frames.

2.12.1 Ca^{2+} Activity

In all figures, Ca^{2+} activity refers to the area under the curve of Ca^{2+} traces. To calculate this value, we isolated z-scored df/f traces (see 2.12, Ca^{2+} imaging analysis) and

took their integral using the MATLAB function trapz. For all figures, excluding Figure 3.6, I and Figure 3.7, N, area under the curve was calculated for 5 s intervals, which was chosen based on average transient length. When calculating the average area under the curve across velocities (Figure 3.6, I and Figure 3.7, N), the process was the same, but intervals were 1 s. These values were calculated for each cell to get its Ca^{2+} activity values. When average Ca^{2+} activity is reported, that refers to the average area under the curve for all cells for each mouse. When Ca^{2+} activity is reported for a subpopulation of cells, that refers to the average area under the curve for all cells in a given subpopulation per mouse.

2.12.2 Single Cell ROC Analysis

Responses of individual cells during different behavioral conditions were assessed within each behavioral trial using receiver operating characteristic (ROC) analysis, as previously described (Li et al., 2017; Kingsbury et al., 2020). The ROC curve demonstrates how well a single neuron's activity matches an animal's behavioral state, which can be quantified by calculating the area under the ROC curve (auROC) (Li et al., 2017; Kingsbury et al., 2020). For each neuron in each behavioral condition, an ROC curve was generated using the true positive rate (TPR) and false positive rate (FPR) values for that cell and behavioral state. TPR and FPR were calculated across multiple binary thresholds applied to z-scored df/f traces of each cell, ranging from the minimum to maximum values of the Ca^{2+} signal. For each threshold, binarized df/f traces were compared to the binary behavioral vectors, which used binary values to indicate an

animal's presence or absence in a specific zone of the arena. TPR and FPR were then plotted against each other to create each ROC curve and auROC was calculated.

To classify cells as stimulus-selective or neutral, we determined whether the cell's auROC value for a given stimulus was high enough to suggest it preferentially activated to a stimulus. To account for any random alignment in our data, we calculated 1000 null values for each cell by applying circular permutations of randomized lengths to the Ca^{2+} data and calculating auROC for each of these randomized versions of the data. A cell was considered selective for a certain stimulus if its auROC was at least 2 SD greater than the mean of the null distribution (auROC > 97.5^{th} percentile). If a cell was not selective for any of the stimuli in a given task, it was classified as a "neutral cell". This ROC classification technique has been used by other groups to identify cells that preferentially activated to social stimuli (Li et al., 2017; Kingsbury et al., 2020). This auROC threshold for designation of selective cells has been utilized to avoid over-estimating statistical significance and has been described as a relatively unbiased approach because it does not use any fixed threshold (Li et al., 2017; Kingsbury et al., 2020; Guido et al., 1995). For Figure 5.1, to calculate the auROC of "super cells", we averaged z-scored df/f traces of all cells that were selective for a given stimulus and re-calculated auROC for that averaged data.

2.12.3 AuROC Analysis Across Tasks

For Figures 5.2 and 5.3, to determine if the same cells were responsive to stimuli in different tasks, we registered cells across EZM and Sociability using CaImAn

(Giovannucci et al., 2019). An advantage of our miniscope is that it is detachable, which allowed us to group house mice, but it was difficult to obtain the same imaging plane across different tasks. Nevertheless, in a subset of mice and VIP^{ACC}, we were able to confidently identify and register cells across tasks (127 registered VIP^{ACC} from all 6 animals). Cells were registered using CaImAn and trained observers examined the images by eye to confirm that the same neurons were found in both tasks. Therefore, any shift of the lens when the miniscope was removed and re-attached is unlikely to contribute to our findings. For each cell and behavioral condition, auROC was calculated (see 2.12.2, Single cell ROC analysis) and cells were considered selective for multiple conditions if they were selective for different stimuli across these tasks.

2.12.4 AuROC Analysis Validation

To validate the auROC analysis (Figures 3.10 and 4.6), we looked for consistent activity changes in the cells we identified as selective. We calculated auROC values using the first half of the EZM or Sociability data, rather than the entire dataset, to identify selective cells (Figures 3.10, A). Next, using these classifications of selectivity, we assessed Ca^{2+} activity from the second half of the data under the cell's preferred and non-preferred conditions (Figures 3.10, B and Figure 4.6). The preferred condition was the one that cell was selective for, whereas non-preferred was the other context or stimulus in that task. To assess whether ROC analysis led to random assignment of cells as selective, we reran our analysis with Ca^{2+} traces that were temporally shifted at

random lengths 1000 times. This allowed us to calculate the average percentage of cells assigned as selective in this randomized control.

2.12.5 Activity Heatmaps

For Figure 3.7, D-E, the activity heatmaps were plotted to visualize the average cell activity in 5x5 pixel spatial bins across the OF arena. Z-scored df/f traces from individual cells were normalized to their maximum value and matched with DeepLabCut centroid coordinates at the closest timestamp. For Figure 3.10, C, heatmaps were made in the same way, using Ca^{2+} data from selective cells that had been circularly shuffled as a control.

2.13 Analysis of Trans-synaptic Tracing Data

For retrograde mapping experiments, brains were scanned to identify signal from starter cells and retrogradely labeled input neurons. We identified retrogradely-labeled brain regions based on landmarks from the DAPI signal and the Allen Mouse Brain Atlas (Allen Institute for Brain Science, 2004) and cells were quantified using ImageJ. Starter cells were defined as cells that were positive for both GFP (from AAV-TVA-Glyco) and mCherry (from EnvA-ΔG-mCherry), whereas input cells were only positive for mCherry. We confirmed with DAPI that all putative starter and retrogradely-labeled cells had a nucleus. Each animal had a different number of starter cells, so to normalize our data, we divided the number of retrogradely-labeled neurons in each region by the number of

starter cells for that mouse (Inputs per starter cell). The number and location of labeled neurons in a given region was independently confirmed by 3 trained scientists.

After quantifying all cells, input brain regions were divided into quartiles by number of input neurons. Only brain regions in the top two quartiles were graphed and included in the data presented here. We did not include RVdG inputs at the site of the ACC injection in this analysis since leakage in viral expression could lead to Cre-independent local labeling (Callaway & Luo, 2015).

To quantify layer specificity of starter cells, histology with starter cells was compared to the Allen Institute Interactive Atlas Viewer (Allen Institute for Brain Sceince, 2008). For each cell type, the layer of each starter cell was identified manually by trained observers and quantified.

2.14 Statistical Analysis

Statistical analyses were performed using Graph Pad Prism 8.0 (GraphPad Software Inc., San Diego, California). For figure preparation, CorelDRAW Graphics Suite X8 (Corel Corporation, Ottawa, Canada) and ImageJ were used. The threshold for significance was set to $\alpha = 0.05$ and $*p<0.05$, $**p<0.01$, $***p<0.001$, $****p<0.0001$. Data are presented as mean ± SEM, unless otherwise noted. t-tests and ANOVAs followed by appropriate post tests were used and are specified in the figure legends. For Fig S3A-B, Fig S4K-L, and Fig S6A-D, frequency distributions were fitted with Gaussians and percentages of selective cells are represented in pie charts. For all behavioral experiments, N = 6 implanted mice for Ca^{2+} imaging and N = 5 control mice

that underwent no surgeries. For EZM, n = 345 cells, for Sociability, n = 310 cells, for Social Novelty Day 2, n = 350 cells, Day 3, n = 232 cells, for Novel Object, n =227 cells, and for OF, n = 273 cells. For VIP tracing experiments, N = 3 mice with n = 705 starter cells and 10107 retrogradely-labeled input cells. For SOM tracing experiments, N = 3 mice with n = 567 starter cells and 18270 retrogradely-labeled input cells. For PV tracing experiments, N = 3 mice with n = 1770 starter cells and 69447 retrogradely-labeled input cells.

CHAPTER THREE

Functional Heterogeneity of VIP^{ACC} Interneuron Subpopulations in Anxiogenic and Anxiolytic Contexts

3.1 Introduction

Despite the prevalence of anxiety disorders (Harvard Medical School, 2007), many questions remain about how the brain encodes information related to anxiety, especially at the level of the neural circuit. The ACC has been implicated in anxiety disorders in humans (Kitayama, Quinn, & Bremner, 2006; Kasai et al., 2008; Cohen et al., 2006; Nitschke et al., 2009) and manipulation of the ACC in rodents is sufficient to induce or diminish anxiety-related behaviors (Weible et al., 2017; Kim et al., 2011). Nonetheless, studies that monitor distinct neural subtypes or assess ACC activity with cellular resolution during anxiety-related tasks are especially rare. Cortical populations sometimes exhibit marked functional heterogeneity (Frost, Haggart, & Sohal, 2021; Liang et al., 2018; Weible et al., 2012; Weible et al., 2009), which would not be detected in studies that monitor bulk ACC activity. VIP interneurons can alter the activity of many other cells in local cortical microcircuits (Pi et al., 2013; Karnani et al., 2016; Melzer et al., 2020), but whether they are involved in encoding anxiogenic or anxiolytic stimuli in the ACC remains unknown. VIP cells are also known to be diverse in their morphology, electrophysiology, and molecular profiles (Ferezou et al., 2002; Cauli et al., 1997; Gonchar, Wang, & Burkhalter, 2008; Kawaguchi & Kubota, 1997; Ketchesin, Huang, & Seasholtz, 2017; Obermayer et al., 2019; Porter et al., 1999; Tasic et al., 2016; Tasic et

al., 2018), and yet it is unknown whether VIP^{ACC} are functionally heterogeneous in vivo. We hypothesized that individual VIP^{ACC} would activate preferentially to different anxiety-related environments, but not all VIP^{ACC} would demonstrate similar stimulus-related activation.

In the following series of experiments, we utilized Ca^{2+} imaging techniques with miniaturized microscopes to determine whether VIP^{ACC} encode anxiety-related information. Miniscopes, viruses, and surgical techniques were all optimized to restrict our Ca^{2+} imaging to VIP^{ACC}, specifically. Animals implanted with miniscopes underwent two anxiety-related assays: the elevated zero maze and the open field. Cellular resolution allowed us to capture the heterogeneity of responses across VIP^{ACC} and determine stimulus-specific activation of individual neurons.

3.2 Results

3.2.1 Ca^{2+} Imaging of VIP^{ACC} Activity with Cellular Resolution in Freely Moving, Behaving Mice

To quantify the activity of VIP^{ACC}, we first needed to optimize our methodology for imaging this specific neural population. We injected an adeno-associated virus (AAV) that expresses GCaMP6f, a genetically encoded calcium indicator (GECI), to visualize calcium transients by measuring changes in fluorescence. GCaMP6f demonstrates brighter expression with faster kinetics as compared to prior versions of GCaMP and to GCaMP6s, respectively (Chen et al., 2013). To achieve cell-type specific imaging, we injected a Cre-dependent AAV (AAV9-CAG-flex-GCaMP6f) into the ACC of VIP-Cre

mice (Figure 3.1, A). To allow for strong viral expression, we waited for three weeks after injection and then implanted a graded-index (GRIN) lens into the ACC (Figure 3.1). We then used miniscopes to image VIP^{ACC} while animals were awake and freely behaving (Figure 3.2).

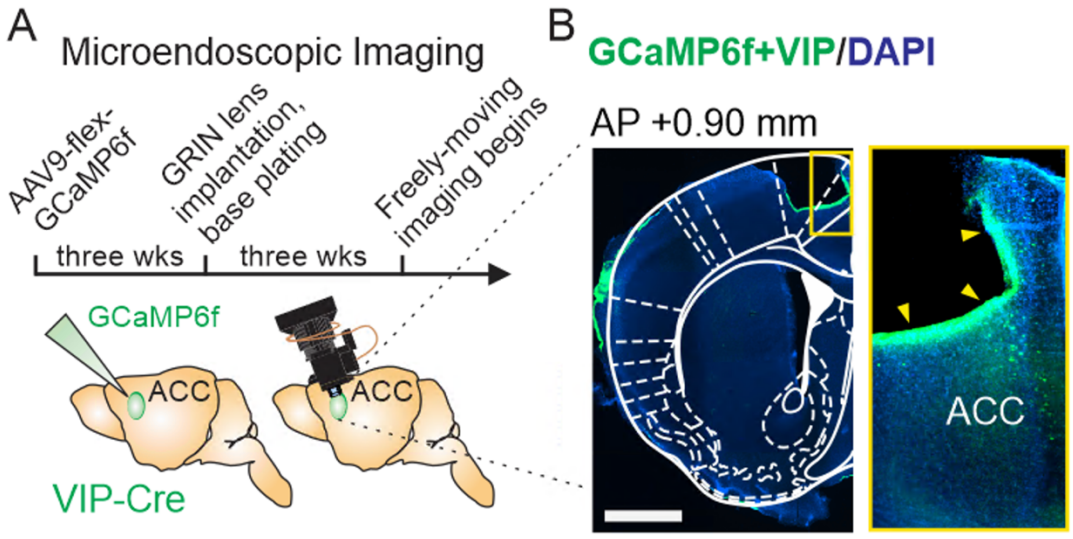

Figure 3.1: Experimental paradigm for Ca^{2+} imaging of VIP^{ACC}. (A) Experimental timeline for Ca^{2+} imaging experiments. (B) Representative image of histology from an animal injected with AAV9-flex-GCaMP6f and with a GRIN lens implanted in the ACC. Image acquired with a 4x objective. Blue: DAPI, green: VIP^{ACC} expressing GCaMP6f. Dotted white overlay: brain regions from the Allen Mouse Brain Atlas (2004). Yellow arrowheads: GRIN lens location in the ACC. **Left**: left hemisphere. **Right**: zoomed image of yellow boxed region in the left panel. Scale bar = 1mm (left panel) or 400 μm (right panel). Note: Surgeries performed by William Yen. Histology and imaging by Lisa Kretsge. Figure preparation by Lisa Kretsge, Alberto Cruz-Martín, and William Yen. Figure published in Johnson, Kretsge & Yen et al., *BioRxiv*, 2020.

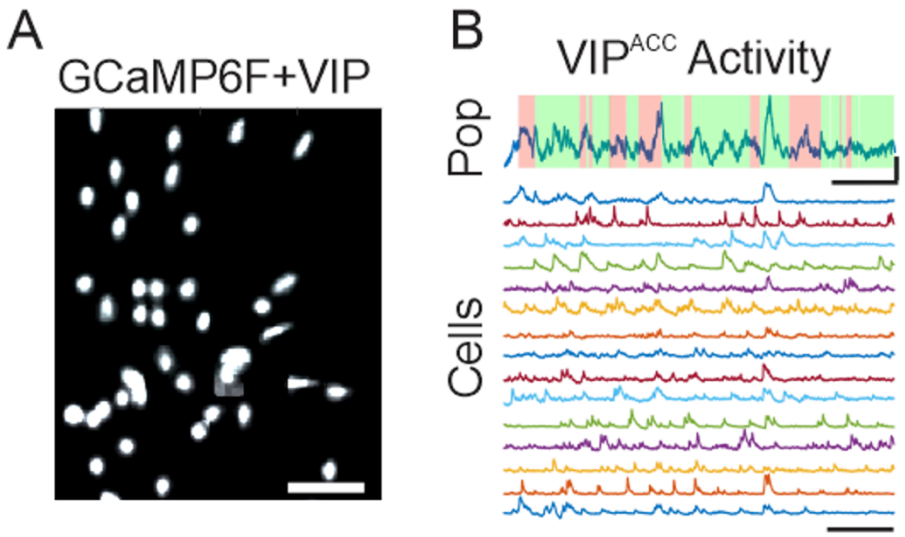

Figure 3.2: Ca^{2+} transients of VIP^{ACC} can be imaged in vivo in awake, behaving animals. (A) Representative image of VIP^{ACC} expressing GCaMP6f (white) in vivo during a behavioral task. Scale bar = 100 μm. (B) Top: population activity of VIP^{ACC} represented as SD. Scale bar = 50 s. The two different shaded colors (pink or green) represent the mouse's location in one of two different locations of a behavioral arena: open (pink) or closed (green) arms of an elevated zero maze. Scale bar = 50 s, 1 SD. Bottom: Example Ca^{2+} transients of individual VIP^{ACC} (normalized to peak activity) were recorded as an animal explored a behavioral arena. Note: Surgeries and in vivo imaging performed by William Yen. Figure preparation by Lisa Kretsge, William Yen, and Alberto Cruz-Martín. Figure published in Johnson, Kretsge & Yen et al., *BioRiv*, 2020.

To optimize these imaging techniques, we needed to ensure that 1) viral expression was limited to VIP^{ACC}, 2) lenses were implanted in the ACC, and 3) miniscopes were optimized for our behavioral experiments. First, we verified that the expression of our virus of interest was restricted to VIP^{ACC}. Previous work has shown that expression of Cre-dependent AAVs can leak into cells without Cre (Callaway & Luo, 2015). To ensure there was no leakage of our AAV, we injected it into the ACC of mice without any Cre expression (C57BL6/J wild type mice, n=3) and waited 3 weeks to allow for viral expression. We compared the histology of these control animals to that of VIP-

Cre animals with the same injection volumes and viral titers (Figure 3.3). We found GCaMP6f-expressing cells in the ACC of the VIP-Cre mice, but not in the wild-type animals (Figure 3.3). Since there was no visible viral expression in the mice without Cre present, this suggests that GCaMP6f expression was appropriately restricted to the Cre+ cells, or VIP cells in VIP-Cre animals.

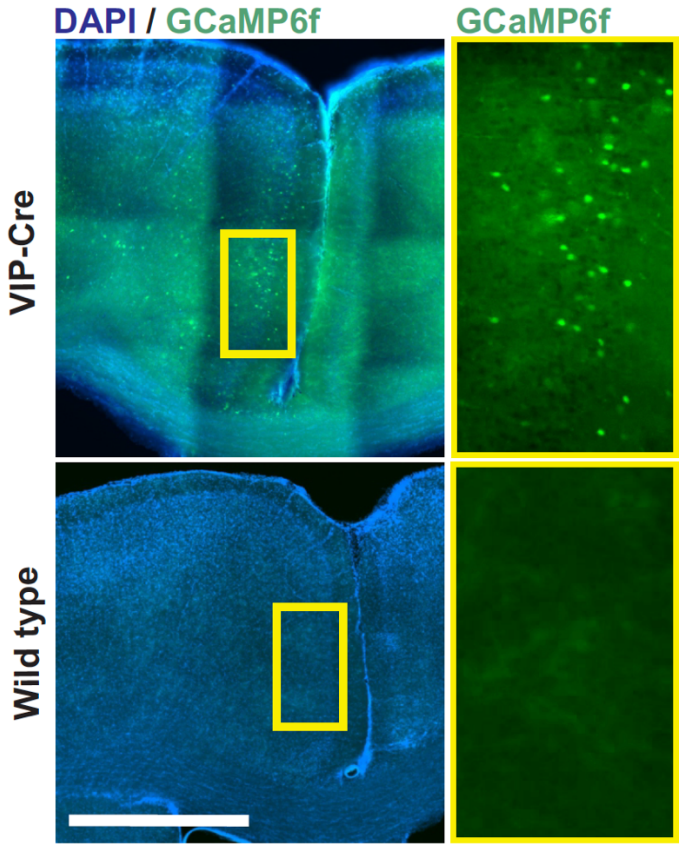

Figure 3.3: GCaMP6f expression in VIP-Cre cells. Histology showing AAV9-flex-GCaMP6f injections in the ACC of a VIP-Cre mouse (top) and wild type mouse (bottom). GCamP6f+ cells are abundant in the VIP-Cre animal (top), but no labelled cells were found when this Cre-dependent virus was injected into wild type mice (bottom). Right panels show zoomed versions of the yellow boxed regions from the left panels. Blue: DAPI, green: GCaMP6f. Scale bar = 1 mm. n = 3 wild type mice. Note: Injections performed by Lisa Kretsge and William Yen. Histology, imaging, and figure preparation by Lisa Kretsge. Figure not previously published.

Next, we verified that GCaMP6f expression and GRIN lenses were located in the ACC of our experimental animals. We found that the best method for GRIN lens implantation was to insert the lenses at a 20-degree angle relative to the midline (Figure 3.4, A-D). This allowed for better access to the ACC while minimizing the risk of puncturing the midline vasculature during surgery. When baseplates were attached to the skull, we also mounted the miniscope at a 20-degree angle, which allowed for alignment to the GRIN lens (Figure 3.4, E-F). For each animal in the following datasets, post-mortem histology showed that injections and lenses were successfully targeted to the ACC (Figure 3.1, B). Because viral expression was limited to VIP cells and lenses were implanted in the ACC, we were able to specifically monitor VIP^{ACC} with our miniscopes (Figure 3.2).

The next alteration in this experimental paradigm was to modify existing designs (Liberti, et al., 2017; Ghosh et al., 2011) of 3D-printed miniscopes. Because we planned to assay social behavior, it was important that our animals could be group-housed, even after lens implantation. Previous work has shown that single housing mice can be a stressor and can lead to abnormal behavior in tasks assaying anxiety and depression-like behaviors, memory, and social behaviors (Koike et al., 2009; Liu et al., 2020; Voikar et al., 2005). Therefore, we wanted our miniscopes to be detachable, such that animals could be group housed without risking damage to the miniscopes from their cagemates. We adapted these previous designs (Ghosh et al., 2011; Liberti, et al., 2017), assembled them in-house, and used them for in vivo Ca^{2+} imaging (Figure 3.4).

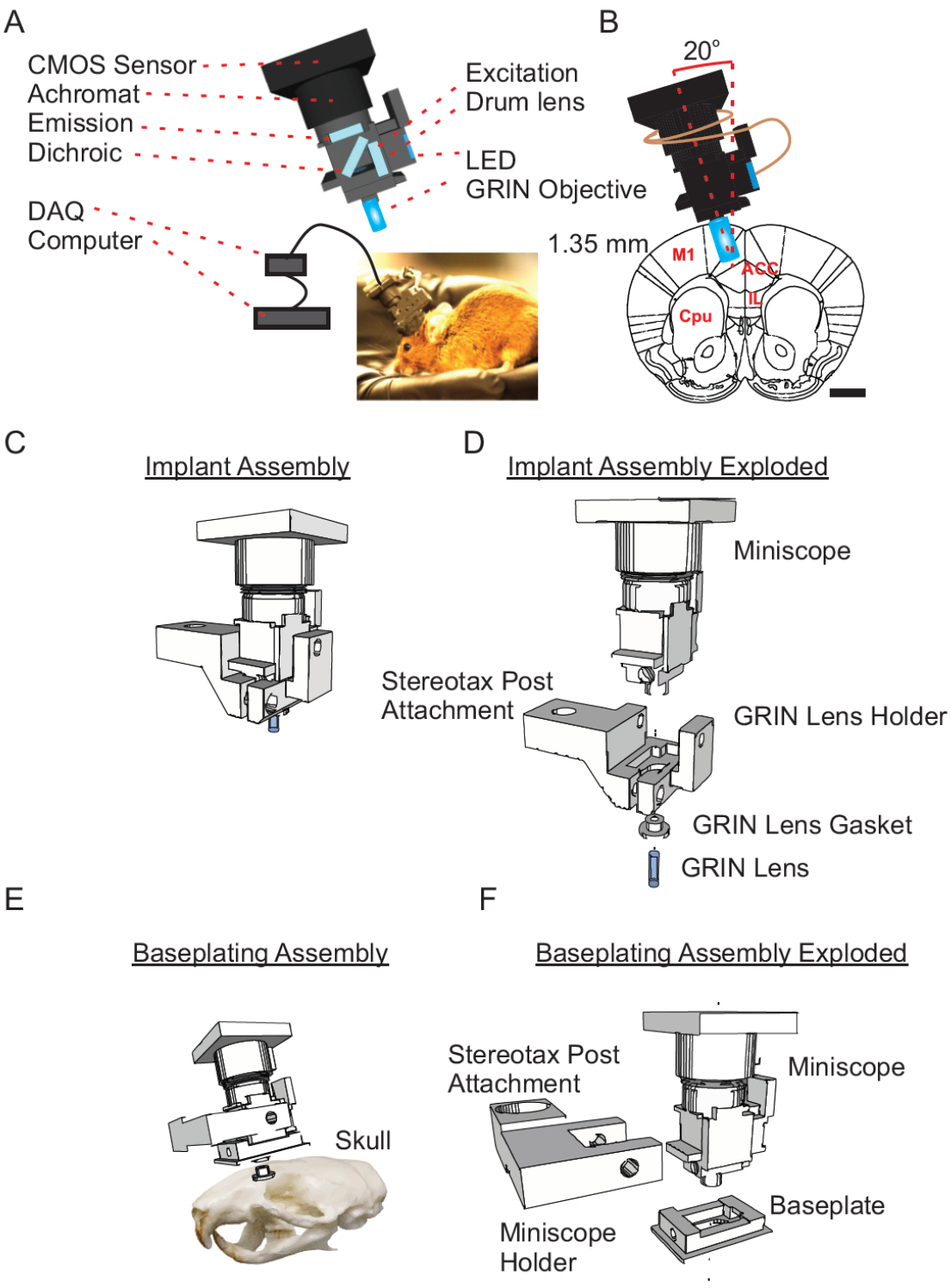
A
CMOS Sensor
Achromat
Emission
Dichroic
DAQ
Computer
Excitation
Drum lens
LED
GRIN Objective
B
20°
1.35 mm
M1
ACC
IL
Cpu
C
Implant Assembly
D
Implant Assembly Exploded
Miniscope
Stereotax Post
Attachment
GRIN Lens Holder
GRIN Lens Gasket
GRIN Lens
E
Baseplating Assembly
Skull
F
Baseplating Assembly Exploded
Stereotax Post
Attachment
Miniscope
Baseplate
Miniscope
Holder

Figure 3.4: 3D-printed miniscope for imaging in the ACC. (A) Model displaying the main components of the miniscope and image of a miniscope implanted in an experimental mouse. (B) Schematic of a miniscope implanted in the ACC (coronal section, implanted at a 20 degree angle). Scale bar = 1.5 mm. (C-D) Implant assembly (C) and exploded version (D) showing stereotax post attachment, GRIN lens holder, and GRIN lens gasket. This is used to surgically implant a GRIN lens. (E-F) Baseplating assembly (E) and exploded version (F) showing stereotax post attachment, miniscope holder, and baseplate. This is used to attach the baseplate. Miniscope models available at https://github.com/CruzMartinLab. Note: 3D printed parts adapted by William Yen from two previous designs (Ghosh et al., 2011; Liberti, et al., 2017) and assembled in-house by William Yen and Connor Johnson. Figure made by Alberto Cruz-Martín, William Yen, and Connor Johnson. Figure published in Johnson, Kretsge & Yen et al., *BioRxiv*, 2020.

As the final step in our protocol optimization, it was essential to determine whether or not our injections, implantations, and miniscopes caused behavioral impairments. The histology (Figure 3.1, B) shows that GRIN lens implantation caused some damage to secondary motor cortex (M2), so it was critical to assess whether this led to any motor impairments. In addition, we wanted to conclude if any of our manipulations lead to abnormal levels of anxiety-like behaviors in these mice. To answer these questions, the behavior of our implanted, miniscope-mounted animals was compared to a cohort of control non-surgerized mice (Figure 3.5). Mice underwent two behavioral paradigms, the open field (OF) and the elevated zero maze (EZM).

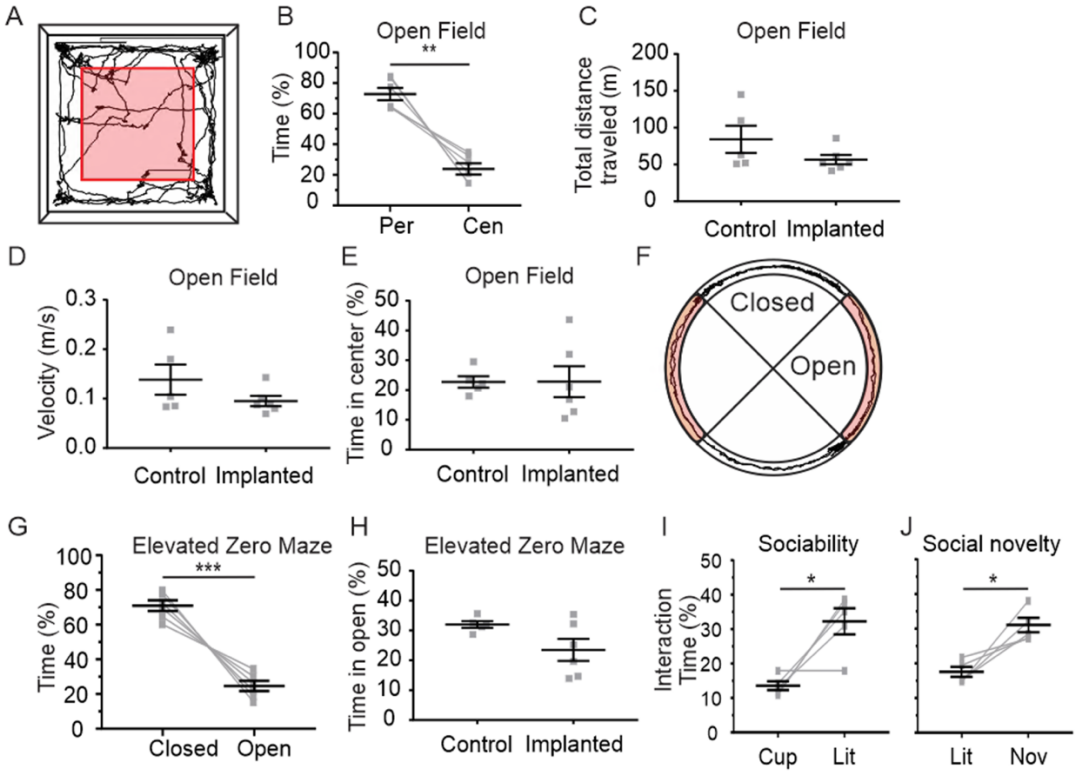

Figure 3.5: Lens implant and miniscope mounting do not impair locomotor, anxiety-like, or social behaviors. (A) Representative trace (black) of locomotor activity in the OF. Pink zone: center. White zone: periphery. (B) Percent time implanted mice spent in the periphery (Per) versus center (Cen) of the OF. **p=0.0014. (C) Total distance traveled by implanted mice versus controls in the OF. p=0.2209. (D) Average velocity of implanted mice versus controls in the OF. p=0.2388. (E) Percent time spent in center of the OF by implanted mice versus controls. p=0.9916. (F) Representative trace (black) of locomotor activity in the EZM. Pink zone: open arms. White zone: closed arms. (G) Percent time implanted mice spent in the closed versus open arms of the EZM. ***p=0.0006. (H) Percent time spent in the open arms of the EZM by implanted mice versus controls. (I) Percent time implanted mice spent interacting closely with either the empty cup (Cup) or littermate (Lit) in Sociability. *p=0.0199. (J) Percent time implanted mice spent interacting closely with either the littermate (Lit) or novel mouse (Nov) in Social Novelty. *p=0.0141. N = 6 implanted mice and 5 control mice. Each replicate in B-E and G-J represents one mouse. All statistics performed with Paired t-test. Note: Surgeries performed by William Yen. Behavioral experiments performed by Lisa Kretsge and William Yen. Data analyzed by Lisa Kretsge, Connor Johnson, and Alexandra O'Connor. Figure made by Lisa Kretsge and Alberto Cruz-Martín. Figure published in Johnson, Kretsge & Yen et al., *BioRxiv*, 2020.

The OF is an empty square arena, which mice were allowed to freely explore for 10 minutes (Figure 3.5, A). Normal animals innately spend more time in the periphery (anxiolytic zone) of the arena than the center (anxiogenic zone) (Hall & Ballachey, 1932; Choleris et al., 2001). Our implanted mice explored both the zones of the OF and, as expected, spent less time (67% less) in the open region, relative to the periphery (Figure 3.5, B). This suggests normal anxiety-related behavior in these implanted animals. There was no difference between implanted mice and controls in their total distance traveled (Figure 3.5, C), average velocity (Figure 3.5, D), or percentage of time spent in the center of the arena (Figure 3.5, E). These data show that implants and miniscopes did not induce abnormal locomotor or anxiety-related behaviors in the OF.

The EZM is an elevated circular arena with two open arms and two closed arms (Figure 3.5, F). In this assay of anxiety-like behavior, healthy animals spend more time in the closed arms (anxiolytic zone) than the open arms (anxiogenic zone) (Shepherd et al., 1994). Similar to the OF data, in the EZM, implanted mice spent approximately 65% less time in the open arms than in the closed (Figure 3.5, G). There was also no difference in percentage of time spent in the open arms between implanted mice and controls (Figure 3.5, H). These data confirm that implants and miniscopes do not impair normal anxiety-like behaviors.

Lastly, we monitored the behavior of these animals in two social tasks: Sociability and Social Novelty assays. In both tasks, mice explored a chamber with an empty mesh cup at each end of a rectangular arena. In Sociability, one cup was empty and the other housed a littermate; in Social Novelty, each cup housed either a littermate or a novel male

mouse. Wire mesh cups ensured that experimental animals could see and smell the stimulus animals. Implanted mice spent more time with their littermate than an empty cup (Figure 3.5, I, 2.4 fold-change), and more time with the novel mouse than the littermate (Figure 3.5, J, 1.8 fold change). These data suggest that implants and miniscopes did not interfere with the animals' normal interest in socialization and preference for novel social stimuli. These behavioral patterns match the expectation for social behavior of a normal, healthy animal (Moy et al., 2004). Taken together, all of these behavioral data suggest that that our experimental manipulations did not induce changes in locomotion, anxiety-like behavior, or social behaviors. This control experiment allowed us to investigate how VIP^{ACC} activity changes during anxiety-related and social behaviors.

3.2.2 Subpopulations of VIP^{ACC} Preferentially Encode Either Open or Closed Arms of the Elevated Zero Maze

To determine whether VIP^{ACC} encode anxiety-related information and whether they are a heterogeneous population, we imaged VIP^{ACC} activity as mice performed behavioral tasks. The elevated zero maze (EZM) was used to quantify anxiety-like behavior – closed arms are anxiolytic and open arms are anxiogenic (Figure 3.5, F). We monitored Ca^{2+} dynamics while animals navigated the EZM to determine whether exploration of anxiogenic areas altered VIP^{ACC} activity. We hypothesized that some subpopulations of VIP^{ACC} would activate to anxiolytic zones, others to anxiogenic zones, and still others would remain neutral. To test this, we extracted Ca^{2+} traces (Figure 3.2) and performed ROC analysis on each VIP^{ACC} as previously described (Li et al., 2017)

(Figure 3.6, B). This analysis provides us with auROC values, which quantify how well each cell's activity matches a behavioral state; values near 0.5 are expected for cells that do not encode behavioral states and higher auROCs reflect better encoding of this information. For each neuron, we calculated an auROC for the closed arms and an auROC for the open arms (Figure 3.6, B).

We identified individual VIP^{ACC} that demonstrated selectively increased activity in one arm type and classified them as open-selective (21%), closed-selective (11%), or neutral (which were not selective for either stimulus, 68%) (Figure 3.6, A-E). When these data were shuffled 1000 times as a control, 5% of cells were selective for each stimulus (data not shown), suggesting that the percentage of selective cells identified was unlikely to occur entirely by chance. The activity of individual selective cells better encoded anxiolytic states, as compared to neutral cells (Figure 3.6, B, F-H). Closed-selective cells showed increased activity while animals were in the closed, as compared to the open arms (Figure 3.6, D, top), whereas open-selective cells showed the opposite effect (Figure 3.6, D, bottom). When the activity of all closed-selective cells was averaged across mice, they were more active in the closed arm than the open (approximately 58% increase, Figure 3.6, F). Open-selective cells were preferentially active in the open arm, as compared to the closed (approximately 60% increase, Figure 3.6, G) and neutral cells did not differ across zones (Figure 3.6, E, H). The majority of auROC values were near 0.5 for both zones (Figure 3.6, J-K), suggesting that most VIP^{ACC} were neutral and did not preferentially activate to a specific context. These data suggest that we can identify

subpopulations of VIP^{ACC} that activate preferentially to either anxiogenic or anxiolytic contexts and that this cell type is functionally heterogeneous in the EZM.

To determine whether locomotion impacted VIP^{ACC} activity, we monitored animal velocity. In the EZM, there was no relationship between the animal's velocity and VIP^{ACC} activity (Figure 3.6, I), which suggests that activity differences in the EZM cannot be explained by changes in the animal's locomotion and may reflect the animal's anxiogenic state. These data suggest that our selectivity classifications accurately reflect the relationship between VIP^{ACC} activity and anxiety-related behaviors.

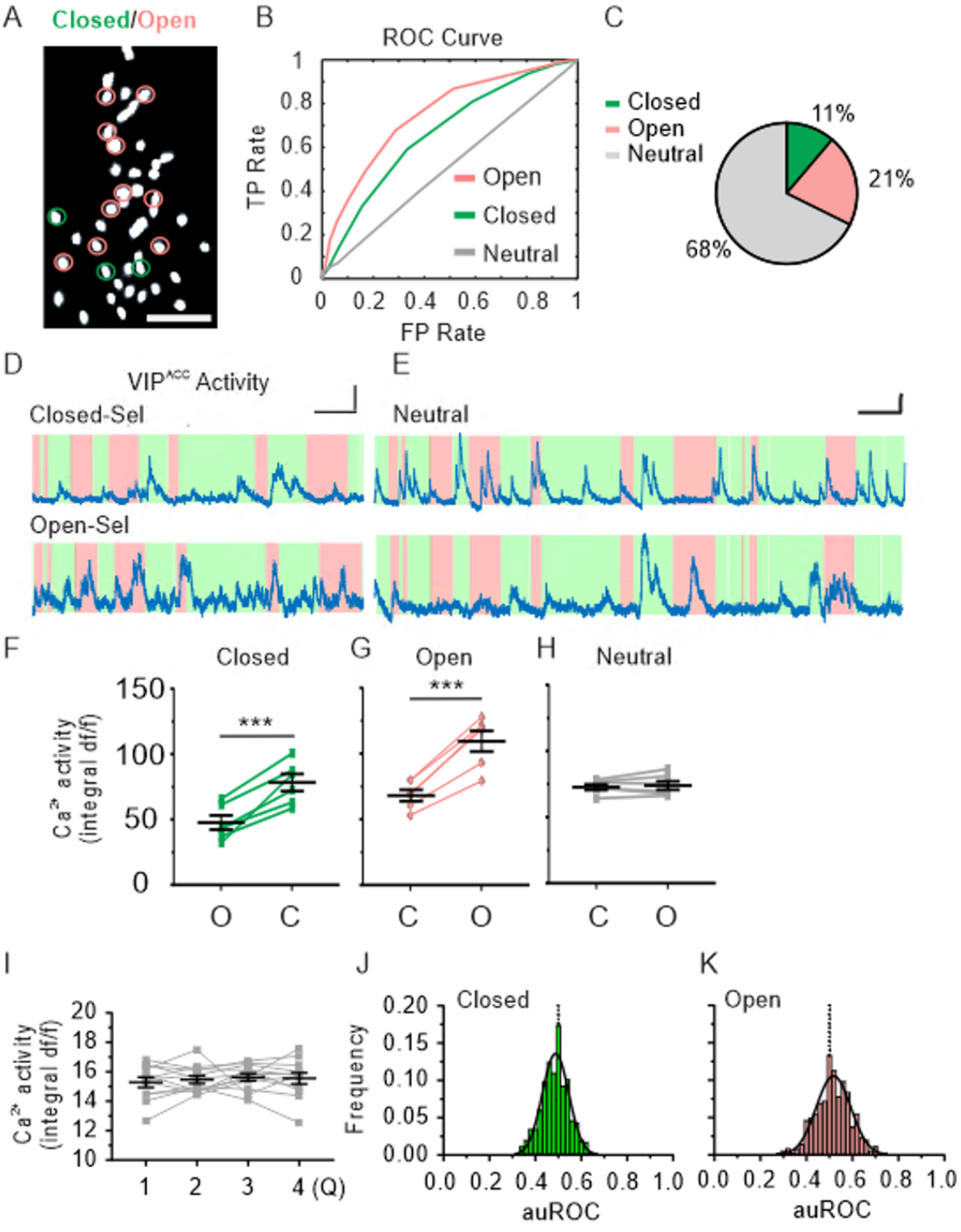
A
Closed/Open
B
ROC Curve
TP Rate
FP Rate
Open
Closed
Neutral
C
Closed
Open
Neutral
11%
21%
68%
D
VIP^Acc Activity
Closed-Sel
Open-Sel
E
Neutral
F
Closed
G
Open
H
Neutral
Ca2+ activity (integral df/f)
***
O
C
I
J
K
Closed
Open
Frequency
auROC
4 (Q)

Figure 3.6: Distinct VIP^{ACC} interneurons can be classified as open- or closed-arm specific in the EZM. preferentially encode anxiogenic or anxiolytic contexts in the EZM. (A) VIP^{ACC} expressing GCaMP6f (white) in vivo while mouse navigates the open and closed arms of the EZM. Pink circles: open-selective, green circles: closed-selective. Neutral cells are not circled. Scale bar = 100 μm. (B) Representative ROC curves demonstrating how well cells encode behavioral states for an open-selective cell (pink, auROC = 0.75), a closed-selective cell (green, auROC = 0.66), and a neutral cell (gray, auROC = 0.51). (C) 21% of VIP^{ACC} were classified as open-selective, 11% as closed-selective, and 68% as neutral. (D) Representative example Ca^{2+} transients from a closed-selective cell (top) and an open-selective cell (bottom). Shaded areas indicate the location of the mouse in either the open (pink) or closed (green) arms of the EZM. Scale bar = 25 s and 2 SD. (E) Ca^{2+} traces of representative neutral cells in the EZM. Location of mouse: open (pink) or closed (green) zones. Top: auROC = 0.51 for closed, 0.51 for open. Bottom: auROC = 0.49 for closed, 0.51 for open. Scale bar = 2 SD and 25 s. (F-H) Ca^{2+} activity of selective VIP^{ACC} in the open (O) versus closed (C) arms of the EZM. Graphs show activity of the closed-selective cells (F, $^{**}p$=0.0016), the open-selective cells (G, $^{***}p$=0.0002), and the neutral cells (H, p=0.5239). (I) Ca^{2+} activity does not differ across 4 quartiles of animal velocity in the EZM. Repeated measures ANOVA with Tukey's test. All quartile comparisons $p > 0.05$. (J-K) Frequency distributions for auROC values for all cells in the EZM for closed (J) or open (K) arms. Black curves are Gaussian fits. (J) Closed arms. Gaussian fit: Amplitude = 0.14, Mean = 0.49, SD = 0.06. (K) Open arms. Gaussian fit: Amplitude = 0.11, Mean = 0.52, SD = 0.07. N = 6 mice, n = 345 cells. All statistics performed with Paired t-tests unless otherwise noted. Ca^{2+} activity refers to the area under the curve (integral df/f). All ROC curves, traces, and images are representative. Each replicate in E-G represents one mouse. Closed-sel: closed selective, Open-sel: open-selective, df/f: Deltaf/f. Note: Surgeries and behavioral testing performed by William Yen. Data analyzed by Lisa Kretsge, Connor Johnson, Alexandra O'Connor, and Alberto Cruz-Martín. Figure made by Lisa Kretsge, Connor Johnson and Alberto Cruz-Martín. Figure published in Johnson, Kretsge & Yen et al., *BioRxiv*, 2020.

3.2.3 Distinct Subgroups of VIP^{ACC} Preferentially Encode Either Center or Periphery Zones of the Open Field

We next assessed whether these effects were context-specific, or they could also be identified in a second task of anxiety-like behavior. Similar to our findings in the EZM, we found that mice in the open field (OF) avoided the anxiogenic center zone

(Figure 3.5, B) and we identified zone-specific cells that encoded the animal's behavioral state (Figure 3.7, A-G). Using ROC analysis, we identified center- and periphery-selective cells and demonstrated that their Ca^{2+} activity better encoded whether the animal was exploring the anxiolytic or anxiogenic zones than neutral cells did (Figure 3.7, H-J). Periphery-selective cells showed increased activity while animals were in the periphery, as compared to the center (Figure 3.7, D, F, and H). Center-selective cells showed increased activity when animals were in the center, as compared to the periphery (Figure 3.7, E, G, and I). These differences were consistent when we averaged the activity of all periphery- (Figure 3.7, H) or center-selective (Figure 3.7, I) cells and when we examined transients of individual selective neurons (Figure 3.7, F and G). As in the EZM data (Figure 3.6, J-K), most auROC values were near 0.5 for both zones (Figure 3.7, K-L), suggesting that most VIP^{ACC} were neutral. Neutral cells showed no change in their activity when the mouse was in the center versus the periphery (Figure 3.7, J and M). These data show that functional heterogeneity of VIP^{ACC} is not unique to the EZM but is a feature of VIP^{ACC} activity across different anxiety-like behavioral assays.

In contrast to the EZM data (Figure 3.6, I), in the OF there was a relationship between the animal's velocity and VIP^{ACC} activity (Figure 3.6, N). In the OF, overall VIP^{ACC} activity was higher when the animal's velocity was faster (Figure 3.6, N). For this reason, we focused the following analysis primarily on the EZM. In the EZM data, we can avoid this potential confound and ensure our selectivity data accurately reflect the relationship between VIP^{ACC} activity and anxiety-related behaviors.

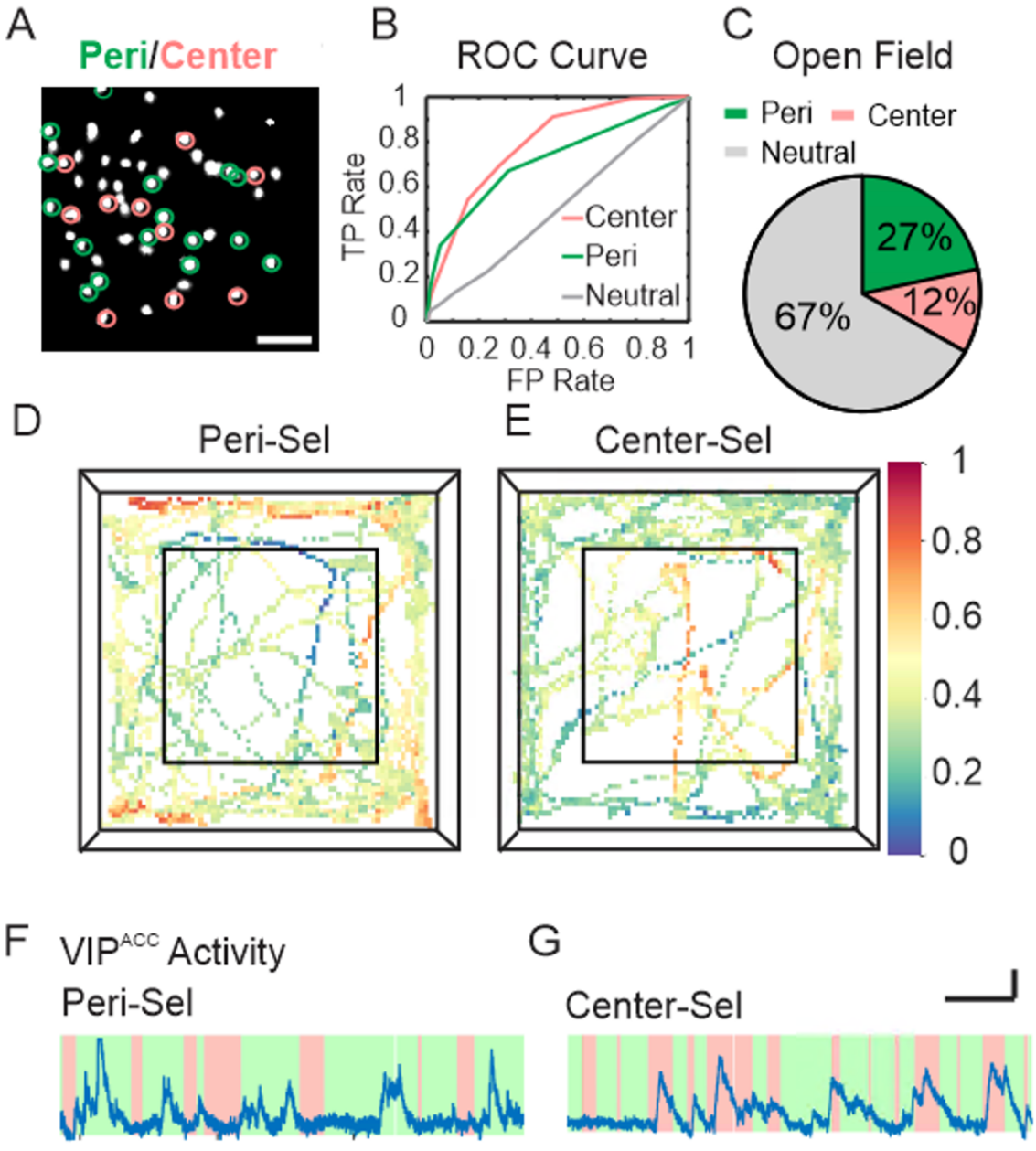
A
Peri/Center
B
ROC Curve
TP Rate
FP Rate
Center
Peri
Neutral
C
Open Field
Peri
Center
Neutral
27%
12%
67%
D
Peri-Sel
E
Center-Sel
1
0.8
0.6
0.4
0.2
0
F
VIP^ACC Activity
Peri-Sel
G
Center-Sel

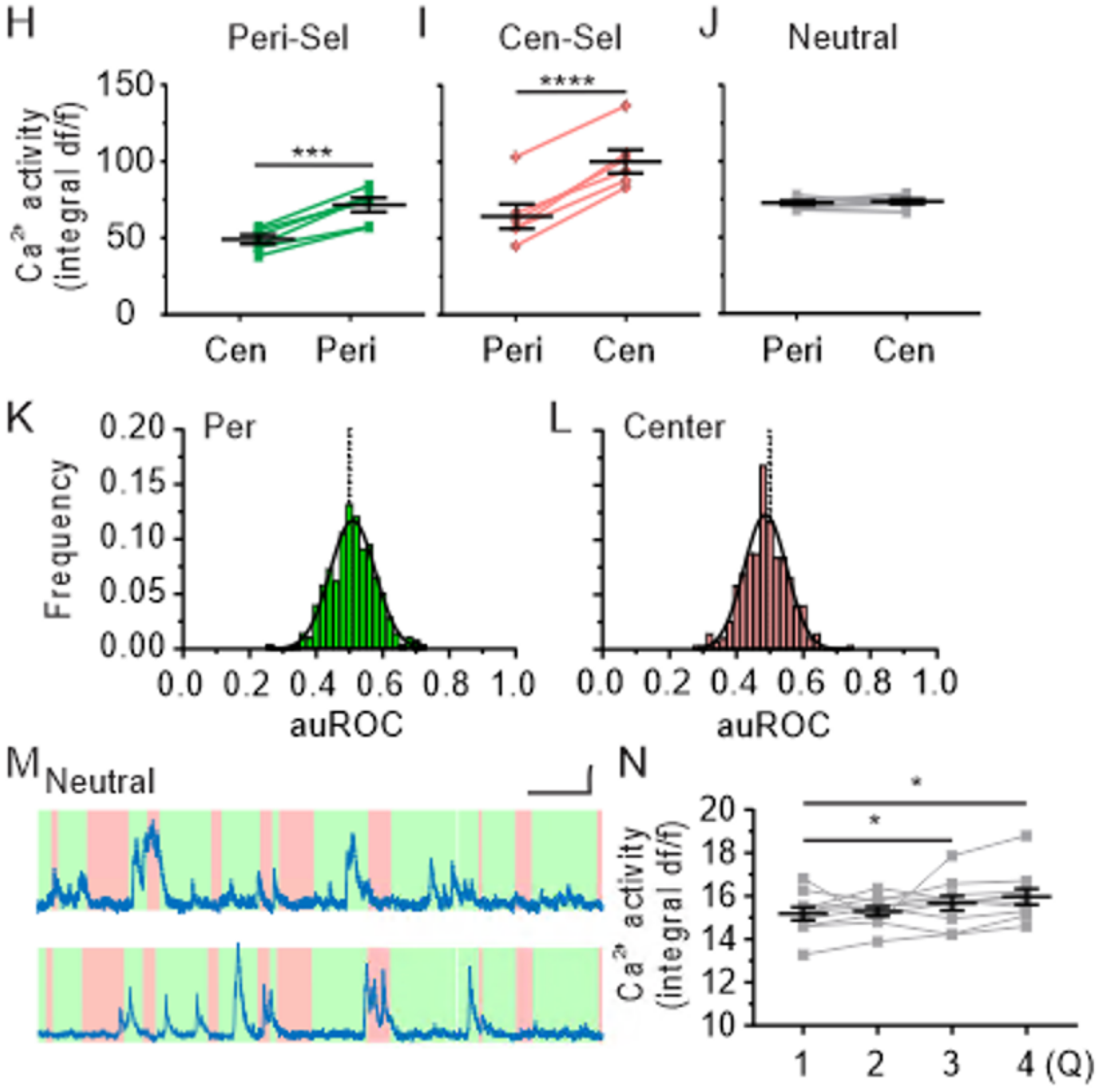
H
Peri-Sel
I
Cen-Sel
J
Neutral
Ca2+ activity (integral df/f)
150
100
50
0
***
****
Cen
Peri
Peri
Cen
Peri
Cen
K
Per
L
Center
Frequency
0.20
0.15
0.10
0.05
0.00
0.0 0.2 0.4 0.6 0.8 1.0
auROC
0.0 0.2 0.4 0.6 0.8 1.0
auROC
M
Neutral
N
*
*
Ca2+ activity (integral df/f)
20
18
16
14
12
10
1
2
3
4 (Q)

Figure 3.7: Subpopulations of VIP^{ACC} preferentially activate to the center or the periphery of the OF. (A) Image of VIP^{ACC} expressing GCaMP6f (white) in vivo. Pink circles: center-selective, green circles: periphery-selective. Neutral cells are not circled. Scale bar = 100 μm. (B) Representative ROC curves for a center-selective (pink, auROC = 0.79), a periphery-selective (green, auROC = 0.72), and a neutral (gray, auROC = 0.50) cell. (C) 12% of VIP^{ACC} were classified as center-selective, 27% as periphery-selective, and 67% as neutral. (D-E) Heatmaps of selective VIP^{ACC} activity normalized to peak activity while mice explore the OF for periphery- (D) or center-selective (E) cells. Inner black line: border between center and periphery. Warmer colors represent greater neural activity than cooler colors. (F-G) Representative examples of Ca^{2+} transients of a periphery-selective (F) and a center-selective (G) cell. Shaded areas represent the animal's location in either the center (pink) or the periphery (green). Scale bar = 25 s and 2 SD. (H-J) Ca^{2+} activity of selective cells in the center (Cen) versus periphery (Peri) of the OF. (H) Periphery-selective cells, ***p=0.0005. (I) Center-selective cells, ****p<0.0001. (J) Neutral cells, p=0.8996. (K-L) Frequency distributions for auROC values all cells in the OF for periphery (K) or center (L). Black curves are Gaussian fits. (K) Periphery-selective. Gaussian fit: Amplitude = 0.12, Mean = 0.51, SD = 0.07. (L) Center-selective. Gaussian fit: Amplitude = 0.12, Mean = 0.49, SD = 0.06. (M) Ca^{2+} traces of 2 representative neutral cells in the OF. Location of mouse: center (pink) or periphery (green). Top cell: auROC = 0.52 for periphery, 0.48 for center. Bottom cell: auROC = 0.47 for periphery, 0.53 for center. (N) Ca^{2+} activity across 4 quartiles of velocity in the OF. Repeated measures ANOVA with Tukey's test. Q1 vs Q3. *p=0.0382. Q1 vs Q4. *p=0.0271. Scale bar = 2 SD and 25 s. N = 6 mice, n = 273 cells. All ROC curves, traces, and images are representative. Each replicate in H-J represents one mouse. All statistics performed with Paired t-test. Per: periphery, Cen: center, df/f: Deltaf/f. Note: Surgeries and behavioral experiments performed by William Yen. Heatmaps made by Sky Ruichen Liu. Data analyzed by Lisa Kretsge, Connor Johnson, Alexandra O'Connor, and Alberto Cruz-Martín. Figure made by Lisa Kretsge, Connor Johnson, Sky Ruichen Liu, and Alberto Cruz-Martín. Figure published in Johnson, Kretsge & Yen et al., *BioRxiv*, 2020.

3.2.4 The Activity of Stimulus-selective Cells Changes Markedly at Behavioral Transitions in the Elevated Zero Maze

To determine how selective VIP^{ACC} activity changes in anxiolytic or anxiogenic contexts, we isolated trials when animals transitioned from one arm to the other and plotted VIP^{ACC} activity (Figure 3.8). Heatmaps and Ca^{2+} activity showed robust

differences during behavioral transitions (Figure 3.8, C-J). Closed-selective cells preferentially activated soon after animals entered the closed arms (27% increase, Figure 3.8, C and G) or prior to entering the open arms (45% increase, Figure 3.8, D and H). Open-selective cells were preferentially active soon after animals transitioned into the open arms (22% increase, Figure 3.8, E and I) or before leaving the closed arms (44% increase, Figure 3.8, F and J). These data suggest that VIP^{ACC} that are selective for different stimuli show opposite patterns of activation during behavioral transitions and that changes in the activity of selective cells can be sustained while the animal remains in a given environment. Differences in the magnitude of the data in Figure 3.8, C-F as compared to G-J may be because the values are averages for G-J are from all selective cells in one animal, rather than for individual neurons normalized to the peak activity of each cell (as in C-F). In addition, the heatmaps show activity in 20 s window around behavioral transitions (Figure 3.8, C-F), rather than a 10 s window (Figure 3.8, G-J).

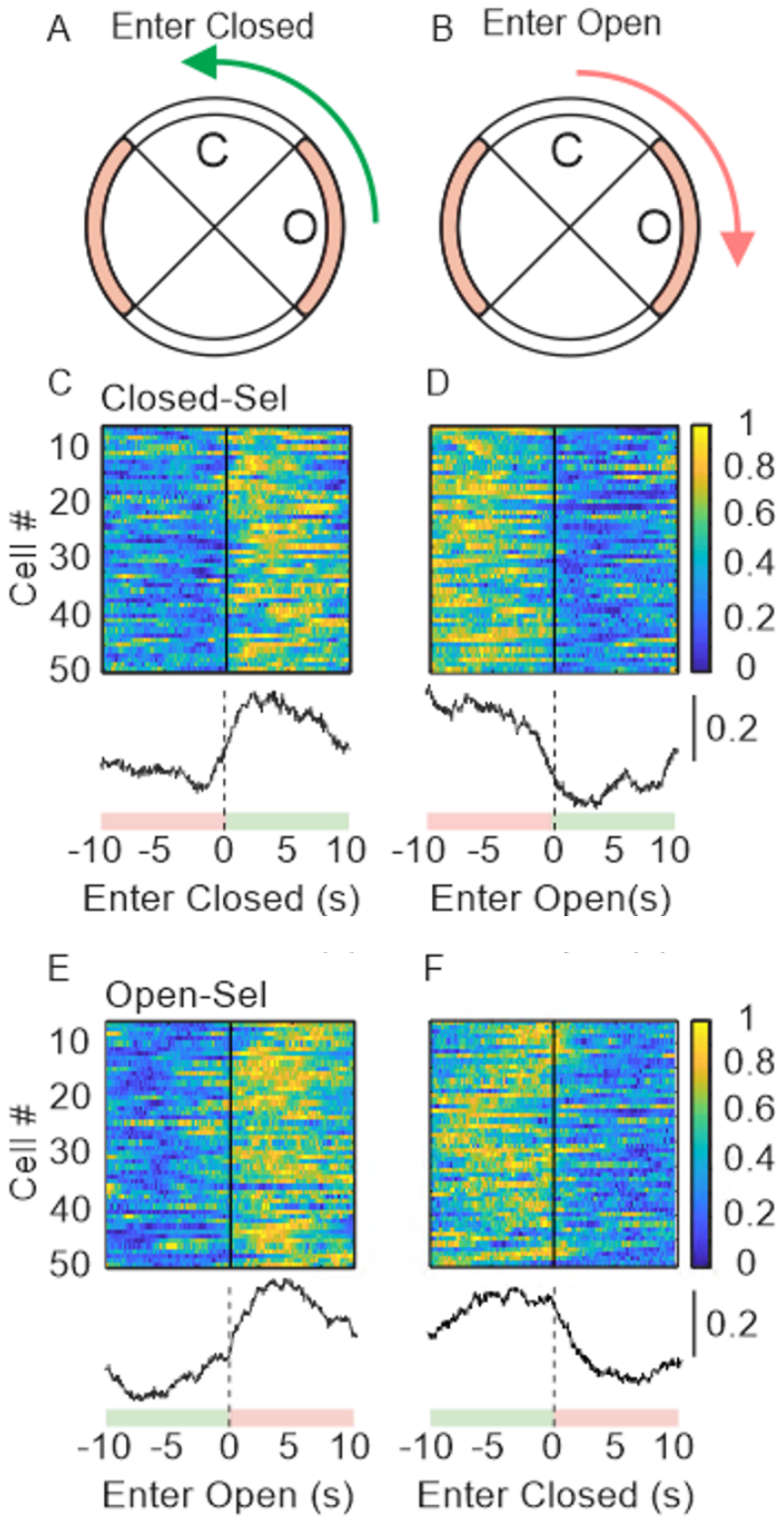
A
Enter Closed
C
O
B
Enter Open
C
O
C
Closed-Sel
Cell #
10
20
30
40
50
-10 -5 0 5 10
Enter Closed (s)
D
1
0.8
0.6
0.4
0.2
0
0.2
-10 -5 0 5 10
Enter Open(s)
E
Open-Sel
Cell #
10
20
30
40
50
-10 -5 0 5 10
Enter Open (s)
F
1
0.8
0.6
0.4
0.2
0
0.2
-10 -5 0 5 10
Enter Closed (s)

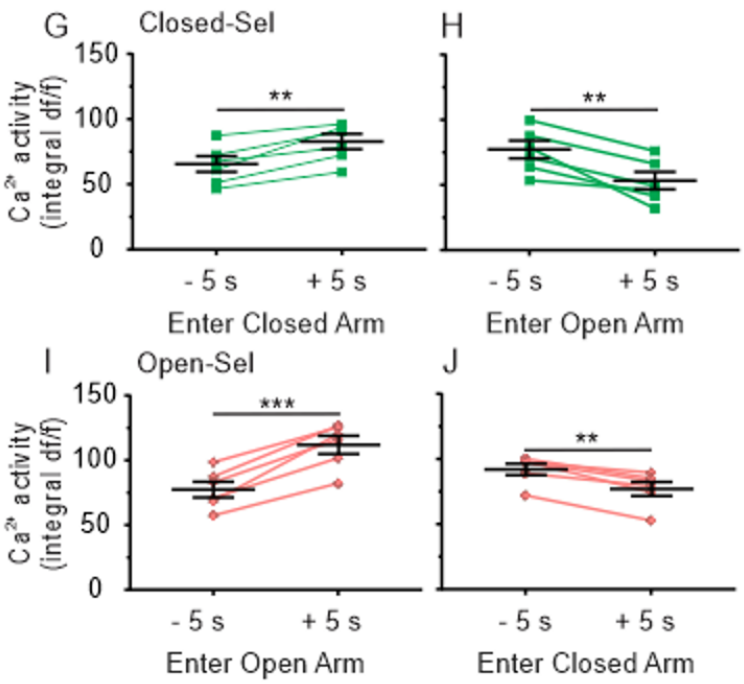

Figure 3.8: Stimulus-selective cells show significantly different Ca2+ activity before and after transitions between EZM arm types. (A-B) Behavioral transitions: movement of a mouse from an open to a closed arm (left) or a closed to an open arm (right) of the EZM. (C-F) Heatmaps (top) show activity of 50 individual selective cells during behavioral transitions. Each colored row represents one neuron's activity and each cell's data is normalized to the peak activity of that neuron. Warmer colors indicate more activity relative to cooler colors. Traces (bottom) show averaged normalized activity from all selective cells during these transitions. (C-D) Activity of closed-selective cells from 10 s prior to 10 s after entering either a closed (C) or an open (D) arm. (E-F) Activity of open-selective cells from 10 s prior to 10 s after entering either an open (E) or closed (F) arm. (G-J) Average Ca^{2+} activity of all stimulus-selective cells during arm-type transitions. -5 vs. +5 s. (G) Closed-selective cells as the animals were entering the closed arms. $^{**}p$=0.0046. (H) Closed-selective cells as the animals were entering the open arms. $^{**}p$=0.0056. (I) Open-selective cells as the animals were entering the open arms. $^{***}p$=0.0004. (J) Open-selective cells as the animals were entering the closed arms. $^{**}p$=0.0015. N = 6 mice, n = 345 cells. All statistics performed with Paired t-tests. Ca^{2+} activity refers to the area under the curve (integral df/f). Each replicate in F-I represents one mouse. C: closed arm, O: open arm, Closed-sel: closed selective, Open-sel: open-selective, df/f: Deltaf/f. Note: Behavioral experiments performed by Lisa Kretsge and William Yen. Data analyzed by Lisa Kretsge, Connor Johnson, and Alexandra O'Connor. Figure made by Lisa Kretsge and Alberto Cruz-Martín. Figure published in Johnson, Kretsge & Yen et al., *BioRxiv*, 2020.

3.2.5 Whole Population Activity of VIP^{ACC} Does not Differ Across Anxiogenic or Anxiolytic Zones of the Open Field or Elevated Zero Maze

Despite differences in behavior and the activity of individual neurons, there was no difference in the average activity of all VIP^{ACC} as mice explored different zones of the EZM or OF (Figure 3.9), which suggests that VIP^{ACC} do not uniformly activate in anxiogenic or anxiolytic contexts. Therefore, despite prior research linking changes in whole ACC activity to differences in anxiety-related behaviors (Weible et al., 2017; Kim et al., 2011), VIP^{ACC} do not uniformly activate in anxiogenic or anxiolytic contexts. Overall, these results support our hypothesis that VIP^{ACC} are a heterogeneous population, where some subpopulations preferentially activate in anxiolytic contexts and others in anxiogenic contexts.

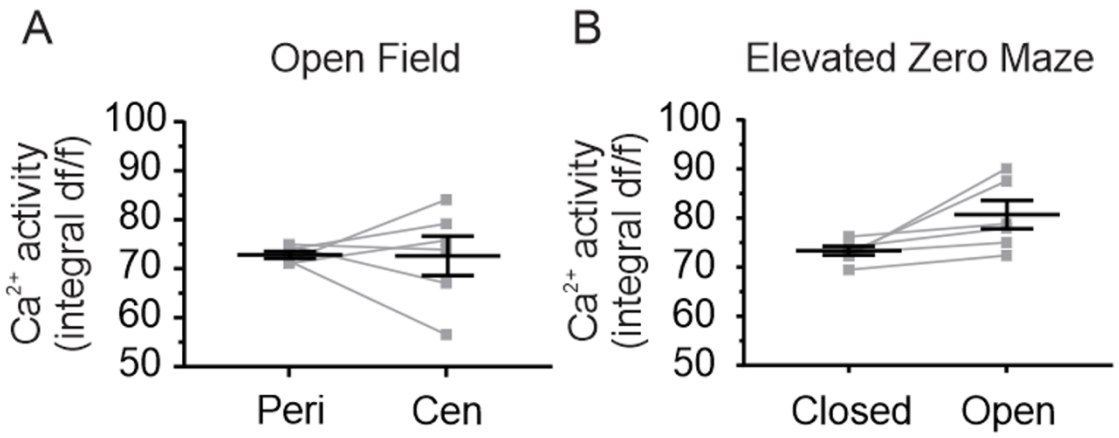

Figure 3.9: Whole populations of VIP^{ACC} do not uniformly activate in anxiolytic or anxiogenic contexts. (A-B) Ca^{2+} activity of all VIP^{ACC} per animal anxiolytic versus anxiogenic zones. Population-level Ca^{2+} activity does not differ between the periphery (Peri) and center (Cen) of the OF (A, p=0.9575) or between the closed and open arms of the EZM (B, p=0.0510). Note: Behavioral and imaging experiments performed by William Yen. Data analyzed by Lisa Kretsge, Connor Johnson, and Alexandra O'Connor. Figure made by Alberto Cruz-Martín. Figure published in Johnson, Kretsge & Yen et al., *BioRxiv*, 2020.

3.2.6 Cell-selectivity Identification Method was Validated for Elevated Zero Maze

We verified that this analysis method was reliable by using half of our data to identify selective cells and using those classifications to perform Ca^{2+} activity analysis on the remaining half of the data (Figure 3.10, A). In this second half of the data, activity of selective cells increased when mice were in the preferred context, relative to the non-preferred (Figure 3.10, B). Differences in the magnitude of this change, as compared to the data in Figure 3.6, F-G are likely becuase these data include both closed- and open-selective cells in one dataset (preferred vs. non-preferred, rather than closed versus open, for example). The direction of this change is consistent with Figure 3.6, however. This suggests that this auROC method was accurately identifying cells that encoded one arm type.

In addition, we performed random circular shuffling of closed- (Figure 3.10, C) or open-selective (Figure 3.10, D) cells to determine whether cells with these activity profiles could be identified as selective by chance. In our real (un-shuffled) data, 12-27% of VIP^{ACC} were selective for each arm type (Figure 3.7, C). After shuffling, the percentage of selective cells that still were identified as stimulus-selective was much

lower (about 5% of all cells), suggesting it is unlikely that our ROC analysis identified all of the cells in our analyses as selective by chance alone. In our real datasets, heatmaps revealed stark changes in activity of selective cells at behavioral transitions between arm types (Figure 3.8, C-F). When these data were shuffled, however, their heatmaps showed no clear pattern of activation at behavioral transitions (Figure 3.10, C-D). This suggests that our real data reflect activity changes that correspond with the animal's behavior, rather than a random alignment. Together these data provide evidence that ROC analysis accurately identified stimulus-selective cells in the EZM and VIP^{ACC} were not designated as stimulus-selective by chance alone.

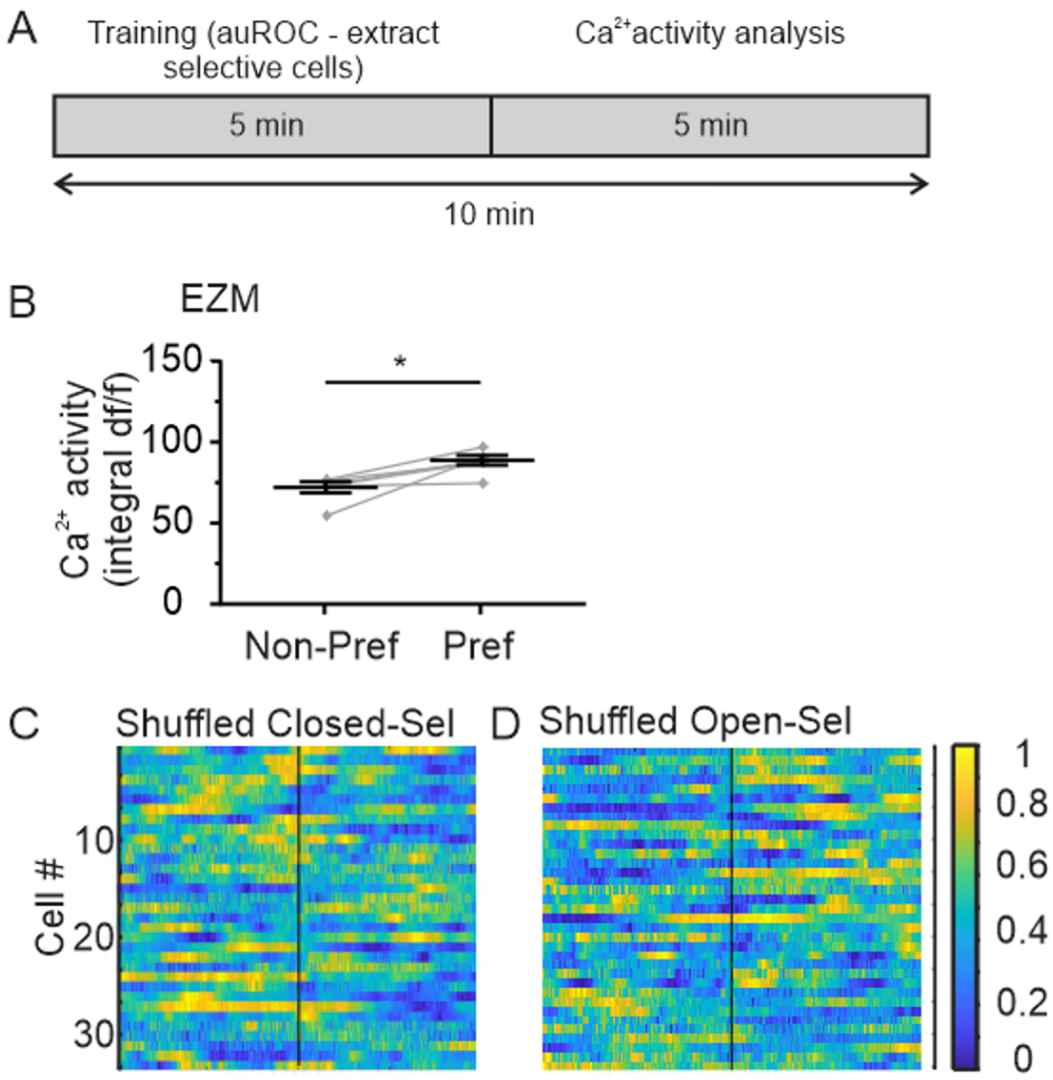
A
Training (auROC - extract selective cells)
Ca2+activity analysis
5 min
5 min
10 min
B
EZM
Ca2+ activity (integral df/f)
150
100
50
0
*
Non-Pref
Pref
C
Shuffled Closed-Sel
D
Shuffled Open-Sel
Cell #
10
20
30
1
0.8
0.6
0.4
0.2
0

Figure 3.10: Validation of VIP^{ACC} activity analysis. (A) Schematic explaining how this analysis was validated. (B) Grouped data for EZM. Cells identified as selective for one arm type using the first half of the data showed more activity in the second half of the data when the animal was in the preferred arm type. *p=0.0166. N = 6 mice, n = 345 cells. Each replicate represents the average data for one mouse. All statistics performed with Paired t-test. (C-D) Heatmaps show activity of individual selective cells during behavioral transitions. Each colored row represents one neuron's activity. Warmer colors indicate more activity relative to cooler colors. (C) Activity of shuffled closed-selective cells from 10 s prior to 10 s after entering a closed arm. (D) Activity of shuffled open-selective cells from 10 s prior to 10 s after entering an open arm. Non-pref: non-preferred, Pref: preferred, df/f: Deltaf/f. Note: Behavioral and imaging experiments performed by William Yen. Data analyzed by Lisa Kretsge, Connor Johnson, and Alexandra O'Connor. Figure made by Connor Johnson and Alberto Cruz-Martín. Figure published in Johnson, Kretsge & Yen et al., *BioRxiv*, 2020.

3.3 Conclusion and Future Directions

These results support our hypothesis that VIP^{ACC} are a heterogeneous population, where subpopulations encode different anxiety-related environments. While it may be expected from previous work that many cells in the ACC would activate in an anxiety-related manner, interestingly our data show that some VIP^{ACC} activate preferentially to opposite EZM arm types and others remain neutral throughout this task. This work underscores the importance of using cellular resolution to uncover functional heterogeneity within this population. This work also demonstrates that our methodologies can be used to monitor and quantify the activity of VIP^{ACC} in vivo with cellular resolution and detachable miniscopes.

We determined that subgroups of VIP^{ACC} preferentially activate in anxiolytic contexts, others in anxiogenic environments, and still others are neutral in anxiety-related tasks. Stimulus-selective cells in the EZM showed dramatic changes in activity during

behavioral transitions between environments. Despite these clear relationships between individual VIP^{ACC} and anxiety-related stimuli, when the all VIP^{ACC} were assessed as one population, these effects disappeared: overall VIP^{ACC} activity does not differ as animals navigate anxiety-related assays. These data are the first to demonstrate a role for VIP^{ACC} in encoding anxiety-related information and to show that VIP^{ACC} activity is not homogenously activated or suppressed in anxiogenic or anxiolytic environments.

Future studies could investigate possible heterogeneity in the neurons up or downstream of VIP^{ACC}, including other neuronal subtypes within the ACC (Pyr, PV, SOM) or in brain regions like AM or RS that are known to project to the ACC. VIP interneurons in the ACC may recruit subpopulations of Pyr (Karnani et al., 2016; Pi et al., 2013) that are behaviorally relevant or encode specific information. For example, anxiogenic-selective VIP cells may correspond with a similar subpopulation of anxiogenic-selective Pyr cells in the ACC. Investigating these different cell types with cellular resolution would further explain how the ACC encodes anxiety-related information throughout the local microcircuit. More broadly, it could determine whether different cortical subtypes show similar functional heterogeneity and elucidate how the cortex uses these different parts of the microcircuit to encode diverse behavioral information.

In addition, our work showed no relationship between animal velocity and VIP^{ACC} activity in the EZM, although increased activity corresponded with increased velocity in the OF. Prior work has shown that VIP cells in the visual cortex demonstrated increased activity when animals were running, as compared to reminaing stationary (Fu et al.,

2014). These data may relate to our findings in the OF, but the lack of effect in the EZM may suggest differences in velocity-related encoding across brain regions. Alternatively, differences may arise because our studies monitor freely behaving mice, where Fu et al. (2014) performed experiments in head-fixed animals.

We set a strict threshold we for classifying a cell as selective, so some cells designated as neutral may still carry some stimulus-related information. In addition, VIP^{ACC} selectivity in the EZM may be more complex than simply encoding for anxiety-related information. For example, an open-selective cell may not encode the aversiveness of the environment, but other sensorimotor or affective features that are relevant during the behavior. If VIP^{ACC} encoding varies in this way, that could contribute to differences in our findings between anxiogenic arenas. Future work should address this and the outstanding question of whether VIP^{ACC} stimulus-selectivity is correlational or whether their activity is sufficient to drive changes in anxiety-related behaviors. Targeting the activity of anxiogenic-specific VIP^{ACC} could provide a therapeutic intervention for anxiety disorders. One way to address this question would be to use advanced genetic tools that allow researchers to selectively express proteins for optogenetic manipulation in cells that were active during a specific time frame (Reijmers et al., 2007; Ramirez, Tonegawa, & Liu, 2014). For example, this experimental design could be used by allowing for optogenetic control of neurons that activated while the animal was in an anxiogenic environment. Utilized in a VIP-Cre mouse line, this could allow researchers to specifically optogenetically inhibit the activity of VIP^{ACC} that activated in an anxiogenic environment and determine whether that is sufficient to diminish anxiety-like behaviors. Overall, the

work presented here shows that VIP^{ACC} are functionally heterogeneous, where subpopulations encode either anxiogenic or anxiolytic stimuli.

CHAPTER FOUR

Activation of Distinct VIP^{ACC} Cells During Social and Non-social Behaviors

4.1 Introduction

In addition to its role in anxiety, the ACC has been implicated in social and cognitive tasks (Di Martino et al., 2009; Rudebeck et al., 2006; Nelson et al., 2015; Guo et al., 2019; Krabbe et al., 2019; Weible et al., 2009; Weible et al., 2012). Nonetheless, a circuit-level understanding of social dysfunction, normal social behavior, and the role of ACC cells in cognition is still lacking. Recent work in rodents has provided some insight into prefrontal cortical function in social behavior by monitoring the activity of excitatory Pyr neurons (Guo et al., 2019; Liang et al., 2018). Excitatory cells in the ACC were found to be more active during socialization and optogenetic stimulation of these cells increased social behaviors (Guo et al., 2019). This study was limited, however, by techniques that lacked cellular resolution, so they could not investigate whether all ACC Pyr cells activate similarly or if distinct subgroups activate to different kinds of stimuli. In addition to social tasks, some ACC neurons have been shown to increase or decrease their activity during interactions with non-social stimuli, like objects (Weible et al., 2012; Weible et al., 2009). Significant changes in activity were found for some ACC neurons during interactions with familiar objects and with novel objects (Weible et al., 2012; Weible et al., 2009).

Using miniscopes and Ca^{2+} imaging of Pyr in the mPFC, recent evidence demonstrates functional heterogeneity of this population during social tasks (Liang et al.,

2018). In tasks used to assay sociability and social novelty, subpopulations of mPFC Pyr activate preferentially to social stimuli, and some are specific to novel or familiar social stimuli (Liang et al., 2018). Similarly, electrophysiological data in ACC neurons has shown heterogeneous responses to interactions with objects (Weible et al., 2012; Weible et al., 2009). While these data provide strong evidence of some cortical functional heterogeneity in encoding social and non-social behaviors, it is unclear whether this heterogeneity occurs in inhibitory cell populations within the ACC. The role of VIP^{ACC} neurons in social and cognitive behaviors has not been investigated.

The following work aimed to determine whether heterogeneity of VIP^{ACC} activity is specific to anxiety-related behaviors or whether it is a feature of how VIP^{ACC} activate across different kinds of behaviors. Using Ca^{2+} imaging and miniscopes during social and cognitive tasks, the following experiments addressed the hypothesis that distinct subpopulations of VIP^{ACC} would activate preferentially to familiar social, novel social, or non-social stimuli.

4.2 Results

4.2.1 Subpopulations of VIP^{ACC} Preferentially Activate to Social or Non-social Stimuli in Two Social Behavioral Tasks

To assay VIP^{ACC} activity during social behaviors, we used a 3-day behavioral paradigm to assess both general sociability and social novelty (Figure 4.1, A). In both Sociability and Social Novelty, animals explored a rectangular arena with one mesh wire cup at each end. On Day 1 (Sociability), one cup housed a littermate (male, VIP-Cre) and

the other was empty. On Days 2 and 3 (Social Novelty), one cup housed a littermate and the other housed an entirely novel male CD-1. The experimental mouse was given 10 minutes to explore the arena and social stimuli. (Figure 4.1, A). We investigated whether individual VIP^{ACC} were selective for social or non-social stimuli by recording their activity as mice interacted with these stimuli over three days (Figure 4.1).

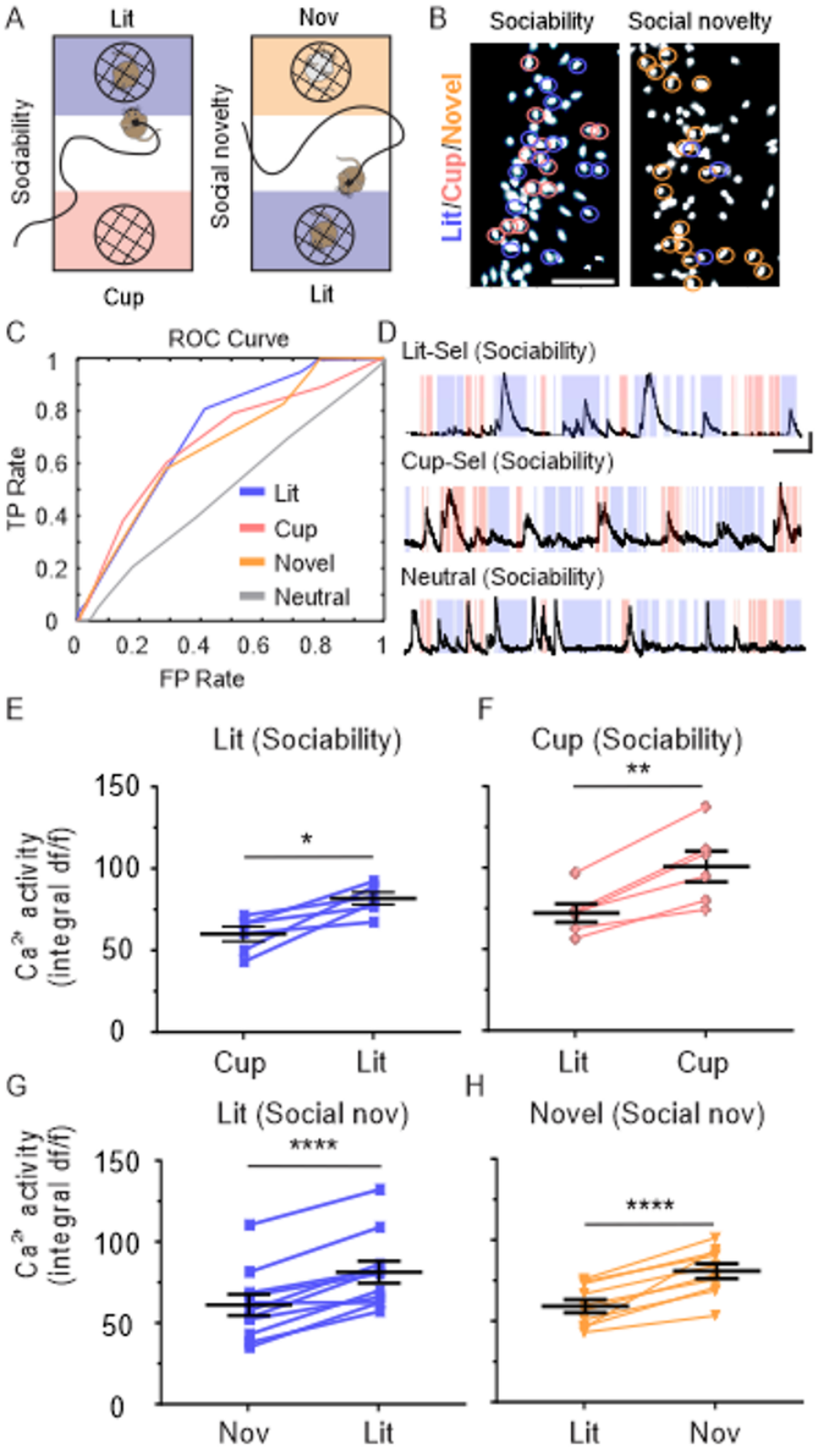
A
Lit
Nov
Sociability
Social novelty
Cup
Lit
B
Sociability
Social novelty
Lit/Cup/Novel
C
ROC Curve
TP Rate
FP Rate
Lit
Cup
Novel
Neutral
D
Lit-Sel (Sociability)
Cup-Sel (Sociability)
Neutral (Sociability)
E
Lit (Sociability)
Ca2+ activity (integral df/f)
Cup
Lit
F
Cup (Sociability)
Lit
Cup
G
Lit (Social nov)
Nov
Lit
H
Novel (Social nov)
Lit
Nov

Figure 4.1: Distinct subpopulations of VIP^{ACC} encode social and non-social stimuli. (A) Behavioral paradigm. Left: Sociability (Day 1). Right: Social Novelty (Days 2 and 3). Littermate zone (purple). Empty cup zone (pink). Novel mouse zone (orange). Neutral zone (white). (B) Images of VIP^{ACC} expressing GCaMP6f (white) in vivo during Sociability (left) or Social Novelty (right). Pink circles: cup-selective, purple circles: littermate-selective, orange circles: novel mouse-selective cells. Neutral cells are not circled. Scale bar = 100 μm. (C) Representative ROC curves for a littermate-selective (purple, auROC = 0.72), a novel-mouse-selective (orange, auROC = 0.67), a cup-selective (pink, auROC = 0.69), and a neutral (gray, auROC = 0.51) cell. (D) Representative Ca^{2+} transients from Sociability: littermate-selective cell (top), cup-selective cell (middle), neutral cell (bottom). Shaded areas indicate location of mouse: littermate (purple), cup (pink), and neutral (white) zones. Scale bars = 25 s and 1 SD. (E-H) Average Ca^{2+} activity of selective cells. (E) Littermate-selective cells in Sociability. Littermate vs. cup. *p=0.0132. (F) Empty cup-selective cells in Sociability. Cup vs. littermate. **p=0.0017. (G) Littermate-selective cells in Social Novelty. Littermate vs. novel mouse. ****p<0.0001. (H) Novel-mouse-selective cells in Social Novelty. Littermate vs. novel mouse. ****p<0.0001. N = 6 mice, n = 310 cells for Sociability, n = 350 cells for Social Novelty Day 2, and n = 232 cells for Day 3. All ROC curves, traces, and images are representative. Each replicate in E-H represents one mouse. All statistics performed with Paired t-tests. Lit: littermate, Nov: novel mouse, Lit-sel: littermate-selective cell, Cup-sel: cup-selective cell, Social nov: Social Novelty, df/f: Deltaf/f. Note: Behavioral and imaging experiments performed by William Yen. Data analyzed by Lisa Kretsge, Connor Johnson, Alexandra O'Connor, and Alberto Cruz-Martín. Figure made by Lisa Kretsge, Connor Johnson, and Alberto Cruz-Martín. Figure published in Johnson, Kretsge & Yen et al., *BioRxiv*, 2020.

Using ROC analysis, we identified cup-, littermate-, and novel-mouse-selective cells and demonstrated that they better encode behavior states than neutral cells (Figure 4.1 B-H, Figure 4.2 E-F). For Sociability, cells were classified as cup-selective (15%), littermate-selective (17%), or neutral (Figure 4.1, B-C). For Social Novelty, cells were classified as littermate-selective (11% Day 2, 20% Day 3), novel mouse-selective (24%, 12%), or neutral (64%, 68%, Figure 4.1, B-C). Data were then shuffled 1000 times as a control and we found that 5% of cells were selective for each stimulus (data not shown),

which suggests the percentages in the real dataset did not occur entirely by chance. Littermate-selective cells showed increased activity while animals interacted with the littermate, as compared to the cup (36% increase, Figure 4.1, E) or novel mouse (33% increase, Figure 4.1, G). Cup-selective VIP^{ACC} were more active when animals interacted with the cup than with the littermate (40% increase, Figure 4.1, F). Novel mouse-selective neurons demonstrated increased activity while mice interacted with novel mice, as compared to the littermates (36% increase, Figure 4.1, H). Similar to the OF and EZM data (Figure 3.6 J-K and Figure 3.7 K-L), most cells (64-68%) were classified as neutral, with auROC values near 0.5 for each stimulus (Figure 4.2 A-D, Figure 4.3). The activity of neutral cells did not change as mice interacted with various stimuli (Figure 4.1, D, bottom, Figure 4.2 E-F). These data demonstrate that VIP^{ACC} functional heterogeneity is not specific to anxiety-related tasks. In addition, they show that some VIP^{ACC} encode social information in sociability and social novelty tasks.

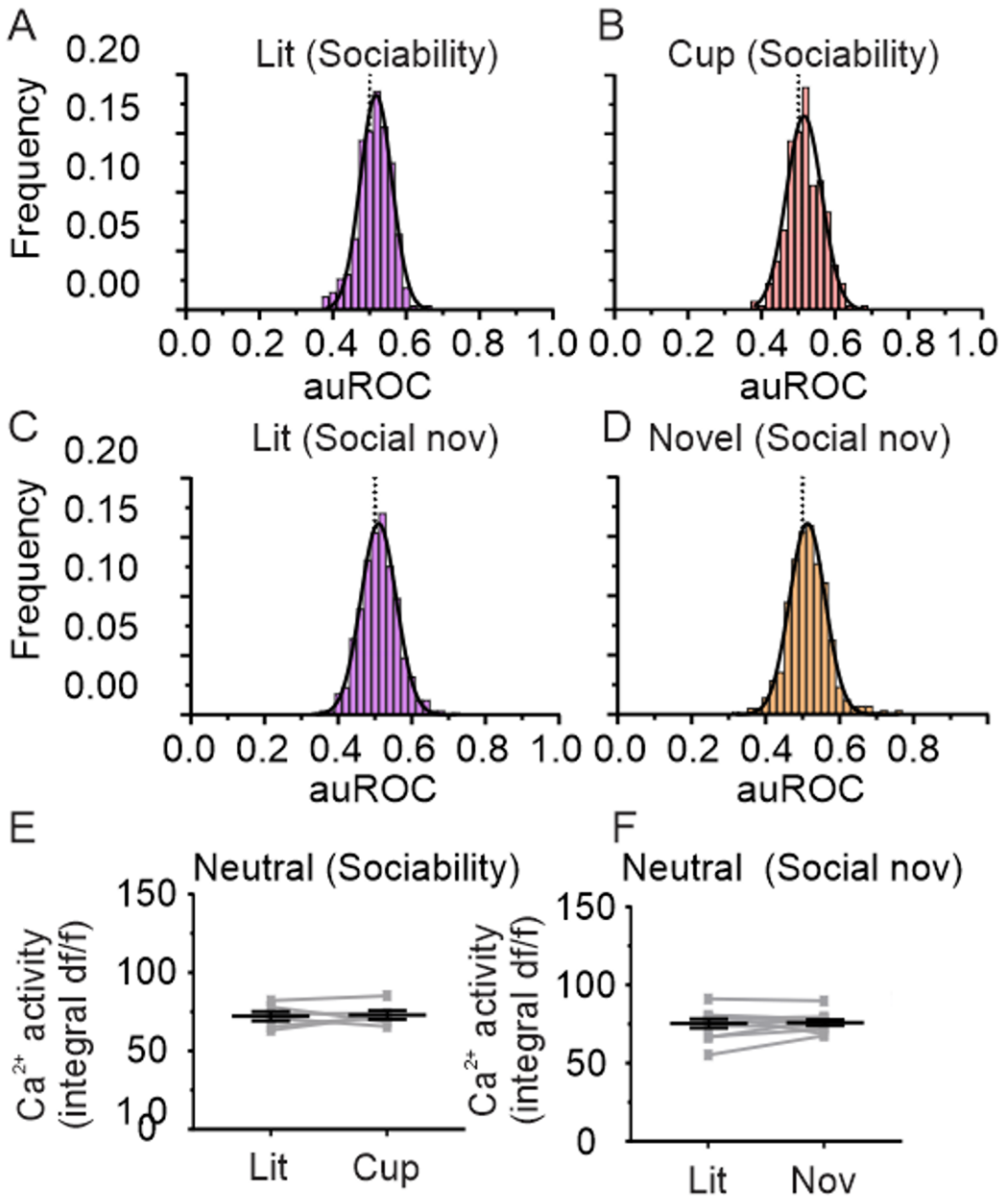
A
Lit (Sociability)
B
Cup (Sociability)
Frequency
0.20
0.15
0.10
0.05
0.00
0.0 0.2 0.4 0.6 0.8 1.0
auROC
C
Lit (Social nov)
D
Novel (Social nov)
E
Neutral (Sociability)
F
Neutral (Social nov)
Ca2+ activity (integral df/f)
150
100
50
0
Lit
Cup
Nov

Figure 4.2: Distribution of selective cells and neutral cells in social tasks. (A-D) Frequency distribution of auROC values in social tasks. Black curves: Gaussian fits. (A) Littermate-selective cells in Sociability. Gaussian fit: Amplitude = 0.18, Mean = 0.52, SD = 0.04. (B) Cup-selective cells in Sociability. Gaussian fit: Amplitude = 0.17, Mean = 0.52, SD = 0.05. (C) Littermate-selective cells in Social Novelty. Gaussian fit: Amplitude = 0.16, Mean = 0.51, SD = 0.05. (D) Novel-mouse-selective cells in Social Novelty. Gaussian fit: Amplitude = 0.16, Mean = 0.51, SD = 0.05. (E) Sociability. Littermate vs. cup. p=0.8026. (F) Social Novelty. Littermate vs. Novel mouse. p=0.7879. Each replicate represents one mouse. N = 6 mice, n = 310 cells for Sociability, n = 350 cells for Social Novelty Day 2, n = 232 cells and Day 3. All statistics performed with Paired t-test. Lit: littermate, Nov: novel mouse, Lit-sel: littermate-selective cell, Cup-sel: cup-selective cell, Social nov: Social Novelty, df/f: Delta f/f. Note: Behavioral and imaging experiments performed by William Yen. Data analyzed by Lisa Kretsge, Connor Johnson, and Alexandra O'Connor. Figure made by Connor Johnson and Alberto Cruz-Martín. Figure published in Johnson, Kretsge & Yen et al., *BioRxiv*, 2020.

4.2.2 Populations of Cells Selective for Different Stimuli in a Social Task are Largely Non-overlapping

To determine whether VIP^{ACC} cells activate preferentially to one or more stimuli in these social tasks, we quantified the percentage of cells that encoded each stimulus. In the EZM and OF datasets, it was impossible for a cell to be classified as both anxiogenic-selective and anxiolytic-selective. Because there were only two regions in these arenas (open or closed/ center or periphery), a cell could not preferentially activate to both zones. If activity was similarly high in both zones, the cell would have been classified as neutral. In the social tasks, however, there are 2 areas surrounding each cup as well as the remaining parts of the arena. This means it is possible for one neuron to be selective for both stimuli in a given social task. We found that very few cells were selective for multiple stimuli within one task (2% in Sociability, 0-1% in Social Novelty) (Figure 4.3).

These data suggest that distinct subpopulations of VIP^{ACC} encode different stimuli and individual VIP^{ACC} rarely activate to multiple stimuli in these social tasks.

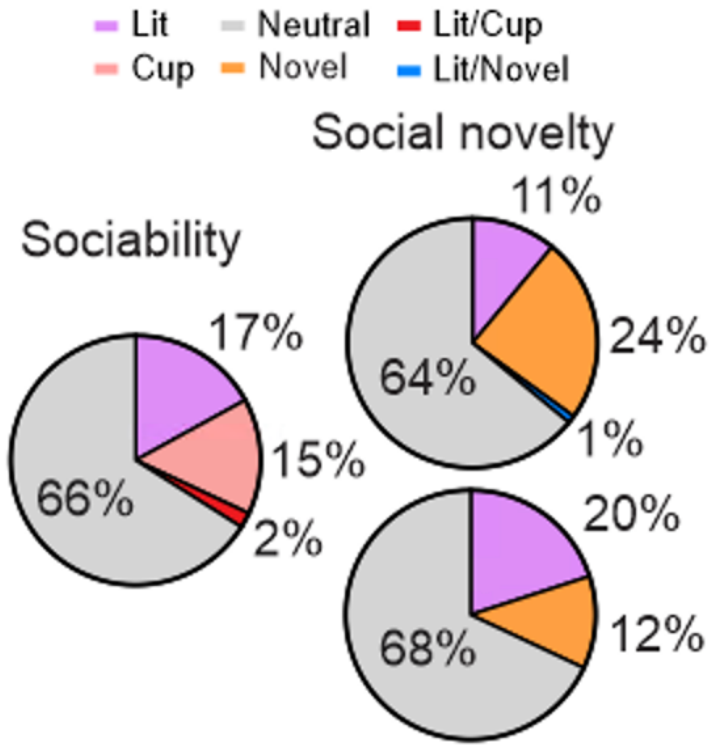

Figure 4.3: Percentage of stimulus-selective cells in social tasks. Left: in Sociability, 17% of VIP^{ACC} were classified as cup-selective, 15% as littermate-selective, 2% as selective for both cup and littermate, and 66% as neutral. Right: in Social Novelty, VIP^{ACC} were classified as littermate-selective (11% Day 2, 20% Day 3), novel-mouse-selective (24% Day 2, 12% Day 3), selective for both littermate and novel (1% Day 2, 0% Day 3), and neutral (64% Day 2, 68% Day 3). N = 6 mice, n = 310 cells for Sociability, n = 350 cells for Social Novelty Day 2, and n = 232 cells for Day 3. Lit: littermate. Note: Behavioral and imaging experiments performed by William Yen. Data analyzed by Lisa Kretsge, Connor Johnson, and Alexandra O'Connor. Figure made by Alberto Cruz-Martín. Figure published in Johnson, Kretsge & Yen et al., *BioRxiv*, 2020.

4.2.3 A Subpopulation of VIP^{ACC} Encode Interactions with Novel Objects

To investigate how VIP^{ACC} activate to non-social novel stimuli, we used the Novel Object task. In Novel Object, a small, plastic object is placed on one end of a rectangular arena and the animal is allowed to freely explore for 5 minutes (Figure 4.4, A). Animals spent about 20% of their time interacting closely with the novel object and about 40% in the zone of the arena near the object (Figure 4.4, B-C). Using ROC analysis, we identified object-selective and neutral subpopulations of VIP^{ACC} (Figure 4.4, D-E) and found that 20% of VIP^{ACC} were preferentially active during close interactions with the novel object (Figure 4.4, F). When analyzed as individual neurons (Figure 4.4, G, top) and when grouped together as a subpopulation (Figure 4.4, H), object-selective cells were more active during object interactions. About 80% of VIP^{ACC} were classified as neutral (Figure 4.4, F) and showed no difference in activity as animals interacted with objects or explored the rest of the arena (Figure 4.4, G, bottom, Figure 4.4, I). The data from this task demonstrate that VIP^{ACC} heterogeneity is not unique to anxiety-related and social tasks. It also shows that not only do some VIP^{ACC} encode social novelty, but some also encode novelty of non-social stimuli.

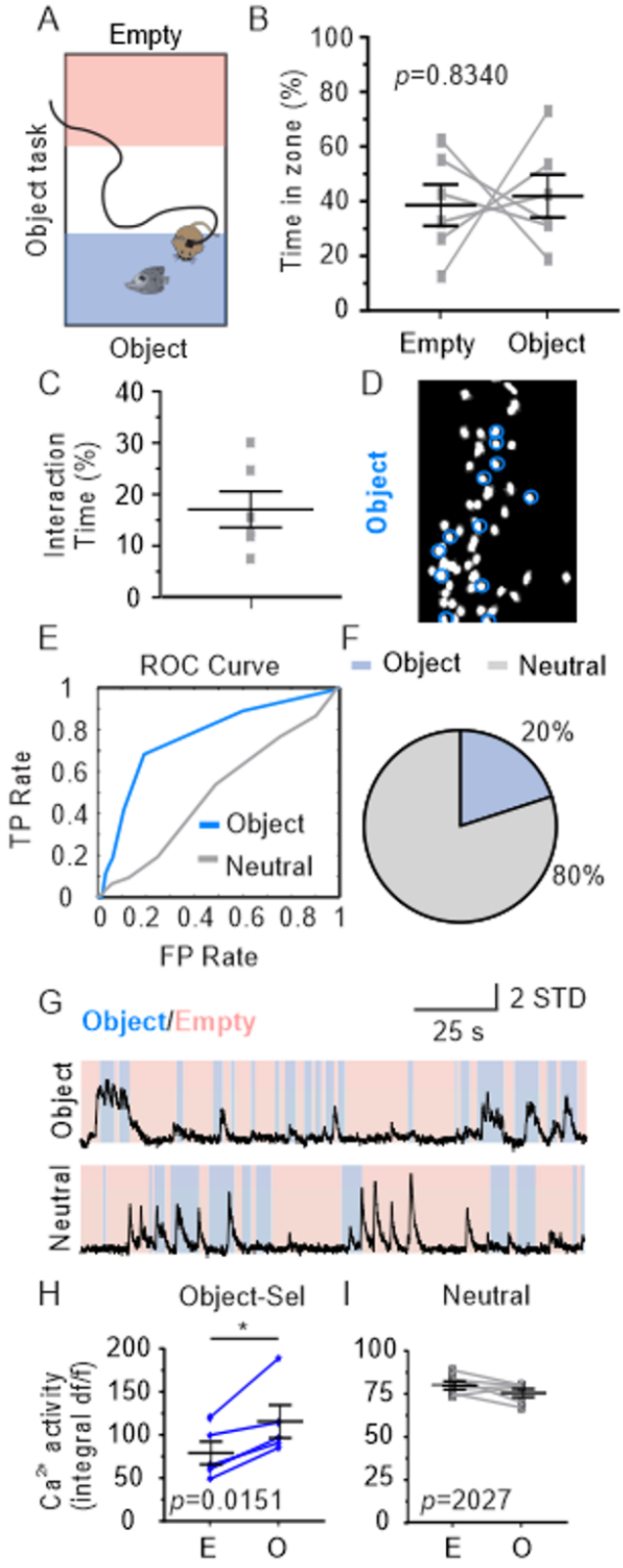
A
Empty
Object task
Object
B
Time in zone (%)
p=0.8340
Empty
Object
C
Interaction Time (%)
D
Object
E
ROC Curve
TP Rate
FP Rate
Object
Neutral
F
Object
Neutral
20%
80%
G
Object/Empty
2 STD
25 s
Object
Neutral
H
Object-Sel
Ca2+ activity (integral df/f)
p=0.0151
E
O
I
Neutral
p=2027
E
O

Figure 4.4. Distinct VIP^{ACC} preferentially encode interactions with a novel object. (A) Behavioral paradigm for the Object task. Object zone (blue). Empty zone (pink). Neutral zone (white). (B) Object task. Interaction time in each zone (%). Object zone vs. empty zone. p=0.8340. (C) Object task. Interaction time with object (%). (D) Image of VIP^{ACC} expressing GCaMP6f (white) in vivo during Object task. Blue circles: object-selective. Neutral cells are not circled. Scale bar = 60 μm. (E) ROC curves for object-selective (blue, auROC = 0.7621) and neutral (gray, auROC = 0.4980) VIP^{ACC}. (F) In the Object task 20% of VIP^{ACC} were classified as object-selective and 80% as neutral. (G) Ca^{2+} transients: object-selective (top) and neutral (bottom). Shaded areas indicate location of mouse: object (blue), empty (pink), neutral (white) zones. Scale bars = 25 s and 2 SD. (H-I) Average Ca^{2+} activity of selective cells per mouse. (H) Object-selective. Empty vs. object. *p=0.0151. (I) Empty-selective. Empty vs. object. p=0.2027. N = 6 mice, n = 227 cells. All ROC curves, traces, and images are representative. Each replicate in B-C and H-I represents one mouse. All statistics performed with Paired t-test. E: empty zone, O: object zone. Note: Behavioral and imaging experiments performed by William Yen. Data analyzed by Lisa Kretsge, Connor Johnson, Alexandra O'Connor, and Alberto Cruz-Martín. Figure made by Lisa Kretsge, Connor Johnson, and Alberto Cruz-Martín. Figure not previously published.

4.2.4 Activity of the Overall VIP^{ACC} Population Does Not Differ as Animals Interact with Social or Non-social Stimuli

Next, we aimed to determine whether whole VIP^{ACC} population activity changed during interactions with social or non-social stimuli. Previous work has shown bulk ACC activation or increased Pyr activity in the ACC during social interactions (Guo et al., 2019), but VIP^{ACC} have not been specifically monitored. Similar to the anxiety-related assays (Figure 3. 9), we found no differences in the average activity of all VIP^{ACC} as mice interacted with the different social (littermate or novel mouse) or non-social (empty cup) stimuli (Figure 4.5). In Sociability, there was no difference in population activity between cup and littermate interactions (Figure 4.5, A). In Social Novelty, there was no population activity difference when comparing interactions with a familiar or novel social

stimulus (Figure 4.5, B). This suggests that there is no global change in the VIP^{ACC} activity during interactions with other mice or objects; VIP^{ACC} do not have an overall homogeneous response to these stimuli.

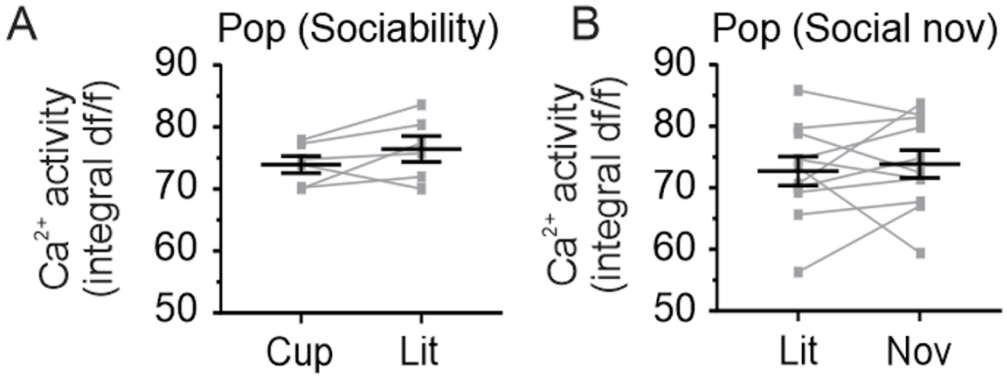

Figure 4.5: Population-level VIP^{ACC} activity does not change as animals interact with social or non-social objects. (A-B) Ca^{2+} activity of whole population VIP^{ACC} per mouse. (A) Sociability. Littermate vs. cup. p=0.1814. (B) Social Novelty. Novel mouse vs. littermate. p=0.6364. (C-D) Activity of neutral VIP^{ACC} in social tasks. (C) Sociability. Littermate vs. cup. p=0.8026. (D) Social Novelty. Littermate vs. Novel mouse. p=0.7879. Each replicate represents one mouse. N = 6 mice, n = 310 cells for Sociability, n = 350 cells for Social Novelty Day 2, n = 232 cells and Day 3. All statistics performed with Paired t-test. Lit: littermate, Nov: novel mouse, Social nov: Social Novelty, Pop: population, df/f: Deltaf/f. Note: Behavioral and imaging experiments performed by William Yen. Data analyzed by Lisa Kretsge, Connor Johnson, and Alexandra O'Connor. Figure made by Connor Johnson and Alberto Cruz-Martín. Figure published in Johnson, Kretsge & Yen et al., *BioRxiv*, 2020.

4.2.5 Cell-selectivity Identification Method was Validated for Sociability

We also verified that this analysis method was reliable, as described above (Figure 3.10, A). We used one half of the Sociability dataset to identify cup- and littermate-selective cells and then used those classifications to perform Ca^{2+} activity analysis on the remaining half of the data (Figure 3.10, A). As in the anxiety-related data

(Figure 3.10, B), we found that the Ca^{2+} activity of selective cells in the second half of the data increased when mice interacted with preferred stimuli (preferred vs. non-preferred, 17%) (Figure 4.6). This suggests the ROC analysis performed accurately identified cells that encoded one stimulus type.

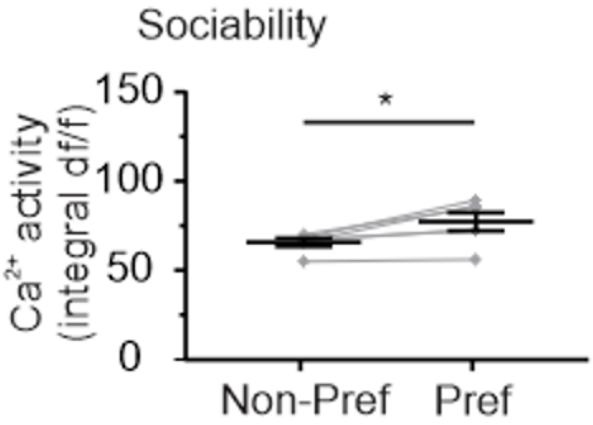

Figure 4.6: Validation of VIP^{ACC} activity for Sociability. Grouped data for the social interaction task. Cells identified as selective for one stimulus (empty cup or littermate) using the first half of the data showed more activity in the second half of the data when the animal was interacting with the preferred stimulus. Preferred vs. Non-preferred, *p=0.0216. N = 6 mice, n = 310 cells. Each replicate represents the average data for one mouse. All statistics performed with Paired t-test. Non-pref: non-preferred, Pref: preferred, df/f: Deltaf/f. Note: Behavioral and imaging experiments performed by William Yen. Data analyzed by Lisa Kretsge, Connor Johnson, and Alexandra O'Connor. Figure made by Connor Johnson and Alberto Cruz-Martín. Figure published in Johnson, Kretsge & Yen et al., *BioRxiv*, 2020.

4.3 Conclusion and Future Directions

This work shows, for the first time, that subpopulations of VIP^{ACC} encode different social, non-social, and novel stimuli. Not only does it demonstrate that VIP^{ACC} are recruited during these behaviors, but it also demonstrates that they are functionally heterogeneous

during these tasks. Using Sociability, Social Novelty, and Novel Object tasks, we were able to identify VIP^{ACC} that preferentially activated to littermates, novel mice, and objects. We also demonstrated that most VIP^{ACC} are either neutral or activate to only one stimulus type. Finally, despite past research showing increased whole ACC activity during socialization, there is no global change in the VIP^{ACC} activity during interactions with other mice or objects. Additionally, we found subgroups of VIP^{ACC} that encoded interactions with objects, which supports past findings that characterized neural correlates in the ACC for object and location recognition and memory consolidation of object and place associations (Weible et al., 2012; Weible et al., 2009).

Interestingly, within the social tasks, very few cells were selective for both stimuli (Figure 4.3, 0-2% of cells). Even in the case of two social stimuli, where one is novel and the other is familiar, there was minimal overlap in the cells that encode them (Figure 4.3, 0-1% of cells). Future work could use more diverse social stimuli (e.g., mice of different sexes, strains, ages) to better understand how VIP^{ACC} subpopulations encode similar information. For example, do VIP^{ACC} that encode interactions with novel males also encode interactions with novel females? To address this, researchers could image VIP^{ACC} in a social task like those described above, but with a novel male in one cup and a novel female in the other. Performing ROC analysis would allow researchers to determine what percentage of cells selectively activated to both stimuli. A similar approach could be taken using a novel mouse and novel object in one assay to determine whether object- and novel mouse-selective cells are comprised of overlapping populations. If they do, those cells may encode novelty itself, rather than novelty specific to either social or non-

social stimuli. It is important to note that the littermate and novel stimulus mice differed not only in their degree of novelty, but also in their strain (VIP-Cre versus CD-1). Prior work has shown that genetic differences in the animals an experimental mouse co-habitiates with can lead to differences in anxiety-related behavior, immune function, and expression of certain genes in the PFC (Baud et al., 2017). It is unknown whether strain differences could also lead to differences in ACC activity, but future work could parse out the effects of strain by repeating these Ca^{2+} imaging studies using familiar CD-1 mice or novel VIP-Cre mice as social stimuli.

Another direction to take this research would be to investigate social anxiety. The neural mechanisms of SAD are still not fully understood. Our work identifies subpopulations of VIP^{ACC} that activate to anxiogenic stimuli as well as groups that activate to social stimuli. Imaging VIP^{ACC} during exposure to a social stressor (as describes above) could elucidate whether some VIP^{ACC} are important in social anxiety-like behaviors. Animals could be exposed to chronic social defeat stress (Harris et al., 2018; Russo et al., 2012) and then VIP^{ACC} activity could be quantified as animals interacted with aggressor mice. Determining whether social stressors activate distinct populations of VIP^{ACC} may provide insight into future therapeutic approaches to address SAD.

One possible interpretation of these data is that VIP^{ACC} may be recruited during interactions with a wide array of salient stimuli. Because so many different kinds of stimuli are encoded by subsets of VIP^{ACC}, it's possible that these cells may be important in complex behaviors that involve combining multiple streams of information (e.g.,

information about whether a stimulus is social versus non-social and novel versus familiar). Murugan et al. (2017) identified neurons in the prelimbic cortex that were active during social investigation, but only in specific spatial locations. Stimulus location was randomized across animals and days, but it remains possible that this factor could contribute to selectivity in our findings. Similarly, cells classified as neutral may be equally activated by multiple or more complex stimuli (Murugan et al. 2017).

Future studies could chemogenetically or optogenetically manipulate VIP^{ACC} to determine whether their normal activity is necessary in tasks that rely upon multiple kinds of stimulus information, like a social memory assay. The work presented in this chapter provide a novel way to understand the neural mechanisms involved in normal social and cognitive behaviors and may also be important in understanding deficits in these behaviors. These data demonstrate that there are distinct subgroups of VIP^{ACC} that encode for interactions with objects, other mice, and social novelty, in addition to our prior data showing subgroups of VIP^{ACC} that encode anxiogenic or anxiolytic contexts.

CHAPTER FIVE

Population-level VIP^{ACC} Encoding Within and Across Tasks

5.1 Introduction

The knowledge that VIP^{ACC} are functionally heterogeneous across a wide variety of behaviors lead us to question how these individual stimulus-selective cells may function as distinct functional groups. In other areas of cortex, past research has shown that clusters of neurons can display task-dependent co-activation (Liang et al., 2018; Krabbe et al., 2019). Subpopulations of Pyr in the mPFC have been identified that activate in multiple distinct groups (Liang et al., 2018). In fact, during social behaviors, researchers found clusters of social stimulus-selective Pyr but also found groups of Pyr that were significantly less active during social interactions (Liang et al., 2018). It has been hypothesized that these groups of cells, despite being the same cell type and located within the same brain region, function in parallel to process unique information (Liang et al., 2018; Cruz-Martin et al., 2014). In addition, this work suggests that selective Pyr in the mPFC better encode information as large populations than as individual selective cells (Liang et al., 2018). This may mean that these cells activate as ensembles to collaboratively improve information processing.

In the context of our research, these data provide a fascinating way in which to interpret the role of stimulus-selective neurons in large-scale cortical information processing. Although this previous work monitored a different cell type and brain region, it may represent one way cortex can encode diverse information. This type of analysis

has not been performed on ACC inhibitory neurons, however, so the following work aimed to determine whether VIP^{ACC} encoding differs when comparing an individual neuron to larger populations of neurons. In addition, we investigated whether functional clusters of VIP^{ACC} have distinct roles in encoding different kinds of stimuli or whether they subpopulations involved in anxiety-like and social behaviors overlap. Our hypotheses were that using information from groups of VIP^{ACC} would better encode information than information from individual VIP^{ACC} and that these subpopulations would preferentially activate to distinct kinds of stimuli. To address these questions, we used super cell analysis and registration of Ca^{2+} imaging data from VIP^{ACC} during the EZM and social behavioral assays.

5.2 Results

5.2.1 Population Coding of Selective VIP^{ACC} Improves Behavioral Encoding

Our analysis thus far demonstrated that individual VIP^{ACC} can reliably encode diverse stimuli. However, it was not known if subsets of selective VIP^{ACC} could work cooperatively to increase the reliability of their coding. To determine whether the activity of groups of selective VIP^{ACC} more reliably encode behavioral states than individual cells, we averaged the Ca^{2+} traces from all cells that were selective for a specific stimulus to create "super cells" for that stimulus (Figure 5.1, A-D).

We compared super cell auROC values from averaged selective cells to auROC values from individual selective cells (Figure 5.1, E-J). In addition, we compared them to auROC values from all VIP^{ACC}, which was calculated by averaging the auROC values for

all cells, rather than only selective cells (Figure 5.1, E-J). In the EZM, auROC values for closed super cells increased by 34% and 12% relative to all cells or individual closed-selective VIP^{ACC}, respectively (Figure 5.1, E). For open super cells, we found increases of 42% and 19% in auROC values relative to all or open-selective VIP^{ACC}, respectively (Figure 5.1, F).

We found this pattern in other behavioral tasks, as well. In Sociability, littermate super cells exhibited a 24% and 11% increase in auROC values relative to all or littermate-selective VIP^{ACC}, respectively (Figure 5.1, G). In Social Novelty, auROC values increased by 27% and 10% relative to all or littermate-selective VIP^{ACC}, respectively (Figure 5.1, I). Cup super cell auROCs increased by 29% and 13% relative to all or cup-selective VIP^{ACC}, respectively (Figure 5.1, H), and novel mouse super cells exhibited 24% and 11% increases in auROC values relative to all or novel-mouse-selective VIP^{ACC}, respectively (Figure 5.1, J). Overall, these data support our previous findings and demonstrate that averaging the activity of stimulus-selective VIP^{ACC} increases the accuracy of their coding, suggesting that including information from selective populations, rather than individual cells or all VIP^{ACC}, leads to better information encoding.

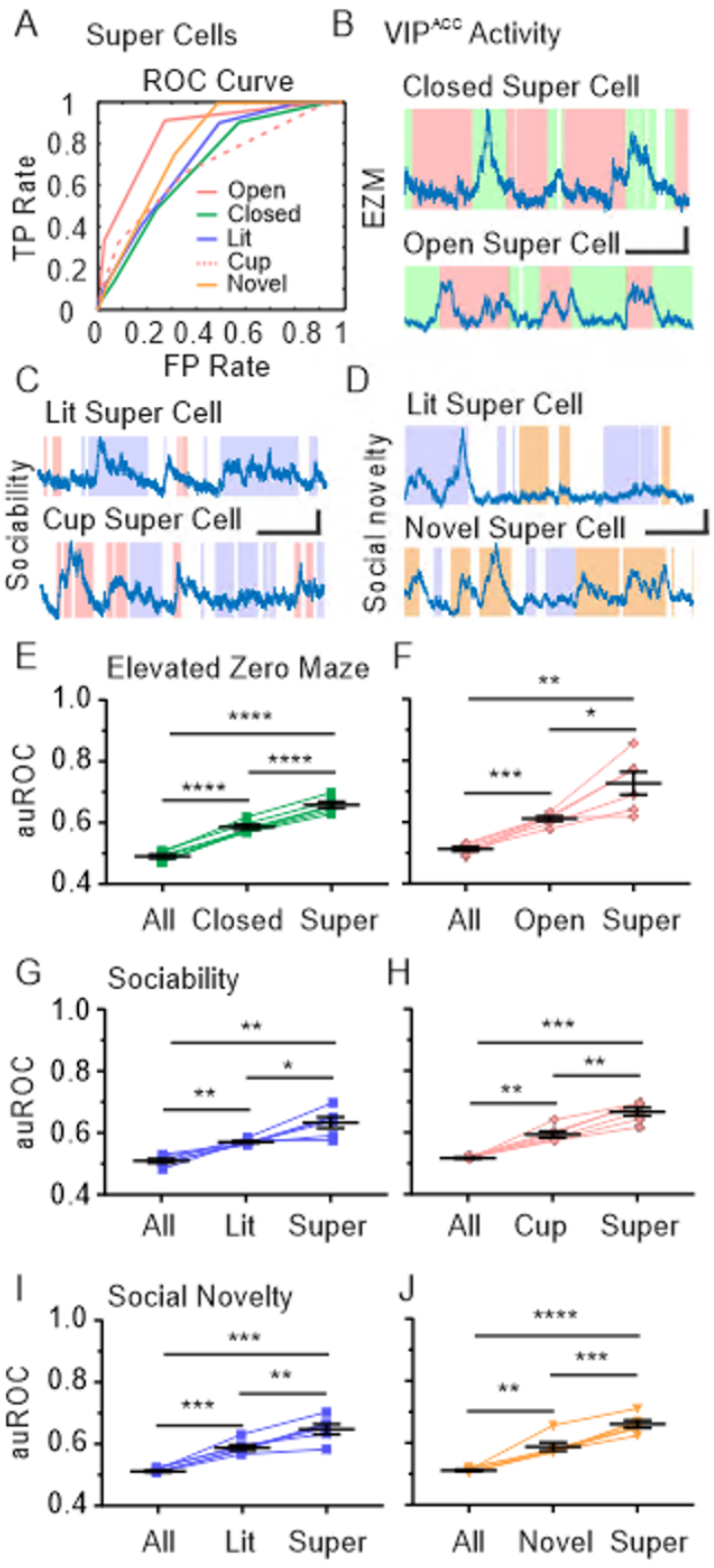
A
Super Cells
ROC Curve
TP Rate
FP Rate
Open
Closed
Lit
Cup
Novel
B
VIP^ACC Activity
Closed Super Cell
Open Super Cell
EZM
C
Lit Super Cell
Cup Super Cell
Sociability
D
Lit Super Cell
Novel Super Cell
Social novelty
E
Elevated Zero Maze
auROC
All Closed Super
F
All Open Super
G
Sociability
All Lit Super
H
All Cup Super
I
Social Novelty
All Lit Super
J
All Novel Super

Figure 5.1: Population coding of selective VIP^{ACC} improves behavioral encoding. (A) Example ROC curves of open- (pink solid, auROC = 0.86), closed- (green, auROC = 0.70), littermate- (purple, auROC = 0.74), empty cup- (pink dotted, auROC = 0.70), and novel-mouse-selective (orange, auROC = 0.79) super cells. (B-D) Ca^{2+} transients of each type of super cell for the EZM (B) and social interaction tasks (C-D). Scale bars = 10 s and 1 SD. Shaded areas represent location of the mouse. Closed arm (B, green), open arm (B, pink), littermate (C-D, purple), empty cup (C, pink), novel mouse (D, orange) or neutral (C-D, white) zones. Ca^{2+} signals overlayed. (E-J) auROC of all cells (All), selective cells, and super cells (Super) per mouse in the EZM (E-F) and social interaction tasks (G-J). In each task, selective cells had higher auROC than the whole population and super cells had higher auROC values than selective cells. (E-F) This pattern was consistent in the EZM for both closed- (E, All vs. closed: ****p<0.0001. All vs. super: ****p<0.0001. Closed vs. super: ****p<0.0001) and open-selective cells (F, All vs. open: ***p=0.0009. All vs. super: **p=0.0047. Open vs. super: *p=0.0370). (G-H) In Sociability, this pattern was consistent for littermate- (G, All vs. littermate: **p=0.0022. All vs. super: **p=0.0011. Littermate vs. super: *p=0.0326) and cup-selective (H, All vs. cup: **p=0.0026. All vs. super: ***p=0.0003. Cup vs. super: **p=0.0010). (I-J) In Social Novelty, this pattern was consistent for littermate- (I, All vs. littermate: ***p=0.0005. All vs. super: ***p=0.0008. Littermate vs. super: **p=0.0073.) and novel-mouse-selective (J, All vs. novel: **p=0.0059. All vs. super: ****p<0.0001. Novel vs. super: ***p=0.0007). ****p<0.0001. N = 6 mice, n = 345 cells for EZM, n = 310 cells for Sociability, n = 350 cells for Social Novelty Day 2, n = 232 cells and Day 3. All ROC curves and traces are representative. Each replicate in E-J represents one mouse. All statistics performed with Repeated measures ANOVA with Tukey's post test. Lit: littermate, Soc: social. Note: Behavioral and imaging experiments performed by William Yen. Data analyzed by Lisa Kretsge, Connor Johnson, Alexandra O'Connor, and Alberto Cruz-Martín. Figure made by Connor Johnson and Alberto Cruz-Martín. Figure published in Johnson, Kretsge & Yen et al., *BioRxiv*, 2020.

5.2.2 VIP^{ACC} Can Be Registered to Determine Their Activation Across Tasks from Different Imaging Sessions

To determine whether diverse neuronal representations are embedded in particular VIP^{ACC} subpopulations, we aimed to monitor the same cells across tasks. Using CaImAn (Giovannucci et al., 2019), we were able to register imaging data across different behavioral assays, even when experiments were performed on different days and the

miniscope was removed and re-attached repeatedly (Figure 5.2). We registered neural data from the EZM and Sociability tasks and were able to identify 127 neurons (out of 655 total neurons) that were visible across both tasks (Figure 5.2). This process allowed us to track their activity in both EZM and Sociability and perform auROC analysis for anxiety-related, social, and non-social stimuli for the same cells.

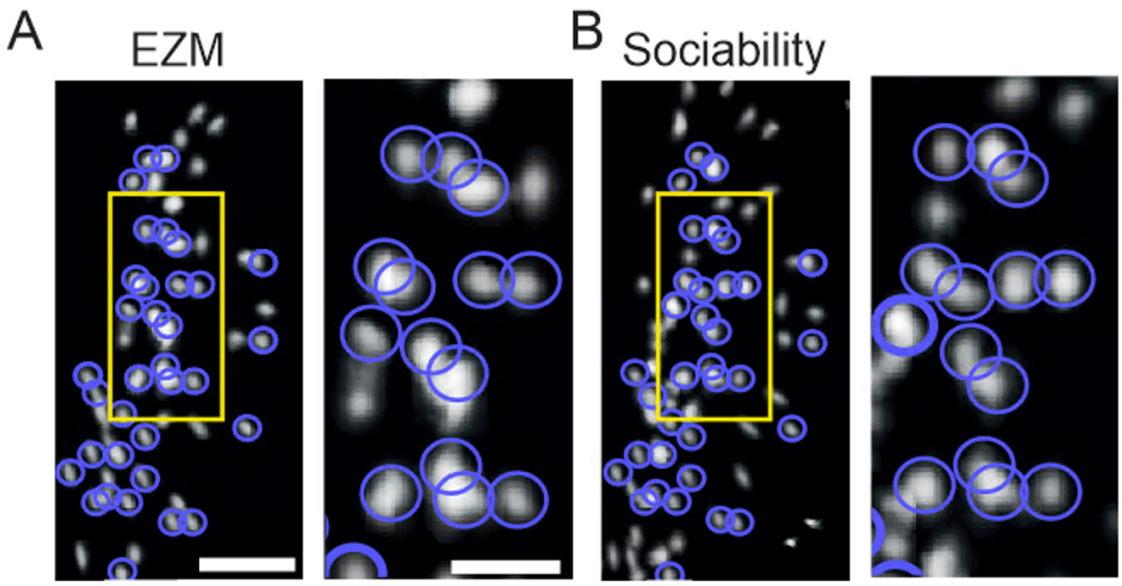

Figure 5.2: VIP^{ACC} cells can be registered and across different imaging sessions and behavioral tasks. (A-B) VIP^{ACC} were registered across tasks. Purple circles: registered cells monitored during both EZM (A) and Sociability (B). Left: Scale bar = 100 μm. Right: zoomed versions of yellow outlined regions in left panels. Scale bar = 40 μm. Note: Behavioral and imaging experiments performed by William Yen. Data analyzed by Lisa Kretsge and Connor Johnson. Figure made by Lisa Kretsge and Connor Johnson. Figure published in Johnson, Kretsge & Yen et al., *BioRxiv*, 2020.

5.2.3 Distinct, Non-overlapping VIP^{ACC} Subpopulations Are Recruited in Different Behavioral States

Although we have already shown that subpopulations of VIP^{ACC} encode anxiety-related and social stimuli, those data did not determine whether the subpopulations that encode these different kinds of information are separate from one another. By registering our data across EZM and Sociability, we identified distinct subpopulations of VIP^{ACC} that showed stimulus selectivity in only one task and others that were selectively active in specific zones of each task (Figure 5.3). 27% of registered VIP^{ACC} were selective in the EZM and neutral during Sociability (Figure 5.3, A). Conversely, about 22% were selective in Sociability, but neutral in the EZM (Figure 5.3, A). Out of all registered VIP^{ACC}, 17% were only open-selective, 9% only closed-selective, 16% only littermate-selective, and 6% only cup-selective (Figure 5.3, A). Taken together, these data show that about half of all registered VIP^{ACC} were only selective for one of these 4 stimuli, whereas only one sixth were selective for 2 or 3 stimuli (e.g., both when the mouse was in the open arm of the EZM and when it interacted with the littermate in Sociability) (Figure 5.3). This demonstrates that, on average, more cells were selective for one stimulus than for two or three (Figure 5.3, B). Unlike in the previous data without registration (Figure 3.7, C and 4.2, A), where the majority of cells were neutral, only 36% of cells were neutral in both tasks (data not shown). These data suggest that, within the ACC, there are non-overlapping VIP interneuron subcircuits dedicated to processing particular stimuli.

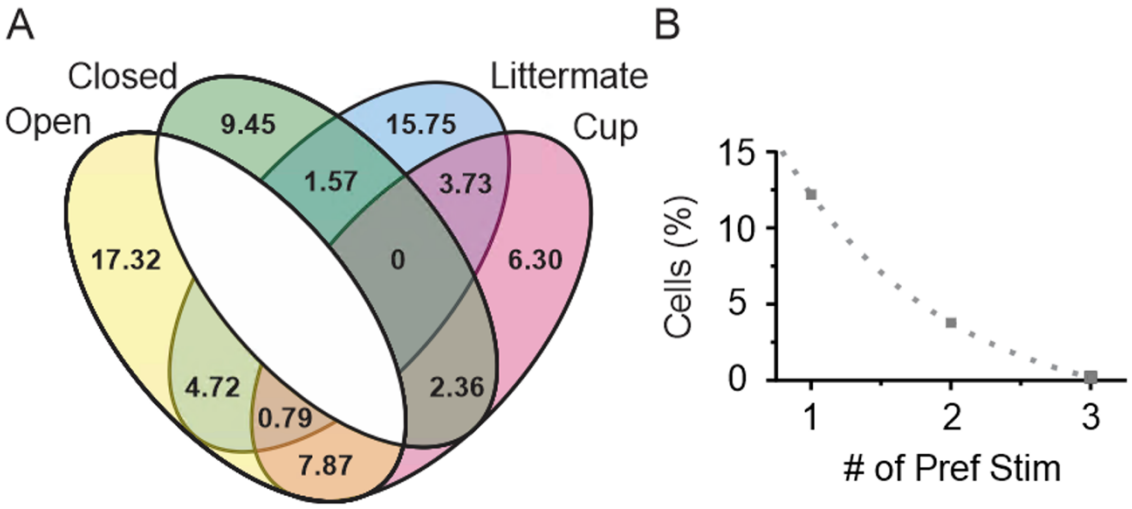

Figure 5.3: VIP^{ACC} subpopulations are non-overlapping and are recruited during distinct behaviors. (A) Venn diagram demonstrating cell selectivity in the EZM and Sociability. Each number indicates what percentage of the registered cells belong to each selectivity category. There is a gap between open and closed because these classifications are mutually exclusive – by definition a cell cannot be selective for both. (B) Percentage of cells selective for one, two, or three stimuli. Dotted line, one phase decay, half-life of 0.81. Pref Stim: preferred stimuli. Note: Behavioral and imaging experiments performed by William Yen. Data analyzed by Lisa Kretsge and Connor Johnson. Figure made by Lisa Kretsge and Connor Johnson. Figure published in Johnson, Kretsge & Yen et al., *BioRxiv*, 2020.

5.3 Conclusion and Future Directions

This chapter has further investigated how VIP^{ACC} subpopulations function to encode diverse stimuli. First, we used super cell analysis to demonstrate that selective VIP^{ACC} have higher auROC values when grouped together than when analyzed as individual neurons, which suggests inclusion of information from many of these selective cells may better encode stimuli than individual neurons. This may mean that these subpopulations function as populations to improve behavioral encoding. In addition, these super cells had higher auROC values than whole VIP^{ACC} populations, which

suggests that including cells that are not specific for a given stimulus decreases the encoding of that stimulus. This finding was consistent across social, non-social, anxiogenic, and anxiolytic stimuli, which suggests it may be a feature of how VIP^{ACC} function across tasks. This approach is a first step that points to the possibility that VIP^{ACC} may encode information as disinhibitory subclusters, but this needs to be further studied. More advanced computational techniques, like principal component analysis, could be used to determine whether VIP^{ACC} activity is sufficient to decode animal behavior or whether clusters or assemblies of VIP^{ACC} with similar functions can be identified (Liang et al., 2018; Spellman et al., 2015; Wang, Zheng, & Ma, 2013; Lopes-dos-Santos et al., 2011).

In addition, we registered VIP^{ACC} cells across behavioral tasks and found surprisingly minimal overlap between cells selective for different stimuli. Most VIP^{ACC} preferentially activated to only one stimulus across the 4 stimuli in EZM and Sociability. While our earlier work demonstrated heterogeneity of within a task, this work shows they also activate heterogeneously across tasks. VIP^{ACC}, therefore, seem to be subdivided into largely distinct functional clusters. It is possible that VIP^{ACC} subpopulations inhibit other groups of interneurons and disinhibit groups of Pyr in a stimulus-dependent manner. Ca^{2+} imaging of other neural subtypes within the ACC could clarify whether there are distinct networks and pathways within this area that function as parallel streams of information (Cruz-Martin et al., 2014). These data may also relate to general cortical function, not only ACC and VIP interneurons. Further work in other brain regions would clarify whether distinct subsets of neurons encode diverse stimuli throughout the cortex.

One caveat of our registration data is that many cells could not be registered across tasks. This is likely because the miniscope was removed and re-attached on these different days, so the focal plane may be slightly different. Registration of our cells needed to be strict to avoid incorrectly matching different cells across tasks, which contributed to the low number of registered neurons. In this study, different behavioral assays were performed on different days to avoid any long recording sessions that could induce bleaching of the GCaMP6f fluorophore. This introduces possible variability in our data because it is unknown whether the functional dynamics of these cells remain stable over days. Future studies could assay anxiety-related and social behaviors within the same imaging session to increase the proportion of cells that can be registered and determine whether the lack of overlap found in the current study remains consistent when monitored within one day. By using brief imaging sessions and inter-trial intervals, it would be feasible to repeat some of these experiments within the same day. These data in this chapter provide new insights into how VIP^{ACC} may function as subclusters and could be used to model how population dynamics in the ACC network contribute to processing anxiety-related and social information.

CHAPTER SIX

Mapping Inputs to VIP^{ACC}

6.1 Introduction

In addition to investigating the functional heterogeneity of VIP^{ACC}, we aimed to determine how other brain regions are connected to VIP^{ACC} and to uncover any connective heterogeneity across ACC interneuron subtypes. Classic tracers have demonstrated that the ACC receives inputs from a wide array of structures, including the motor cortex, nearby frontal cortical subregions, retrosplenial cortex, and anteromedial and mediodorsal thalamus (AM and MD, respectively) (Shibata, 1993; Shibata, 1993; Shibata & Naito, 2005; Shibata, Kondo, & Naito, 2004; Allen Institute for Brain Science, 2011; Jones, Groenewegen, & Witter, 2005). The ACC also receives many interareal projections (from contralateral and ipsilateral ACC cells) (Shibata, 1993; Shibata, 1993; Shibata & Naito, 2005; Shibata, Kondo, & Naito, 2004; Allen Institute for Brain Science, 2011; Jones, Groenewegen, & Witter, 2005; Harris et al., 2018). Advanced synaptic mapping techniques, like mono-synaptic rabies tracing, allow for specific labelling of cells that project to different neural subtypes (DeNardo et al., 2015; Sun et al., 2019; Callaway & Luo, 2015). Previous work has shown differences in connectivity even between nearby cortical regions (Sun et al., 2019), different interneuron subtypes within the same region (Pouchelon et al., 2020), or across cortical layers of different depths (Cruz-Martin et al., 2014), so this could be a potential source of heterogeneity in the ACC. It remains unknown whether different cell types within the ACC all receive inputs

from the same brain regions or whether different patterns of connectivity emerge when examined with cell-type specific techniques.

VIP cells in other cortical areas are known to receive long-range inputs from other brain regions, which may allow them to coordinate the activity of the ACC with other brain regions and respond to diverse stimuli (Lee et al., 2013; Melzer et al., 2020; Karnani et al., 2016). Mapping inputs to VIP^{ACC} could provide important context to learn more about their behavioral relevance. For example, VIP^{ACC} may receive projections from brain areas implicated in anxiety, social behavior, or novel object recognition. Identifying the existence of these inputs to VIP^{ACC} could illuminate circuits that could be studied or manipulated to better understand the neural mechanisms involved in these behaviors. In addition, better understanding connectivity differences between three prevalent cortical interneuron subtypes (VIP, SOM, and PV) may improve our understanding of long-range ACC circuits and overall cortical connectivity.

We hypothesized that ACC interneurons would receive many projections from areas known to project to the ACC (the ACC itself, motor, frontal, and retrosplenial cortex, AM and MD thalamus) (Shibata, 1993; Shibata, 1993; Shibata & Naito, 2005; Shibata, Kondo, & Naito, 2004; Allen Institute for Brain Science, 2011; Jones, Groenewegen, & Witter, 2005). Similarly, we hypothesized that VIP^{ACC} would receive inputs from brain regions implicated in anxiety, social behavior, and cognition. Lastly, we hypothesized that the distribution of inputs from different areas would differ between VIP, SOM, and PV, forming unique cell-type specific maps of ACC connectivity. To test this, we used Cre-dependent rabies trans-synaptic tracing in interneuron-Cre mice to

fluorescently label and quantify monosynaptic inputs to VIP, SOM, and PV cells in the ACC (VIP^{ACC}, SOM^{ACC}, and PV^{ACC}, respectively).

6.2 Results

6.2.1 Rabies Tracing Allows for Specific Labelling of Mono-synaptic Inputs to VIP^{ACC}

To map inputs to VIP^{ACC}, we used rabies virus-mediated trans-synaptic mapping (Figure 6.1). This technique allows us to retrogradely label only neurons that synapse onto VIP^{ACC}. First, we injected AAV-TVA-Glyco-GFP, a helper AAV that expresses target proteins in a Cre-dependent manner, into the ACC of VIP-Cre mice (Figure 6.1, A). After 4 weeks of viral expression time, we injected RV*dG* into the ACC of these same mice (Figure 6.1, A). These two viruses work together to ensure cell-type specific infection and labelling of monosynaptic inputs to Cre+ cells in the area of interest (Figure 6.1, B-C). The AAV contains genes to express EGFP, TVA, and Glyco and RV*dG* is an EnVA pseudotyped, glycoprotein gene deleted (ΔG) rabies virus. Glyco is the rabies virus glycoprotein, which must be present for the ΔG rabies to move through the synapse and infect presynaptic neurons (Kohara et al., 2014; Callaway & Luo, 2015; Wall et al., 2016; Haubensak et al., 2010). TVA is a receptor that allows cells to be infected by viruses pseudotyped with EnVA (Callaway & Luo, 2015; Kohara et al., 2014; Haubensak et al., 2010). EGFP and mCherry fluorescently label infected neurons, so that they can be easily located and quantified. Starter neurons (Cre+ ACC cells, in the following experiments) express both EGFP and mCherry, whereas input cells (cells that project

onto Cre+ ACC cells) only express mCherry (Figure 6.1, B-C and Figure 6.2). When used in VIP-Cre mice, this methodology allowed us to specifically identify VIP^{ACC} starter cells and monosynaptic inputs to VIP^{ACC} throughout the brain (Figure 6.2).

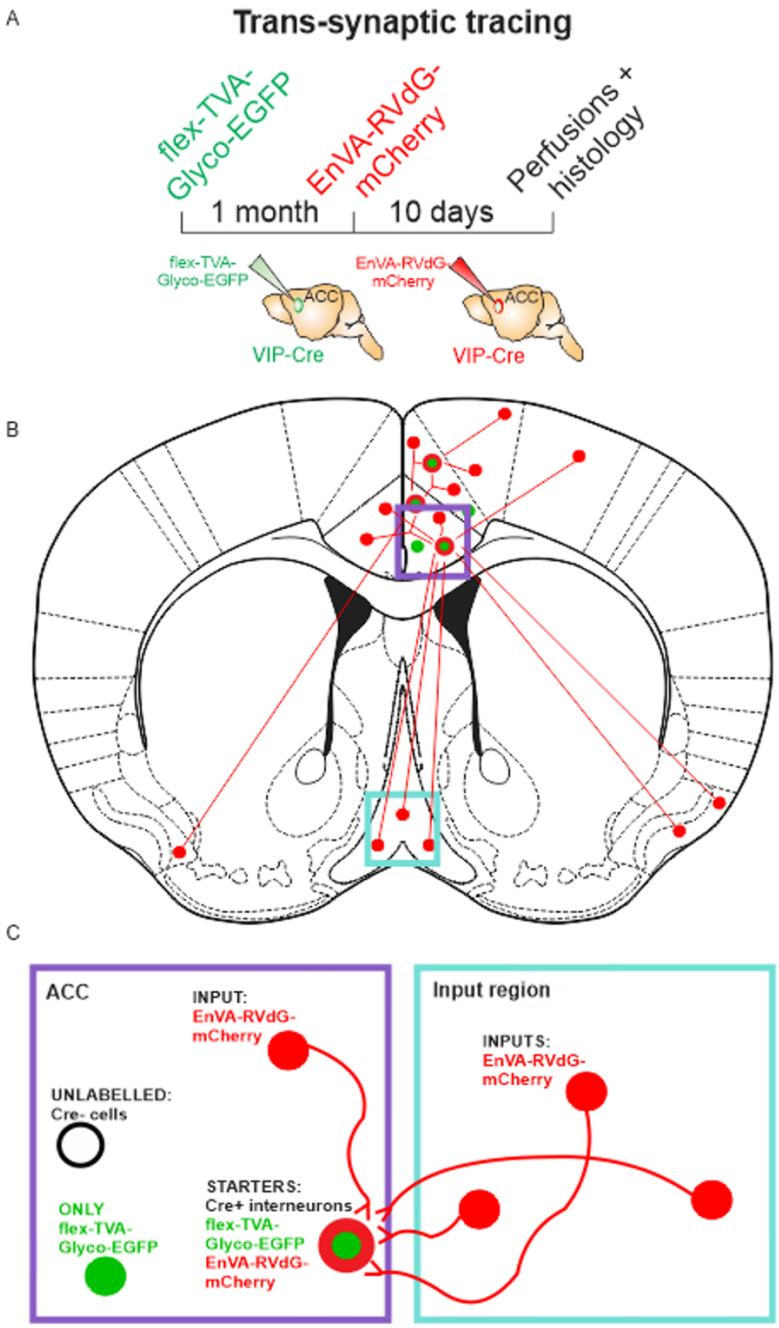

Figure 6.1: Schematic and timeline for trans-synaptic tracing experiments. (A) Timeline for trans-synaptic tracing experiments. (B-C) Schematic of rabies tracing methods to identify inputs to Cre+ cells in the ACC. Colors represent neurons infected with one or both rabies tracing viruses. Red: EnVA-RVdG-mCherry, green: flex-TVA-Glyco-EGFP, white: no viral expression. Starter cells (Cre+ cells in ACC, expressing with both flex-TVA-Glyco-EGFP and EnVA-RVdG-mCherry) and input cells (cells throughout the brain, expressing only EnVA-RVdG-mCherry. (B) Example image of a brain section (black) (Allen Institute for Brain Science, 2004) with input and starter cells labelled. (C) Zoomed regions to demonstrate input and starter cells, as well as unlabeled and single-labelled (flex-TVA-Glyco-EGFP only) cells. Note: Figure made by Lisa Kretsge and not previously published. Figure based on data from prior research using these techniques (Callaway & Luo, 2015; DeNardo et al., 2015).

To determine whether viral expression was limited to cells expressing Cre, we injected AAV-TVA-Glyco-GFP and RV*dG* in Cre-negative mice (C57BL6/J, N = 3) using the same methods and timeline described above (Figure 6.1, A). We identified some mCherry-positive cells at the injection site (ipsilateral ACC), but very few labelled cells elsewhere in the brain (Figure 6.3). In Cre+ mice, the contralateral ACC (clACC) is highly labeled with RV*dG*-mCherry (Figure 6.4, B), but this pattern is not seen in these control mice (Figure 6.3). This suggests minimal leaky expression of the rabies virus in input regions. The non-Cre-dependent mCherry expression at the injection site is in expected based on prior work with these viruses (Callaway and Luo, 2015). To avoid any inaccurate quantification from leaking viruses, the following analyses exclude RV*dG* inputs at the site of the ACC injection (ipsilateral ACC).

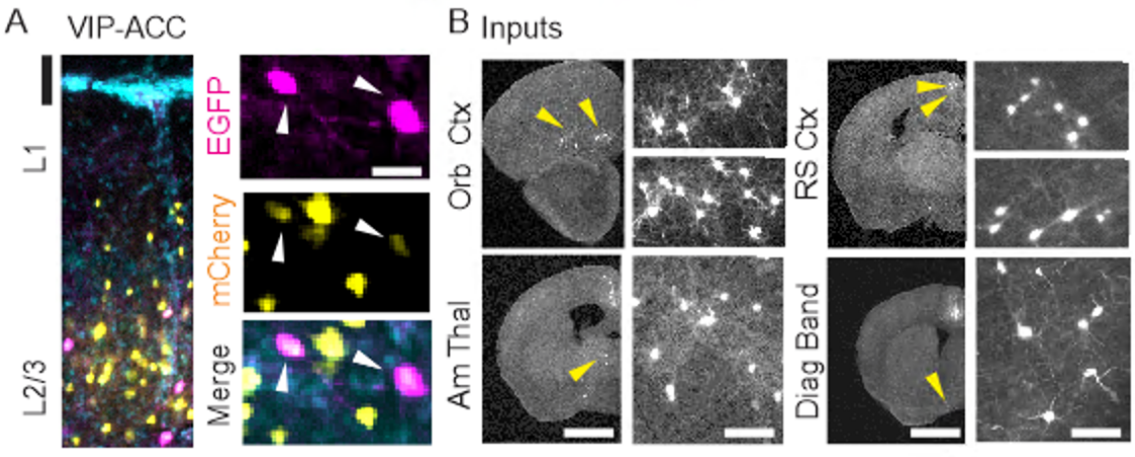

Figure 6.2: Rabies tracing to map monosynaptic inputs onto VIP^{ACC}. (A) Image of starter VIP^{ACC} expressing both EGFP (pseudo colored magenta, also expressing TVA and ΔG) and mCherry (pseudo colored yellow, infected by RV*dG)*, and retrogradely-labeled input cells only expressing mCherry. Coronal section. Left: overlay of both fluorophores and DAPI (cyan). Scale bar = 50 μm. Right: zoomed in superficial layers showing overlap (starter cells, white arrows). Scale bar = 15 μm. (B) Images of retrogradely-labeled input neurons (white) in the orbitofrontal (Orb) cortex (Ctx), anterior thalamic nuclei (Am Thal or AM), retrosplenial (RS) cortex, and diagonal band of Broca (Diag Band, part of the medial septal complex, MSC). Left panels: left hemisphere. Scale bar = 1.5 mm. Right panels: zoomed views of the retrogradely-labeled brain regions (yellow arrowheads in left panel). Scale bar = 100 μm. Note: Surgeries performed by Connor Johnson, Tushare Jinadasa, and Erelle Fuchs. Histology, imaging, and cell counting performed by Lisa Kretsge, Tushare Jinadasa, Erelle Fuchs, Eli Spevack, Berta Escude Velasco, and Frances Hausmann. Data analyzed by Lisa Kretsge, Connor Johnson, and Tushare Jinadasa. Figure made by Lisa Kretsge, Tushare Jinadasa, and Alberto Cruz-Martín. Previously published in Johnson, Kretsge & Yen et al., *BioRxiv*, 2020.

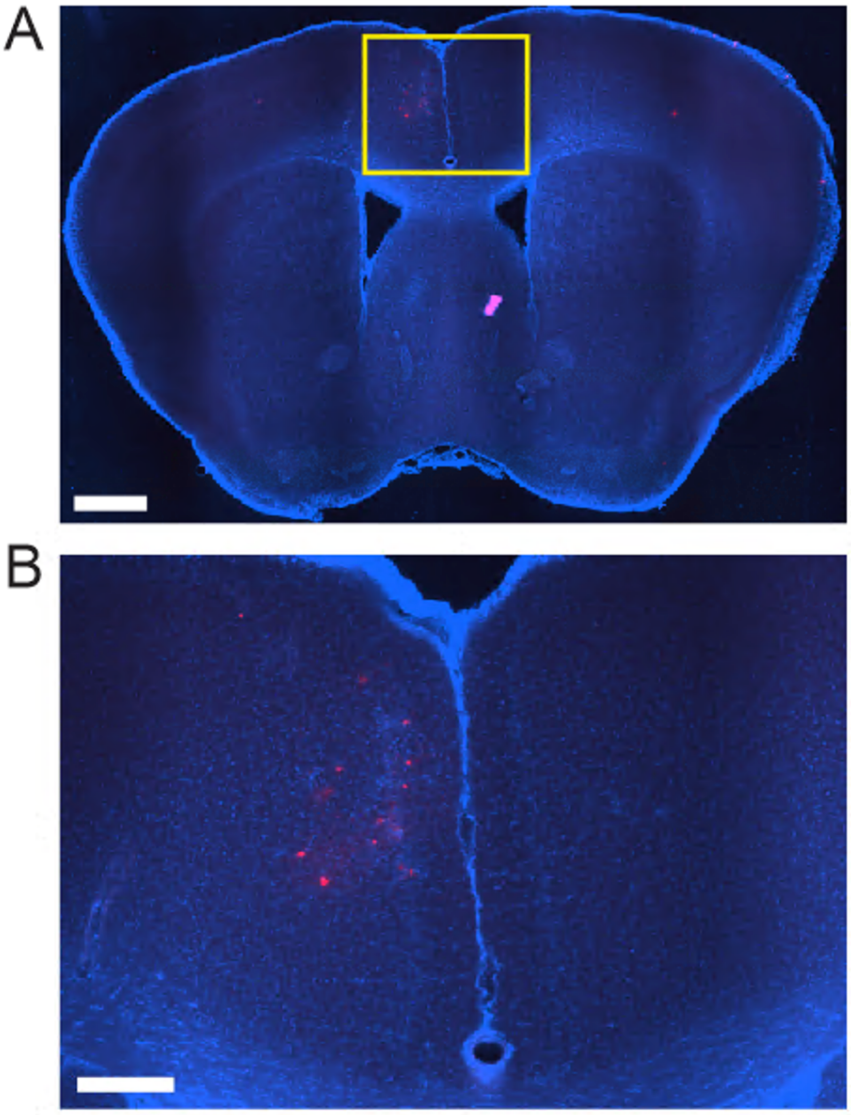

Figure 6.3: Leakage of rabies virus is restricted to the injection site. AAV-TVA-Glyco-GFP and RV*dG* were injected into the ACC of Cre- mice to determine whether labelling was Cre-specific. (A-B) Representative brain section at the viral hotspot. Blue: DAPI, red: RV*dG* expressing cells. Left hemisphere: injection site, right hemisphere: contralateral ACC. (A) Image of the full brain section. Scale bar = 100 µm. (B) Zoomed image from the yellow boxed region in (A). Scale bar = 50 µm. Note: Injections, histology, and imaging performed by Kelly Wingfield. Figure made by Lisa Kretsge and not previously published.

6.2.2 Mapping Mono-synaptic Inputs to VIP^{ACC} Reveals Widespread Connections

To determine whether VIP^{ACC} receive projections from other brain areas involved in anxiety and social behavior, we used rabies virus-mediated trans-synaptic mapping (Figure 6.1). Using the techniques outlined above, we quantified the starter and input cells throughout the brains of VIP-Cre mice and normalized the number of input cells to starters for each animal. We found retrogradely-labeled neurons were most prominent in other regions of the PFC (about 18% of all labeled regions), primary and associative areas (prim/asso), thalamic nuclei, and the medial septal complex (MSC), suggesting that these regions were highly connected to VIP^{ACC} (Figure 6.4, A). We further partitioned the regions with the greatest number of retrogradely-labeled neurons into subregions and determined that VIP^{ACC} received connections from the contralateral (cl) ACC (77% of retrogradely-labeled PFC neurons, Figure 6.4, B), prelimbic cortex (PrL, 12% of retrogradely-labeled PFC neurons, Figure 6.4, B), retrosplenial cortex (RS, including RS granular (RSG) and dysgranular (RSD), 86% of retrogradely-labeled prim/asso neurons, Figure 6.4, C), anteromedial thalamic nucleus (AM) (46% of retrogradely-labeled thalamic neurons, Figure 6.4, D), and lateral posterior thalamic nucleus medio rostral part (LPMR, 8% of retrogradely-labeled thalamic neurons, Figure 6.4, D). Our data show that VIP^{ACC} receive long-range projections, not only from regions implicated in emotional regulation and social cognitive behavior, but also areas important for neuromodulation, memory formation, and motor actions. In addition, they demonstrate connectivity from areas of cortex and thalamus that support existing studies that mapped inputs to the ACC without cell type specificity (Shibata, 1993; Shibata, 1993; Shibata & Naito, 2005;

Shibata, Kondo, & Naito, 2004; Allen Institute for Brain Science, 2011; Jones, Groenewegen, & Witter, 2005).

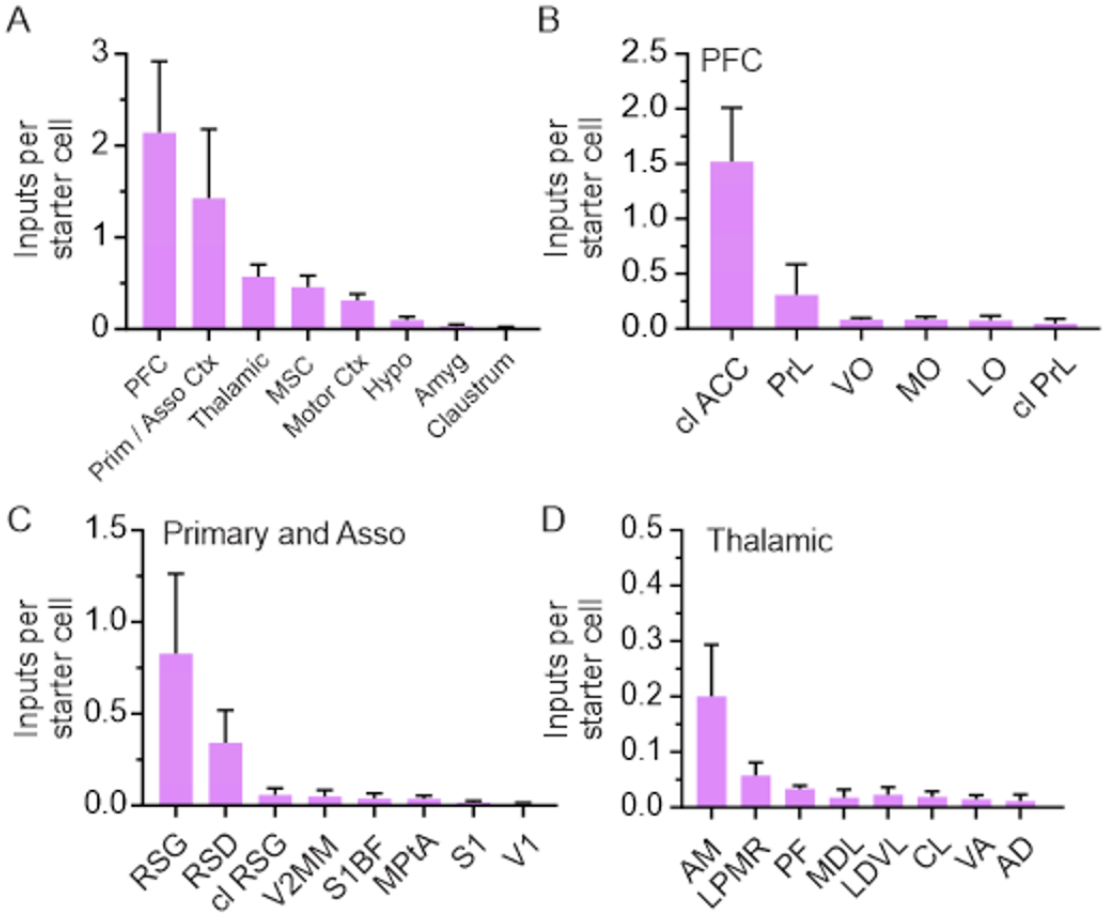

Figure 6.4: VIP^{ACC} receive inputs from brain regions implicated in emotional control and social behaviors. Regions that are the most highly connected to VIP^{ACC}. (A) Rabies trans-synaptic mapping revealed that the prefrontal Ctx (PFC), primary and association Ctx (Prim/asso), thalamic regions, and MSC are highly connected to VIP^{ACC}. (B-D) Highly connected areas (PFC, B, Prim/asso, C, thalamic, D) divided into subregions. Error bars represent SEM. N = 6 mice for Ca^{2+} imaging, n = 345 cells for EZM, n = 310 cells for Sociability. For tracing experiments, N = 3 mice with n = 705 starter cells and 10107 input cells. All images are representative. Hypo: hypothalamus, Amyg: amygdala, cl: contralateral, PrL: prelimbic Ctx, VO: ventral orbital Ctx, MO: medial orbital Ctx, LO: lateral orbital Ctx, RSG: retrosplenial granular Ctx, RSD: retrosplenial dysgranular Ctx, V2MM: secondary visual Ctx mediomedial area, S1BF: primary somatosensory Ctx barrel field, MPtA: medial parietal association Ctx, S1: primary somatosensory Ctx, V1: primary visual Ctx, LPMR: lateral posterior thalamic nucleus medio rostral part, PF: parafascicular thalamic nucleus, MDL: mediodorsal thalamic nucleus lateral part, LDVL: laterodorsal thalamic nucleus ventrolateral part, CL: centrolateral thalamic nucleus, VA: ventral anterior thalamic nucleus, AD: anterodorsal thalamic nucleus. Note: Surgeries performed by Connor Johnson, Tushare Jinadasa, and Erelle Fuchs. Histology, imaging, and cell counting performed by Lisa Kretsge, Tushare Jinadasa, Erelle Fuchs, Eli Spevack, Berta Escude Velasco, and Frances Hausmann. Data analyzed by Lisa Kretsge, Connor Johnson, and Tushare Jinadasa. Figure made by Lisa Kretsge, Tushare Jinadasa, and Alberto Cruz-Martín. Figure published in Johnson, Kretsge & Yen et al., *BioRxiv*, 2020.

6.2.3 Long-range Inputs to ACC Cells Differ Across Interneuron Subtypes

Next, we aimed to determine whether patterns of connectivity differ between interneuron subtypes in the ACC. To answer this question, we employed the same rabies tracing methods as described above (Figure 6.1) in 3 different Cre line mouse strains (Figure 6.5). By injecting AAV-TVA-Glyco-GFP and RV*dG* into the ACC of either VIP-Cre, SOM-Cre, or PV-Cre mice, we were able to visualize brain-wide inputs to all 3 cell types (Figure 6.5).

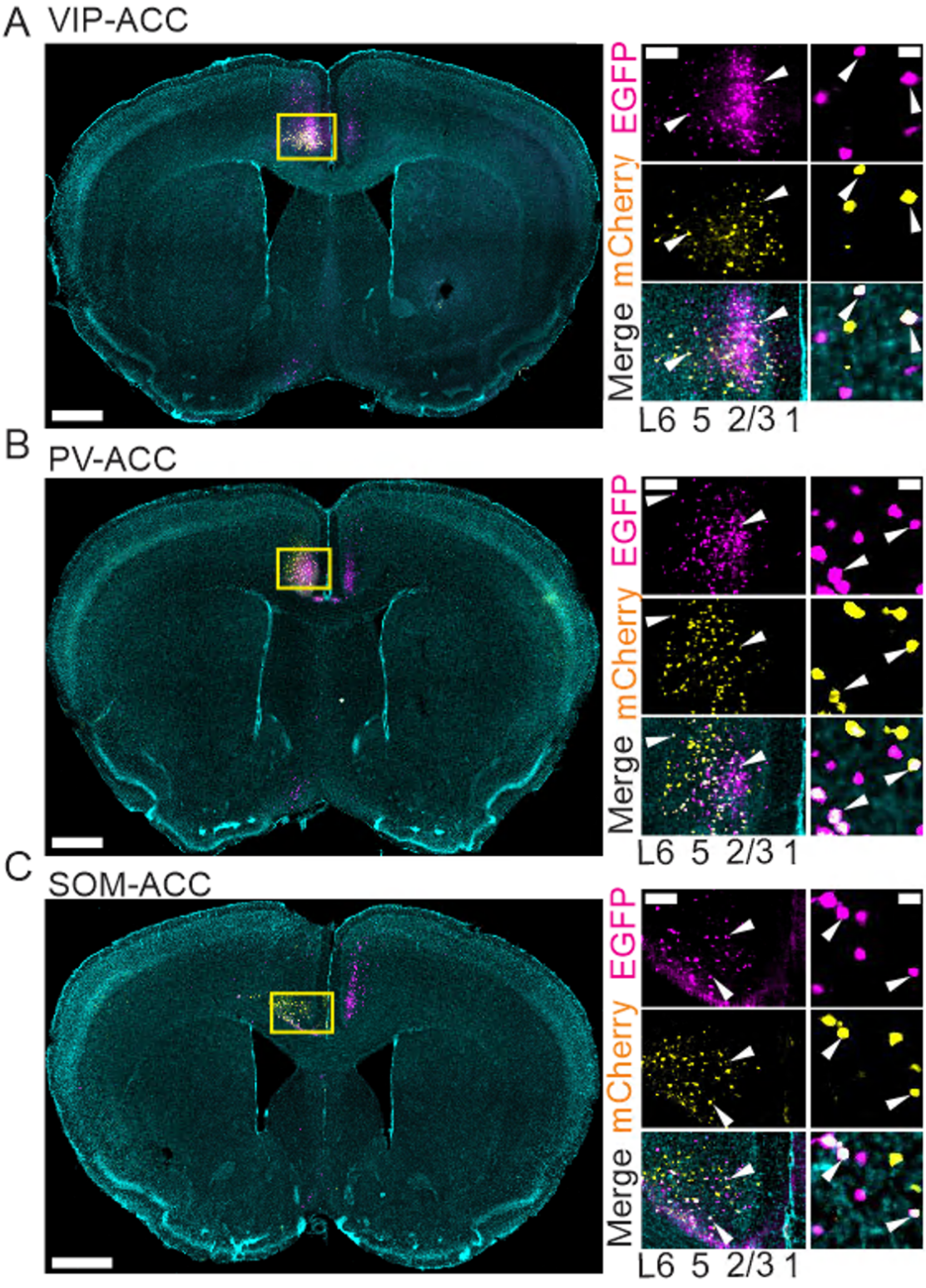
A VIP-ACC
B PV-ACC
C SOM-ACC
EGFP
mCherry
Merge
L6 5 2/3 1

Figure 6.5: Rabies tracing labels inputs to different interneuron subtypes in the ACC. Images of injection sites for trans-synaptic tracing experiments in VIP-Cre (A), PV-Cre (B), and SOM-Cre (C) mice. Starter cells express both EGFP (pseudo colored magenta, also expressing TVA and ΔG) and mCherry (pseudo colored yellow, infected by RV*dG)*. Retrogradely-labeled input cells only express mCherry. Coronal sections. Left: full section showing overlay of both fluorophores and DAPI (cyan). Scale bar = 100 μm. Middle: zoomed version of yellow boxed region showing viral expression in layers I-VI in ACC. White arrows: starter cells. Scale bar = 50 um. Right: zoomed images to show overlap (starter cells, white arrows). Scale bar = 15 μm. Surgeries performed by Connor Johnson, Tushare Jinadasa, and Erelle Fuchs. Histology, imaging, and cell counting performed by Lisa Kretsge, Tushare Jinadasa, Erelle Fuchs, Eli Spevack, Berta Escude Velasco, Frances Hausmann, Kelly Wingfield, Charlotte Yeung, Rhushikesh Phadke, Alison Brack, and Luke Fournier. Data analyzed by Lisa Kretsge. Figure made by Lisa Kretsge. Figure not published.

The numbers of input and starter cells varied widely by cell type, but all data presented here are normalized to the number of starter cells per animal (total starters for VIP: 705, SOM: 567, and PV: 1770; total inputs for VIP: 10107, SOM: 18270, and PV: 69447). Each cell type demonstrated different numbers of inputs labeled per starter, as well (inputs per starter cell for VIP: 14.63, SOM: 33.40, and PV: 40.00). For all 3 cell types, the vast majority of starter cells were successfully targeted to the ACC, rather than adjacent brain regions (percent of starters in ACC for VIP: 98.01%, SOM: 96.47%, and PV: 98.09%). Starter cells were distributed throughout all layers of cortex, with the highest number of starters located in L2/3 and L5 for VIP and PV, but similar proportions of starters in L2/3, 5, and 6 for SOM (Figure 6.6).

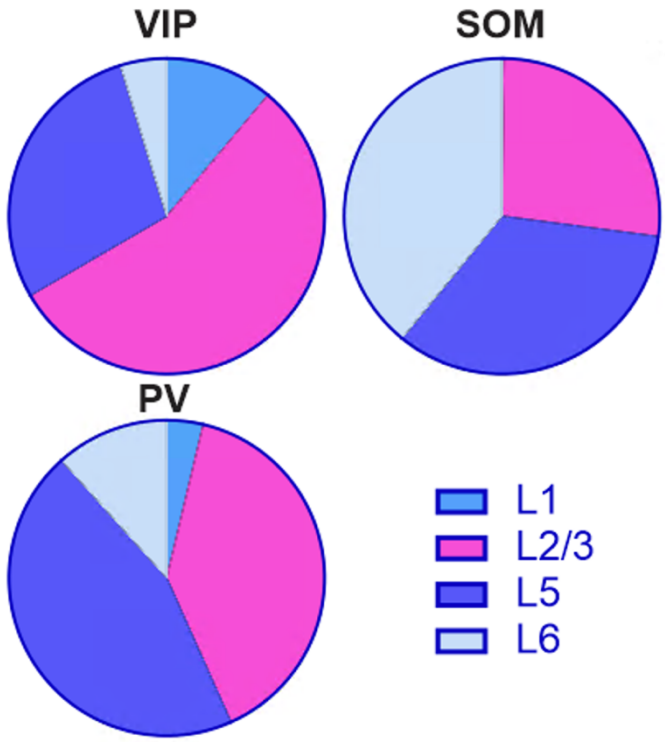

Figure 6.6: Starter cells are dispersed across cortical layers. Pie charts demonstrate the average percentage of starter cells in each cortical layer for all mice of a given Cre-line. Starters were identified and quantified for VIP-Cre (top left), SOM-Cre (top right), and PV-Cre (bottom left) mice. Legend (bottom right) shows which color corresponds to each cortical layer. Surgeries performed by Connor Johnson, Tushare Jinadasa, and Erelle Fuchs. Histology, imaging, and cell counting performed by Lisa Kretsge, Tushare Jinadasa, Erelle Fuchs, Eli Spevack, Berta Escude Velasco, Frances Hausmann, Kelly Wingfield, Charlotte Yeung, Rhushikesh Phadke, Alison Brack, and Luke Fournier. Data analyzed by Lisa Kretsge, Rhushikesh Phadke, and Luke Fournier. Figure made by Lisa Kretsge. Figure not previously published.

Input neurons were quantified and graphed for the most highly labelled brain regions with the most input cells for each cell type (Figure 6.7) and for the top subregions within those larger areas (Figure 6.8). Primary and association cortex was the top region for VIP^{ACC}, SOM^{ACC}, and PV^{ACC} (Figure 6.7, A). The regions with the second and third

most inputs varied across cell types, where VIP^{ACC} received the most inputs from the PFC and thalamus, SOM^{ACC} received the most inputs from the MSC and motor cortex, and PV^{ACC} received most of their inputs from the PFC and motor cortex (Figure 6.7, A).

The three interneuron subtypes also showed different patterns in their most highly connected subareas (Figure 6.7, B). Some inputs regions were consistent across all 3 interneuron subtypes. For example, retrosplenial granular cortex (RSG), retrosplenial dysgranular cortex (RSD), and secondary motor cortex (M2) were within the top 5 labelled areas for VIP, SOM, and PV (Figure 6.7, B). However, some of the top 5 most connected regions differed by cell type. The top 5 subregions labelled included the nucleus of the horizontal limb of the diagonal band (HDB) for VIP and SOM, but not PV (Figure 6.7, B). They also included prelimbic cortex (PrL) for VIP, but neither other cell type, dorsal subiculum (DS) only for SOM, and secondary visual cortex mediomedial area (V2MM) and ventral orbital cortex (VO) only for PV (Figure 6.7, B).

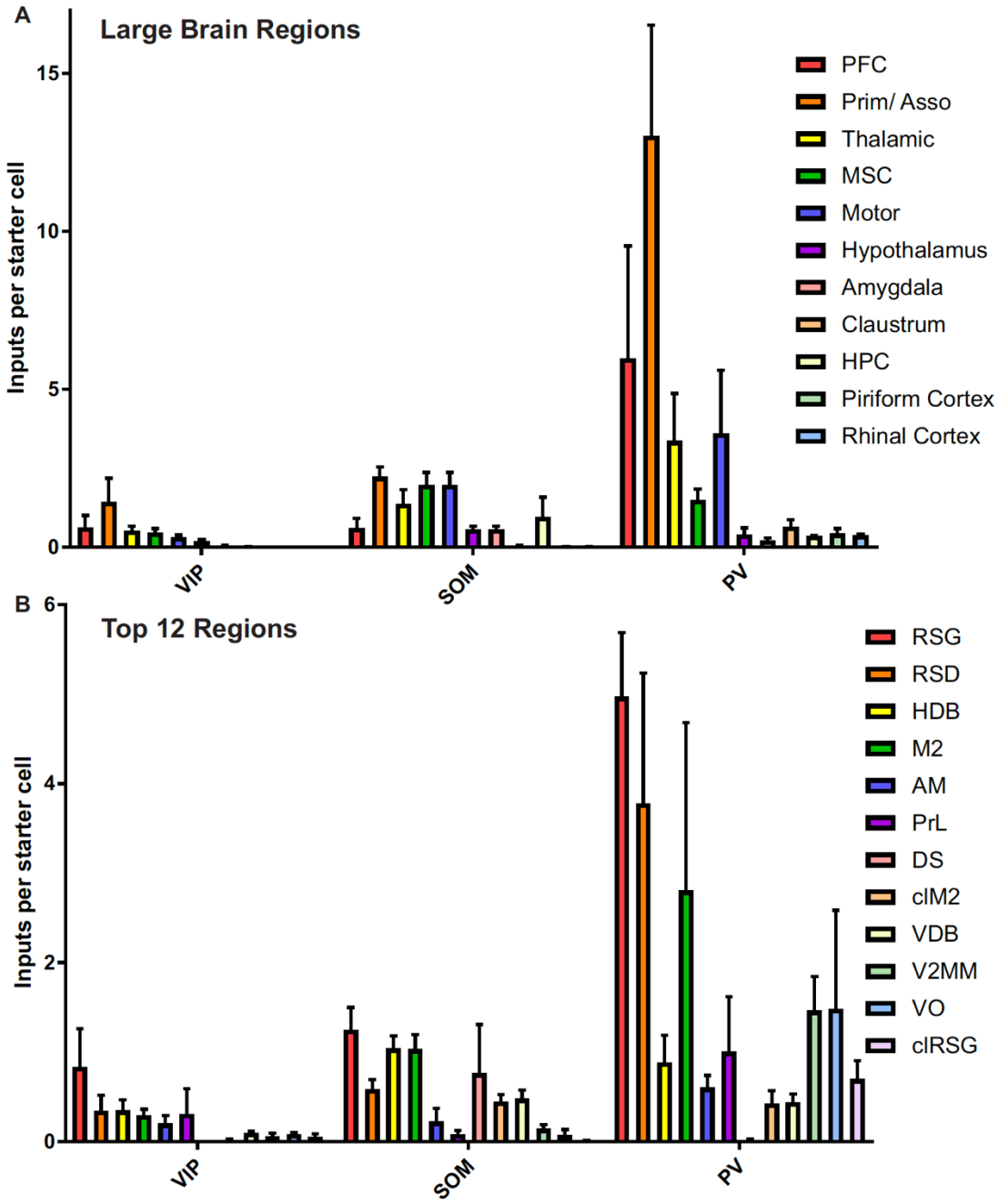
A
Large Brain Regions
Inputs per starter cell
15
10
5
0
VIP
SOM
PV
PFC
Prim/ Asso
Thalamic
MSC
Motor
Hypothalamus
Amygdala
Claustrum
HPC
Piriform Cortex
Rhinal Cortex
B
Top 12 Regions
Inputs per starter cell
6
4
2
0
VIP
SOM
PV
RSG
RSD
HDB
M2
AM
PrL
DS
clM2
VDB
V2MM
VO
clRSG

Figure 6.7 Large brain regions and top regions for inputs to VIP^{ACC}, SOM^{ACC}, and PV^{ACC}. Rabies trans-synaptic mapping revealed brain regions that are highly connected to VIP^{ACC}, SOM^{ACC}, and PV^{ACC}. (A) Large brain regions that are the most highly connected to VIP^{ACC}, SOM^{ACC}, and PV^{ACC} include the prefrontal Ctx (PFC), primary and association Ctx (Prim/asso), thalamic regions, motor cortex and MSC. (B) The most highly connected regions to ACC interneurons. Error bars represent SEM. For VIP cells: N = 3 mice with n = 705 starter cells and 10107 input cells. For SOM cells: N = 3 mice with n = 567 starter cells and 18270 input cells. For PV cells: N = 3 mice with n = 1770 starter cells and 69447 input cells. Ctx: cortex, MSC: medial septal complex, Motor: motor cortex, HPC: hippocampus, RSG: retrosplenial granular Ctx, RSD: retrosplenial dysgranular Ctx, HDB: nucleus of the horizontal limb of the diagonal band, M2: secondary motor cortex, AM: anteromedial thalamic nucleus, PrL: prelimbic Ctx, DS: dorsal subiculum, cl: contralateral, VDB: nucleus of the vertical limb of the diagonal band, V2MM: secondary visual Ctx mediomedial area, VO: ventral orbital Ctx. Note: Surgeries performed by Connor Johnson, Tushare Jinadasa, and Erelle Fuchs. Histology, imaging, and cell counting performed by Lisa Kretsge, Tushare Jinadasa, Erelle Fuchs, Eli Spevack, Berta Escude Velasco, Frances Hausmann, Kelly Wingfield, Charlotte Yeung, Rhushikesh Phadke, Alison Brack, and Luke Fournier. Data analyzed by Lisa Kretsge. Figure made by Lisa Kretsge. Figure not published.

We next examined connectivity to VIP^{ACC}, SOM^{ACC}, and PV^{ACC} in subareas within the frontal cortex, primary and association cortex, and thalamic nuclei (Figure 6.8). Again, some connectivity patterns were consistent across cell type; for example, within retrosplenial connectivity all cell types were most highly connected to RSG, then to RSD, and then to clRSG (Figure 6.8, B). Nonetheless, some cell-type specific differences emerged, like which thalamic subareas were most highly connected to each interneuron type (Figure 6.8, E). All 3 interneuron subtypes received extensive projections from the anteromedial thalamus (AM), but VIP^{ACC} received most other thalamic connections from the lateral posterior thalamic nucleus mediorostral part (LPMR) and parafascicular thalamic nucleus (PF), SOM^{ACC} received most from

anterodorsal thalamic nucleus (AD) and mediodorsal thalamic nucleus lateral part (MDL), and PV^{ACC} received the most from ventrolateral thalamic nucleus (VL) and centrolateral thalamic nucleus (CL) (Figure 6.8, E). Overall, these data from VIP, SOM, and PV demonstrate that connectivity patterns are not consistent across interneuron subtypes within the ACC. Each subtype receives projections from different long-range circuits and may therefore be involved in different functional roles, as well.

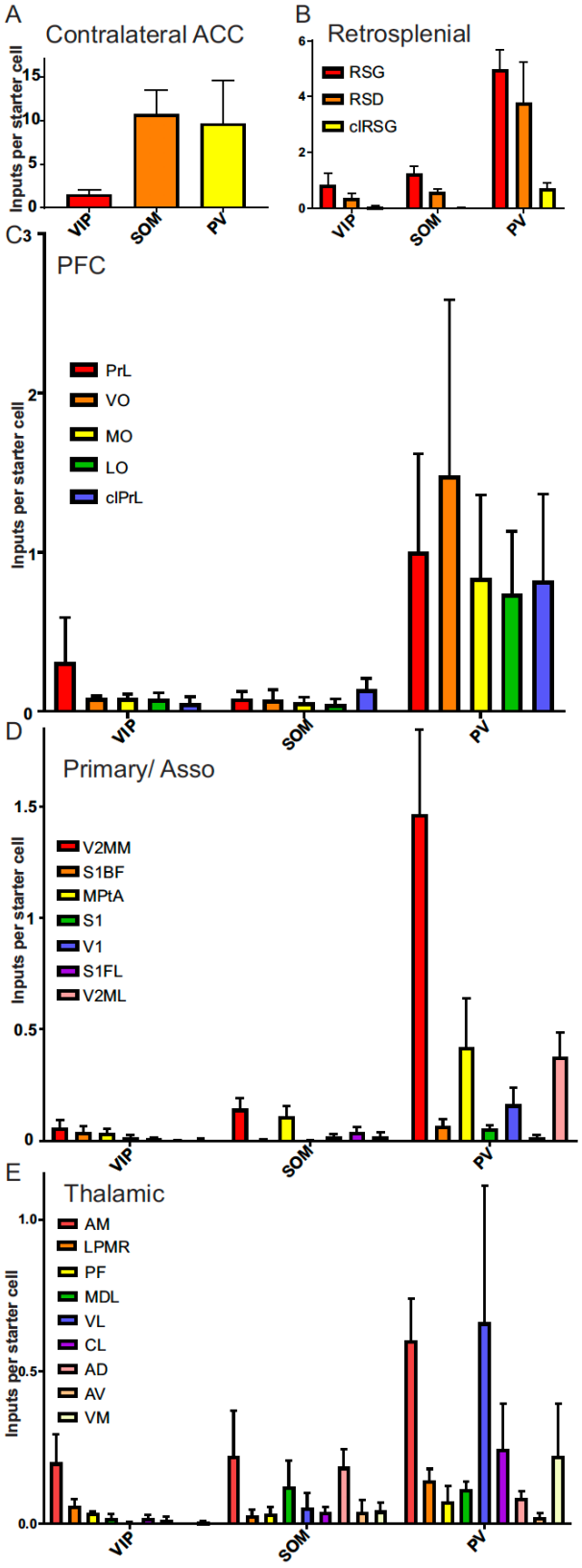
A
Contralateral ACC
Inputs per starter cell
15
10
5
0
VIP
SOM
PV
B
Retrosplenial
RSG
RSD
clRSG
6
4
2
0
VIP
SOM
PV
C3
PFC
PrL
VO
MO
LO
clPrL
Inputs per starter cell
2
1
0
VIP
SOM
PV
D
Primary/ Asso
V2MM
S1BF
MPtA
S1
V1
S1FL
V2ML
Inputs per starter cell
1.5
1
0.5
0
VIP
SOM
PV
E
Thalamic
AM
LPMR
PF
MDL
VL
CL
AD
AV
VM
Inputs per starter cell
1.0
0.5
0.0
VIP
SOM
PV

Figure 6.8: Subareas of cortex and thalamus with inputs to VIP^{ACC}, SOM^{ACC}, and PV^{ACC}. Subregions of prefrontal Ctx (PFC), primary and association Ctx (Prim/asso), and thalamus that are the most highly connected to VIP^{ACC}, SOM^{ACC}, and PV^{ACC} as determined using rabies trans-synaptic tracing. Inputs from (A) contralateral ACC (clACC), (B) retrosplenial Ctx, (C) PFC, (D) Prim/asso Ctx, and (E) thalamic regions. Error bars represent SEM. For VIP cells: N = 3 mice with n = 705 starter cells and 10107 input cells. For SOM cells: N = 3 mice with n = 567 starter cells and 18270 input cells. For PV cells: N = 3 mice with n = 1770 starter cells and 69447 input cells. Ctx: cortex, RSG: retrosplenial granular Ctx, RSD: retrosplenial dysgranular Ctx, cl: contralateral, PrL: prelimbic Ctx, VO: ventral orbital Ctx, MO: medial orbital Ctx, LO: lateral orbital Ctx, V2MM: secondary visual Ctx mediomedial area, S1BF: primary somatosensory Ctx barrel field, MPtA: medial parietal association Ctx, S1: primary somatosensory Ctx, V1: primary visual Ctx, S1FL: primary somatosensory Ctx, forelimb region, V2ML: secondary visual Ctx mediolateral area, AM: anteromedial thalamic nucleus, LPMR: lateral posterior thalamic nucleus medio rostral part, PF: parafascicular thalamic nucleus, MDL: mediodorsal thalamic nucleus lateral part, VL: ventrolateral thalamic nucleus, CL: centrolateral thalamic nucleus, AD: anterodorsal thalamic nucleus, AV: anteroventral thalamic nucleus, VM: ventromedial thalamic nucleus. Note: Surgeries performed by Connor Johnson, Tushare Jinadasa, and Erelle Fuchs. Histology, imaging, and cell counting performed by Lisa Kretsge, Tushare Jinadasa, Erelle Fuchs, Eli Spevack, Berta Escude Velasco, Frances Hausmann, Kelly Wingfield, Charlotte Yeung, Rhushikesh Phadke, Alison Brack, and Luke Fournier. Data analyzed by Lisa Kretsge. Figure made by Lisa Kretsge. Figure not published.

6.3 Conclusion and Future Directions

Using rabies trans-synaptic mapping, we provided a brain-wide map of inputs to three different interneuron subtypes in the ACC. Using different genetic Cre mouse lines, we identified which brain regions send projections specifically to VIP^{ACC}, SOM^{ACC}, and PV^{ACC}. Prior experiments used classic neural tracers to identify inputs to the whole ACC without cell type specificity (Shibata, 1993; Shibata & Naito, 2005; Shibata, Kondo, & Naito, 2004; Jones, Groenewegen, & Witter, 2005). Our work replicates some of these findings, such as high connectivity from AM and RS to all three interneuron types (Shibata, 1993; Shibata & Naito, 2005; Shibata, Kondo, & Naito, 2004; Jones, Groenewegen, &

Witter, 2005). We also found connections between VIP^{ACC} and brain areas that have been implicated in anxiety-related, social, and cognitive behaviors. These circuits may therefore be especially important in execution of these different behaviors. By investigating all three cell types, we showed that some brain regions are highly connected to all three cell types (like RS and AM), but there are some unique connections that vary dramatically by cell type. These data support previous findings that different cell types within the same brain region do not necessarily receive the same long-range inputs (Sun et al., 2019). For example, aside from AM, the thalamic regions that were most highly connected to the ACC varied largely by interneuron type. VIP^{ACC} received more thalamic connections from the LPMR and PF, SOM^{ACC} received more from some more dorsal thalamic regions (AD and MDL), and PV^{ACC} received more from lateral subareas (VL and CL) (Figure 6.8, E). This suggests ACC interneuron subtypes maybe be a part of different neural circuits and may even be important to different behaviors.

This work presents the first brain-wide maps of inputs to ACC interneurons and the first data showing VIP, SOM, and PV cells within the ACC do not have identical patterns of connectivity. Better understanding cell-type specific neural connectivity provides a much fuller understanding of neural circuitry and provides a framework to further investigate the role of distinct ACC circuits in behavior. With the knowledge that VIP^{ACC} receive extensive projections from AM and RS, future work could interrogate these circuits and their impact on animal behavior. For example, the AM has been linked memory formation (Van der Werf et al., 2000; Perry & Mitchell, 2019; Tanimizu et al., 2017), and we have shown that some VIP^{ACC} are recruited during interactions with familiar or novel

social stimuli, so AM-VIP^{ACC} projections may be important for social memory. Previous research has shown a role for AM-ACC projections in itch-induced scratching behavior (Deng et al., 2020), but it remains plausible that this network could be composed of different pathways for parallel processing of different stimuli (Cruz-Martin et al., 2014). Alternatively, future research could focus on the RS-VIP^{ACC} circuit. The RS is involved in learning, autobiographical and fear memories, and navigation (Van der Werf et al., 2000; Vann, Aggleton, & Maguire, 2009; Fischer et al., 2020; Alexander et al., 2020; Corcoran et al., 2011), so this pathway may be important for normal exploration of anxiety-related and social arenas. Manipulation of this circuit could impair memory of (and therefore time spent interacting with) stimulus locations or arm types. We also showed high connectivity between VIP^{ACC} with PFC and clACC. This replicates findings from human imaging studies that highlight the importance of ACC-PFC networks (Gehrig & Knight, 2000; Etkin et al., 2006). These circuits seem to play a role in emotional processing (Etkin et al., 2006) and may therefore be especially important in better understanding anxiety-related behaviors and pathology.

Future examination of the AM-VIP^{ACC}, RS-VIP^{ACC}, or PFC-VIP^{ACC} pathways may show different behavioral relevance than the overall AM, RS, or PFC to ACC pathways that include all cell types. Because our work has shown a role of some VIP^{ACC} in anxiety-related, social, and non-social behaviors, interrogation of these distinct subcircuits may reveal different effects on animal behavior that elucidate ACC encoding of diverse stimuli at the level of the long-range neural circuit. To test this, future work could manipulate VIP^{ACC}-specific circuits by injecting Cre-dependent retrograde optogenetic AAVs

(Addgene #84445-AAVrg, Addgene #20298-AAVrg) into the ACC of VIP-Cre mice. This strategy would make it possible to activate or inhibit retrogradely labelled input cells in the AM, RS, or PFC. In VIP-Cre mice, these viruses would infect VIP^{ACC} and travel retrogradely to their input cells. By implanting optical fibers in either the AM, RS, or PFC, one could limit optogenetic activation or inhibition to AM-VIP^{ACC}, RS-VIP^{ACC}, or PFC-VIP^{ACC} pathways. During optogenetic manipulation, animals could undergo anxiety-related, social behavioral, or object recognition testing to determine the impact of each precise circuit on these varied behaviors.

CHAPTER SEVEN

Concluding Remarks and Future Directions

7.1 Functional Heterogeneity and Cortical Information Processing

7.1.1 VIP^{ACC} are a Functionally Heterogeneous Population

Using in vivo Ca^{2+} imaging with cellular resolution in freely behaving mice, we showed that VIP cells in the ACC are made up of distinct subcircuits that encode for the animal's behavioral state or their interactions with various stimuli. In the OF and EZM, ROC analysis identified stimulus-selective VIP^{ACC} that encoded anxiety-related information. Using the same approach, we identified stimulus-selective cells that encoded for interactions with familiar and novel mice, as well as with objects. We did not find a difference in the overall activity of VIP^{ACC} as animals navigated anxiogenic, anxiolytic, social, or non-social stimuli. These data are the first to analyze VIP^{ACC} activity in vivo with cellular resolution. This work demonstrates functional heterogeneity, not just within the ACC, but even within one interneuron subtype in the ACC.

7.1.2 The Significance of Cortical Heterogeneity

Heterogeneity is a critically important concept in how we understand VIP cells. Prior work has shown that VIP cells in other brain regions can have dissimilar molecular, electrophysiological, and morphological properties (Ferezou et al., 2002; Cauli et al., 1997; Gonchar, Wang, & Burkhalter, 2008; Kawaguchi & Kubota, 1997; Ketchesin, Huang, & Seasholtz, 2017; Obermayer et al., 2019; Porter et al., 1999; Tasic et al., 2016; Tasic et al.,

2018). Our data show that this heterogeneity extends to functional properties in the ACC, as well. It remains to be seen whether functional subpopulations of VIP^{ACC} share similarities in their other characteristics that could more easily be used to identify them. If there are different subgroups of VIP^{ACC} with distinct characteristics and functional roles, it may become less useful to group VIP cells together to study them and it may be a better practice to separate them into even smaller, more precisely defined cell types.

Our data support some previous findings that identified social-selective and non-social-selective subgroups of neurons in the PFC (Liang et al., 2018; Frost, Haggart, & Sohal, 2021). One explanation for these previous findings could be that these datasets likely included recordings from both interneurons and Pyr in PFC, rather than isolating distinct cell types. For example, the heterogeneity found by Liang et al. (2018) and Frost, Haggart & Sohal (2021) could reflect a network of activity where VIP and Pyr cells are largely prosocial, but PV and SOM cells are selectively active during non-social behaviors. In the context of our data, however, it is not probable that would be enough to explain the subpopulations found in prior datasets (Liang et al., 2018; Frost, Haggart, & Sohal, 2021). Instead, it seems more likely that different subpopulations within classically defined cortical cell types activate to different kinds of stimuli. Our data suggest that a more likely explanation of the heterogeneity data in the PFC is that clusters of cortical neurons, even those defined as the same cell type, activate preferentially to different stimuli. It may be possible to extrapolate these findings to broadly understand how complex information is processed across cortical regions, but further work would need to repeat similar

experiments in other regions of cortex to determine whether these effects are specific to the ACC or to VIP cells.

Our work calls into question how to interpret previous findings that pooled data from all VIP cells or all ACC cells together. Our results highlight the importance of techniques that allow for cell-type specific analyses and cellular resolution in studies of cortical activity. Without these technical innovations, it would be impossible to decipher any differences between VIP^{ACC} subpopulations. Because individual VIP cells are known to disinhibit subgroups of Pyr, VIP heterogeneity may be an important feature of the local circuit that leads to stimulus-specific activity in clusters of Pyr (Pi et al., 2013; Karnani et al., 2016). Following the hypothesis that functional heterogeneity may be a feature of other ACC cell types, future studies could re-examine prior imaging data in the ACC that was acquired without cellular resolution. For example, prior work demonstrates overall increased Pyr activity during socialization using fiber photometry (Guo et al., 2019). Reassessing this finding with techniques that provide cell-level data would allow us to determine whether the majority of individual Pyr are social-stimulus selective. Future studies could also use GCaMP in VIP cells and a red calcium indicator (RCaMP or RGECO) in Pyr to simultaneously image both populations. This would provide temporal information that could elucidate whether stimulus-specific changes in VIP^{ACC} subpopulation activity precedes changes in the activity of distinct Pyr clusters. One caveat of using Ca^{2+} imaging in our work is that we can only visualize VIP^{ACC} with bright expression of GCaMP6f. Cells that are minimally active may be hard to detect due to their lack of fluorescence, so the data presented here may preferentially reflect the more highly

active VIP^{ACC} cells. Investigating heterogeneity in both cell types would provide a fuller picture of how the ACC encodes information and may inform our understanding of general cortical information processing.

7.1.3 Neuromodulation of VIP Interneurons

While the current study addressed functional heterogeneity in VIP^{ACC} cells, prior research has identified many other ways in which VIP cells can differ from one another. Some VIP interneurons express neuromodulator receptors, and these receptors are not uniformly expressed across all VIP cells (Porter et al., 1999; Tasic et al., 2016; Tasic et al., 2018; Obermayer et al., 2019; Bayraktar et al., 1997; Gonchar, Wang, & Burkhalter, 2008; Ferezou et al., 2002; Drake & Milner, 2002). Subpopulations of VIP cells have been shown to express genes or proteins of nicotinic ACh receptors or ChAT, serotonergic receptors, noradrenergic signaling, or opioid signaling (Porter et al., 1999; Tasic et al., 2016; Tasic et al., 2018; Obermayer et al., 2019; Bayraktar et al., 1997; Gonchar, Wang, & Burkhalter, 2008; Ferezou et al., 2002; Drake & Milner, 2002). For example, about 15% of cortical VIP cells are positive for ChAT (Obermayer et al., 2019; Bayraktar et al., 1997; Tasic et al., 2018; Gonchar, Wang, & Burkhalter, 2008) and about 30% are positive for 5-HT receptors (Ferezou et al., 2002). Using electrophysiological or Ca^{2+} activity recordings with pharmacological manipulations, it has been shown that ACh and 5-HT are both able to modulate the activity of some VIP interneurons clusters (Ferezou et al., 2002; Poorthuis, Enke, & Letzkus, 2014; Pronneke et al., 2020; Fu et al., 2014).

Our data from the Social Novelty and Novel Object tasks showed approximately 20% of VIP^{ACC} are engaged by novel social stimuli about 20% are engaged by a novel object. Neuromodulator receptors, like those for norepinephrine, may allow VIP interneurons to respond selectively to novel stimuli. Locus coeruleus (LC) neurons, the primary source of norepinephrine in the forebrain, are recruited by novel stimuli, so this neuromodulator and brain region may be important in novelty encoding (Gompf et al., 2010; Uematsu, Tan, & Johansen, 2015). Additionally, the encoding of novel stimuli may be linked to overall arousal. Normally, mice exhibit elevated arousal (behaviorally and in electroencephalogram recordings) when exposed to novel stimuli, but this effect is diminished in animals with ACC or LC lesions (Gompf et al., 2010). Noradrenergic modulation of VIP^{ACC} may be a substrate for novelty or arousal (Gompf et al., 2010). In the cortex, norepinephrine differentially regulates the activity of interneurons (Kawaguchi & Shindou, 1998; McCormick & Prince, 1988), but it is unknown whether recruitment of VIP^{ACC} by novel social or non-social stimuli is dependent on particular neuromodulators.

Neuromodulation may allow long-range projections to alter VIP^{ACC} activity in a task-dependent manner (Lee et al., 2013; Melzer et al., 2020; Karnani et al., 2016). Our data showed that subgroups of VIP^{ACC} are engaged by particular stimuli. Through the actions of neuromodulators, VIP interneurons in the ACC may recruit subpopulations of Pyr that are behaviorally relevant or encode specific information. Future studies could administer agonists or antagonists of serotoninergic, nicotinic or noradrenergic receptors in animals implanted with miniscopes to determine how these neuromodulators impact the

activity of stimulus-specific VIP^{ACC} and animal behavior in anxiety-related and social tasks.

7.1.4 Molecular, Genetic, and Morphological Heterogeneity in VIP Interneurons

In addition to discrepancies in neuromodulation, subpopulations of stimulus-selective VIP^{ACC} may be identifiable by their molecular, genetic, or morphological differences. Some VIP interneurons exhibit distinct dendritic and axonal branching patterns (Pronneke et al., 2015). These features differ across cortical layers (Pronneke et al., 2015) and our experiments were not layer-specific. The field of view in our imaging experiments was large (800 μm × 600 μm), almost spanning all cortical layers (I-VI). Because of this, our data likely include VIP^{ACC} across cortical layers and therefore with different morphologies. Future studies could assess laminar differences in VIP^{ACC} function by registering in vivo cell images with histology to determine the location of selective cells.

In addition, functional VIP^{ACC} subgroups may express unique genes or protein markers. In other regions of cortex, some VIP express combinations of the proteins ChAT, CCK, and CR, which have been linked to differences in morphology or electrophysiology (Obermayer et al., 2019; Gonchar, Wang, & Burkhalter, 2008; Kawaguchi & Kubota, 1997; Ferezou et al., 2002; Cauli et al., 1997). In addition, transcriptomic data show that VIP interneurons can be subdivided into many groups based on differences in their genetics (Tasic et al., 2016; Tasic et al., 2018; Hodge et al., 2019). Recent studies have divided VIP cells into over 20 groups with a wide range of genetic profiles, but one finding of particular interest was the array of genes related to

neuromodulation, including those involved in ACh and Oxt signaling (Tasic et al., 2016; Tasic et al., 2018). It remains possible that VIP diversity in neuromodulatory signaling (involving ACh, Oxt, 5-HT, or opioid signaling) may differentiate VIP^{ACC} functions in varied behaviors. For example, ACh is linked to attention, memory, and cognition, Oxt to socialization, and enkephalin to social memory (Hasselmo, 2006; Hasselmo & McGaughy, 2004; Sarter & Bruno, 1997; Heinrichs, von Dawans, & Domes, 2009; Feldman, 2012; Leroy et al., 2021). From these previous findings in other brain regions and cell types, one could hypothesize that, for example, Oxt+ VIP^{ACC} may be preferentially recruited in social behaviors, so these cells may be more likely to be the littermate-selective or novel mouse-selective neurons found in our data. Because our work was the first to monitor the activity of individual VIP^{ACC} in awake, behaving animals, it is not known whether these molecular or morphological profiles correspond to different functional properties. Future work should aim to identify any characteristics that can differentiate VIP^{ACC} subpopulations with different stimulus-selectivity from one another. To achieve this, experimenters could perform Ca^{2+} imaging and then label genes or proteins of interest using in situ hybridization or immunohistochemistry, respectively. Registration of in vivo imaging and stained slices of brain tissue could allow researchers to match stimulus-selective cells with genes or proteins that may be highly expressed in only some functional subpopulations. If there were markers that differentiated anxiolytic versus anxiogenic-selective cells, for example, that would provide a much more specific target for therapeutic interventions to ameliorate anxiety symptoms. Without some way to isolate cells selective for a given stimulus, any therapeutic approaches would be

modulating both cells that correspond with increased and with decreased anxiety-like behaviors, so the impact of each subpopulation could cancel each other out and provide little improvement for patients.

7.2 Largely Non-overlapping VIP^{ACC} Subpopulations Improve Encoding of Behavioral Information

We also determined that super cells better predict the animal's behavior than individual selective cells or the whole VIP^{ACC} population, suggesting that including information from multiple selective VIP^{ACC} improves behavioral encoding. In addition, cells were registered across two tasks and we determined that most VIP^{ACC} were either selective for only one stimulus or were neutral, which demonstrates that functionally distinct subpopulations are largely non-overlapping. These data show that distinct groups of VIP^{ACC} may work cooperatively to encode stimulus-specific information, which provides a framework for how the ACC encodes information across diverse behavioral states.

When we averaged the activity of stimulus-selective VIP^{ACC}, the reliability of their coding increased across diverse stimuli. Electrical coupling has been observed within inhibitory networks, including VIP interneurons (Galarreta & Hestrin, 1999; Karnani et al., 2016). VIP cells can disinhibit members of their own population, leading to increased co-activation of the population, which may allow these subnetworks to encode stimuli as a population and amplify the population output (Melzer et al., 2020; Karnani et al., 2016; Pi et al., 2013). Because we found VIP^{ACC} subpopulations that activate to opposite stimulus

types (e.g., anxiolytic verses anxiogenic cells), this suggests that VIP^{ACC} may function optimally using sparse firing patterns, rather than uniform activation to certain stimuli. Perhaps if all VIP^{ACC} were activated simultaneously, too many clusters of Pyr would be disinhibited and the specificity of an animal's appropriate behavioral response would be impaired. Future research should manipulate either all VIP^{ACC} (using chemogenetics or optogenetics) or only VIP^{ACC} that activate to specific stimuli (Ramirez, Tonegawa, & Liu, 2014; Reijmers et al., 2007). It may be expected that stimulation of anxiogenic environment-activated VIP^{ACC} would lead to increased anxiety-like behavior. However, activation of all VIP^{ACC} may lead to abnormal behavioral patterns throughout a variety of tasks if a sparse code is important for their normal function.

Our work shows that approximately 70% of VIP^{ACC} were neutral in each anxiogenic and social behavioral task, but this percentage drops to about 35% in our data that registered EZM and Sociability. This suggests that many of the cells that were neutral in anxiety-related assays encode some social or non-social information, and vice versa. The high prevalence of neutral cells in any individual task may therefore reflect the multimodal nature of the ACC, where these cells encode other kinds of stimuli. For example, previous work highlighted the role of the ACC in pain processing (Fuchs et al., 2014). Perhaps many of the cells that were neutral in our study are specifically recruited by stimuli we did not directly test, such as painful stimuli.

Alternatively, cells that were classified as neutral may be equally activated by multiple stimuli. For example, neutral EZM cells may preferentially activate to both anxiogenic and anxiolytic stimuli and be involved in encoding both. This could be tested

by using more analytical techniques in addition to ROC analysis. For example, future work could use advanced computational modeling techniques in an attempt to decode behavior using neural data and could assess both selective and neutral VIP^{ACC} (Liang et al., 2018; Spellman et al., 2015). Future work should include also registration across more behavioral tasks to determine whether cells that activate to novel objects and novel social stimuli show more overlap than cells with more different behavioral roles (like anxiety versus social behavior). We were limited in how many cells could be registered across imaging sessions on different days, so future studies could perform different types of assays on the same day to minimize this issue.

It is possible that signaling from different neuromodulators may impact distinct groups of VIP^{ACC} and simultaneous release of different neuromodulations could allow for the co-activation of segregated VIP^{ACC} clusters (Kampa, Letzkus, & Stuart, 2006). This could therefore lead to co-activation of other ACC cell types and could enable ACC networks to bind multiple streams of information to guide behavioral actions or monitor optimal performance (Kampa, Letzkus, & Stuart, 2006; Vann, Aggleton, & Maguire, 2009). In the context of our findings for anxiety-related and social stimuli, this binding could be important for disorders like SAD that encompass features of both anxiety and social behavior. In humans, ACC volume is inversely correlated with symptom severity in individuals with social anxiety disorder (Frick et al., 2013), suggesting the ACC may be important for integration of these two types of information. In fact, because some VIP^{ACC} activate to either anxiogenic or social stimuli, this population could be involved in the integration of information related to both anxiety and sociability and therefore relevant to

the neural mechanisms of SAD. One way to further address this question would be to perform Ca^{2+} imaging of VIP^{ACC} during exposure to a social stressor, like chronic social defeat stress (Harris et al., 2018; Russo et al., 2012). In addition, manipulation of VIP^{ACC} activity during interactions with an aggressor mouse could elucidate whether these cells have a causal relationship with approaching or avoiding social stressors. Research investigating the activity of VIP^{ACC} during tasks that require social and anxiety-related information may provide insight into future therapeutic approaches to address SAD.

7.3 Whole Brain Mapping of Long-range Direct Inputs to VIP^{ACC}, SOM^{ACC}, and PV^{ACC}

Using rabies trans-synaptic mapping we showed that VIP^{ACC} receive long-range inputs from regions implicated in emotional regulation and social cognition and that these connections are not identical across ACC interneuron types. We also demonstrated that VIP^{ACC} (as well as SOM^{ACC} and PV^{ACC}) receive extensive connections from the AM, RS, and PFC. Experiments with classic neural tracers have demonstrated that the RS and AM thalamic nuclei are extensively connected to the ACC, so our data support these previous findings (Allen Institute for Brain Science, 2011; Shibata & Naito, 2005; Shibata, 1993; Shibata, Kondo, & Naito, 2004; Jones, Groenewegen, & Witter, 2005). Our injections and lenses were located at the border between the A24a and A24b subregions of the ACC (Allen Institute for Brain Science, 2004; van Heukelum et al., 2020). Past research shows that A24 receives projections from the amygdala, orbitofrontal cortex, thalamus, RS, and motor cortex and moderate projections from hippocampus, hypothalamus, and autonomic

brain nuclei (Allen Institute for Brain Science, 2011; Shibata & Naito, 2005; Shibata, 1993; Shibata, Kondo, & Naito, 2004; Jones, Groenewegen, & Witter, 2005). Although our data is mostly consistent with these findings, a major difference is that we used trans-synaptic viral mapping in a cell-type specific manner, while other studies used classic neuronal tracers to map connectivity to all ACC neurons.

7.3.1 Potential Roles of Long-range Circuits to VIP^{ACC}

The heterogeneity of activity presented in our work may reflect populations of VIP^{ACC} that comprise distinct neural circuits. This heterogeneity may correspond to groups of VIP cells that either inhibit or disinhibit Pyr or project onto different cell types. Although most VIP synapse onto other inhibitory cells, disinhibiting excitatory Pyr, some can synapse directly onto Pyr, leading directly to their inhibition (Obermayer et al., 2019, Lee et al., 2013). These groups have the potential to have radically different effects on the activity of other neurons in the local circuit. The functional connectivity of VIP in the ACC, in particular, has not been completely characterized. Future studies could use paired in vitro electrophysiological recordings from genetically identified cell types to characterize local ACC circuits and determine whether they mirror the circuits found in other cortical regions (Cichon et al., 2017; Karnani et al., 2016; Melzer et al., 2020; Pi et al., 2013).

Alternatively, VIP^{ACC} that receive long-range inputs from different regions and could reflect subpopulations with different functional roles. The AM-ACC pathway may be important in novelty-related tasks due to the roles of the AM and the ACC in memory (Van der Werf et al., 2000; Aggleton et al., 2016), as well as our data showing they are

highly connected. Performing tasks that induce long-term social memories leads to increased expression of immediate-early genes in the ACC, suggesting a role for the ACC in social memory (Tanimizu et al., 2017). In addition, VIP cells in the auditory cortex facilitate learning about unexpected, salient auditory stimuli (Krabbe et al., 2019). Future work should study the AM-VIP^{ACC} pathway to determine whether it is important for learning and memory. It may also be a useful target in altering social memory-related responses. For example, when rodents are exposed to social stressors (like chronic social defeat stress), some individuals develop social avoidance behaviors, while others are more resilient to these stressful experiences and perform normal social behaviors (Harris et al., 2018; Russo et al., 2012). If the AM-VIP^{ACC} circuit is important for normal recognition of and interaction with novel social stimuli, manipulation of this pathway could be sufficient to rescue social defeat induced avoidance behaviors. AM-ACC projections have been shown to regulate histaminergic itch-induced scratching behavior (Deng et al., 2020), so further investigation of this circuit would illuminate whether it has roles in different behavioral functions and whether this function is found across all ACC cells or only certain ACC cell types.

The RS plays a role in learning, memory, and navigation and is highly connected to the anterior thalamic nuclei and hippocampus (Alexander et al., 2020; Vann, Aggleton, & Maguire, 2009; Fischer et al., 2020). Navigation-related information conveyed to VIP^{ACC} from the RS could guide motor actions that shape an animals' exploration of social and anxiety-related arenas (Alexander et al., 2020; Vann, Aggleton, & Maguire, 2009; Fischer et al., 2020). Recently, circuit-mapping approaches have demonstrated parallel

pathways of inputs onto distinct RS cells originating from the ACC and anterior thalamus (Brennan et al., 2020). These parallel pathways may allow RS-ACC-thalamic networks to process spatial and emotional information (Brennan et al., 2020).

VIP^{ACC} are also highly connected to other frontal cortex subregions and to the clACC, which supports human imaging studies of ACC-PFC networks (Etkin et al., 2006; Gehrig & Knight, 2000). Human imaging studies demonstrate that the distinct ACC-PFC networks are involved in diverse aspects of emotional processing including appraisal and expression of negative emotions and generating emotional responses (Etkin et al., 2011, Milad et al., 2007, Critchley et al., 2003, Critchley et al., 2004, Mobbs et al., 2009, Johnstone et al., 2007, Bush et al., 2000, Mechias et al., 2010, Lavin et al., 2013). ACC-PFC connectivity may therefore be especially important in better understanding the role of VIP^{ACC} in anxiety-related behaviors.

To investigate the roles of these specific pathways, future studies could manipulate them and monitor their effects on VIP^{ACC} subpopulation activity and animal behavior. VIP^{ACC}-specific pathways could be targeted by injecting Cre-dependent retrograde optogenetic AAVs into the ACC of VIP-Cre mice and implanting optical fibers in the AM, RS, or PFC. During optogenetic manipulation, animals could undergo anxiety-related, social, or object recognition testing. This approach would allow researchers to determine the impact of manipulating these highly specific circuits. First, performing these manipulations during anxiety-related or social behaviors would determine whether this is sufficient to cause changes in these behaviors. Secondly, the combination of optogenetics and Ca^{2+} imaging during tasks like the EZM would illuminate whether the activity of cells

that activated preferentially to the open or closed arms could be altered by manipulation of these pathways. If open-selective cells receive extensive connections from the PFC, for example, optogenetic stimulation of the PFC-VIP^{ACC} pathway could induce increased activity in open-selective, but not closed-selective cells. These experiments would determine whether functional heterogeneity was a result of subpopulations of VIP^{ACC} receiving different long-range connections.

7.3.2 M2-ACC Connectivity in Miniscope Implanted Mice

One caveat in our imaging data is that implanting lenses in the ACC induced some damage to M2. The rabies tracing data revealed extensive connections between M2 and VIP^{ACC} in non-implanted mice. Although these animals had no locomotor impairments or abnormal behavior in the EZM or social tasks, it still remains likely that normal M2-ACC circuits were damaged in this process. Aberrations in these connections may have impacted our imaging data in more subtle ways than gross motor deficits. Unfortunately, miniscope imaging of this brain region relies on the implantation of a lens into the neural tissue, but future work may be able to minimize damage to M2-ACC circuits by using 2-photon microscopy in head fixed mice. This technique allows deeper optical penetration, but also limits the behavioral assays that are feasible due to head-fixation. Each technique has features that make it beneficial and others that are a detriment to addressing our research questions, but combining the knowledge gained from both techniques would provide the most thorough investigation of these cells and their functions.

7.3.3 Interneuron Subtype-specific Connectivity in the Frontal Cortex

Some regions that are highly connected to ACC interneurons are also highly connected to other frontal cortical areas. Tracing experiments show high connectivity from the ACC to the mPFC, which, combined with our data, suggests strong reciprocal connections between the ACC and the PFC (DeNardo et al., 2015). The IL and PrL receive extensive projections from local areas, motor and sensory cortex, as well as the hippocampus and amygdala (DeNardo et al., 2015). Many of these areas were also found to be highly connected to ACC interneurons in our data. However, the previous data in IL and PrL indicated especially high thalamic inputs in the dorsal thalamus (DeNardo et al., 2015), whereas ACC interneurons were most connected to anterior and lateral thalamic nuclei.

In agreement with our data, cell-type specific tracing in the mPFC showed connectivity differences across VIP, SOM, and PV cells within the mPFC (Sun et al., 2019). This work, much like ours, found that PV cells in the mPFC received more cortical inputs than SOM, especially from the RS (Sun et al., 2019). They also found that SOM received more subcortical inputs than PV cells (Sun et al., 2019). While our data show more inputs to PV cells in general, SOM cells did receive more inputs from HPC, hypothalamus, and the medial septal complex than PV cells. In addition, both the mPFC and our ACC data show more connectivity from the diagonal band (HDB and VDB) to SOM than to VIP or PV (Sun et al., 2019). Some findings seem to be specific to ACC versus mPFC, however. For example, for both LO and M2 inputs, more connections were found to VIP than SOM or PV in the mPFC (Sun et al., 2019), but our data show more LO-

PV and M2-PV than any other ACC interneuron. In addition, no differences were found across cell type in inputs from local mPFC in the mPFC data (Sun et al., 2019), but we found more local clACC inputs in PV than in SOM or VIP. Taken together, these data suggest that ACC and mPFC do not show identical patterns of overall or cell-type specific connectivity patterns. However, both datasets are similar in that they show both similarities and some robust differences in inputs between cortical interneuron subtypes.

The data presented in our work show that different cell types can receive vastly different inputs within a given brain region. In conjunction with prior research in the mPFC, this suggests that different connectivity patterns across interneuron subtypes may be a feature of inhibitory circuits across frontal cortex. Because these interneurons receive information from different networks, they may therefore be implicated in different behavioral functions. Future studies could investigate not only region specific inputs to VIP^{ACC} (like AM-VIP^{ACC} circuits), as discussed above, but could also use different Cre mouse lines to examine differences in the roles of inputs to different interneuron subtypes (like AM-VIP^{ACC} versus AM-SOM^{ACC}).

7.4 Subregions within the ACC

Human imaging studies have shown that ACC activity increases as individuals perform social and emotional tasks, as compared to non-social tasks (Di Martino et al., 2009). This pattern was found both in individuals with ASD and in neurotypical controls (Di Martino et al., 2009). Interestingly, this work demonstrates heterogeneous activation of different subregions within the ACC, where increased activity of the perigenual ACC

and rostral ACC is implicated in social tasks and dorsal ACC is selectively activated in non-social cognitive tasks, such as reading comprehension and attention-related tasks (Di Martino et al., 2009). Our histological analysis revealed that GRIN lenses were located at the border of the dorsal and ventral subregions of the ACC (A24a and A24b subregions). Future research could monitor VIP cells in different ACC subregions to determine whether the whether the selectivity distributions found in this work are consistent across both areas.

7.5 Concluding Remarks

Using in vivo imaging with cellular resolution in freely moving mice, we showed that VIP^{ACC} are functionally heterogeneous, where distinct subcircuits encode for diverse stimuli. ROC analysis identified stimulus-selective VIP^{ACC} that encoded anxiety-like behaviors or interactions with mice and objects, even though there was no difference in overall VIP^{ACC} activity. Averaging the activity of selective VIP^{ACC} enhanced their ability to encode for specific stimuli. We also determined that most VIP^{ACC} were either selective for only one stimulus or were neutral. Lastly, we used trans-synaptic mapping to provide maps of ACC interneuron subtype connectivity and show that VIP^{ACC} receive inputs from regions implicated in emotional regulation, social cognition, and memory formation. To our knowledge, these data provide the first evidence of functional heterogeneity of VIP^{ACC} in vivo and show that population coding of selective VIP^{ACC} may encode stimulus-specific information, which provides a framework for how the ACC encodes information across diverse behavioral states.

Like many prefrontal cortical regions, the ACC is implicated in a wide range of behavioral functions. Our work supports past findings by connecting ACC activity with anxiety-related and social behavior and identifies a neural substrate for processing of multimodal stimuli. However, an important facet of our findings is that a diverse range of neuronal representations are encoded in subgroups of VIP^{ACC}, which points to the varied roles of the ACC. Previous data has quantified the activity of the whole ACC or of all VIP cells grouped together, which could lead to the expectation that all VIP^{ACC} would all activate homogenously to anxiety-related and social stimuli. Interestingly, our data show that whole populations of VIP^{ACC} do not preferentially activate to one anxiety-related or social stimulus, but largely distinct subgroups of VIP^{ACC} activate to different anxiogenic, anxiolytic, social, or non-social stimuli.

These data are significant because they elucidate how one cortical subtype can encode complex and diverse behavioral stimuli. In addition, they highlight the need for more cell-type specific Ca^{2+} studies with cellular resolution. Without this technical advance, we would have been led to believe that VIP^{ACC} cells had no role in any of the behaviors assayed. Lastly, better understanding the complexity of cortical encoding provides a stronger ground to develop therapeutics. Future approaches to rescue abnormally high levels of anxiety or social impairments may benefit from the knowledge that manipulating the whole ACC or even all VIP^{ACC} may not be the most beneficial strategy, as different VIP^{ACC} have essentially opposite functional roles. Future work should aim to identify commonalities that tie VIP^{ACC} functional subpopulations together and manipulate these even more precise groups to rescue anxiety-like or social impairments.

BIBLIOGRAPHY

Aggleton, J. P., Pralus, A., Nelson, A. J., & Hornberger, M. (2016). Thalamic pathology and memory loss in early Alzheimer's disease: moving the focus from the medial temporal lobe to Papez circuit. *Brain, 139*(7), 1877-1890.

Aharoni, D., Khakh, B. S., Silva, A. J., & Golshani, P. (2019). All the light that we can see: a new era in miniaturized microscopy. *Nature Methods, 16*(1), 11-13.

Alexander, A. S., Carstensen, L. C., Hinman, J. R., Raudies, F., Chapman, W., & Hasselmo, M. E. (2020). Egocentric boundary vector tuning of the retrosplenial cortex. *Science Advances, 6*(8), eaaz2322.

Allen Institute for Brain Sceince. (2008). Allen Brain Atlas Brain Explorer.

Allen Institute for Brain Science. (2004). *Allen Mouse Brain Atlas.*

Allen Institute for Brain Science. (2011). *Allen Mouse Brain Connectivity Atlas*. Retrieved from https://connectivity.brain-map.org/

Amir, N., Beard, C., Taylor, C. T., Klumpp, H., Elias, J., Burns, M., & Chen, X. (2009). Attention training in individuals with generalized social phobia: A randomized controlled trial. *Journal of Consulting and Clinical Psychology, 77*(5), 961.

Askew, C. E., Lopez, A. J., Wood, M. A., & Metherate, R. (2019). Nicotine excites VIP interneurons to disinhibit pyramidal neurons in auditory cortex. *Synapse, 73*(9), e22116.

Batista-Brito, R., Vinck, M., Ferguson, K. A., Chang, J. T., Laubender, D., Lur, G., . . . Hernandez, V. G. (2017). Developmental dysfunction of VIP interneurons impairs cortical circuits. *Neuron, 95*(4), 884-895.

Baud, A., Mulligan, M. K., Casale, F. P., Ingels, J. F., Bohl, C. J., Callebert, J., ... & Stegle, O. (2017). Genetic variation in the social environment contributes to health and disease. *PLoS Genetics*, *13*(1), e1006498.

Bayraktar, T. J., Staiger, J. F., Acsady, L., Cozzari, C., Freud, T. F., & Zilles, K. (1997). Co-localization of vasoactive intestinal polypeptide, γ-aminobutyric acid and choline acetyltransferase in neocortical interneurons of the adult rat. *Brain Research, 757*(2), 209-217.

Becht, A. I., Klapwijk, E. T., Wierenga, L. M., van der Cruijsen, R., Spaans, J., can der Aar, L., . . . Crine, E. A. (2020). Longitudinal associations between structural prefrontal cortex and nucleus accumbens development and daily identity

formation processes across adolescence. *Developmental Cognitive Neuroscience, 46*, 100880.

Bishop, S., Duncan, J., Brett, M., & Lawrence, A. D. (2004). Prefrontal cortical function and anxiety: controlling attention to threat-related stimuli. *Nature, 7*(2), 184-188.

Bollimunta, A., Santacruz, S. R., Eaton, R. W., Xu, P. S., Morrison, J. H., Moxon, K. A., ... & Nassi, J. J. (2021). Head-mounted microendoscopic calcium imaging in dorsal premotor cortex of behaving rhesus macaque. *Cell Reports*, *35*(11), 109239.

Brennan, E. K., Sudhakar, S. K., Jedrasiak-Cape, I., John, T. T., & Ahmed, O. J. (2020). yperexcitable neurons enable precise and persistent information encoding in the superficial retrosplenial cortex. *Cell Reports, 30*(5), 1598-1612.

Callaway, E. M., & Luo, L. (2015). Monosynaptic circuit tracing with glycoprotein-deleted rabies viruses. *Journal of Neuroscience, 35*(24), 8979-8985.

Cauli, B., Audinat, E., Lambolez, B., Angulo, M. C., Ropert, N., Tsuzuki, K., . . . Rossier, J. (1997). Molecular and physiological diversity of cortical nonpyramidal cells. *Journal of Neuroscience, 17*(10), 3894-3906.

Chen, P., & Hong, W. (2018). Neural circuit mechanisms of social behavior. *Neuron, 98*(1), 16-30.

Chen, T. W., Wardill, T. J., Sun, Y., Pulver, S. R., Renninger, S. L., Baohan, A., . . . Looger, L. L. (2013). Ultrasensitive fluorescent proteins for imaging neuronal activity. *Nature, 499*(7458), 295-300.

Choleris, E., Thomas, A. W., Kavaliers, M., & Prato, F. S. (2001). A detailed ethological analysis of the mouse open field test: effects of diazepam, chlordiazepoxide and an extremely low frequency pulsed magnetic field. *Neuroscience & Biobehavioral Reviews, 25*(3), 235-260.

Chung, E. K., Zhang, X., Li, Z., Zhang, H., Xu, H., & Bian, Z. (2007). Neonatal maternal separation enhances central sensitivity to noxious colorectal distention in rat. *Brain Research, 1153*, 68-77.

Cichon, J., Blanck, T. J., Gan, W. B., & Yang, G. (2017). Activation of cortical somatostatin interneurons prevents the development of neuropathic pain. *Nature Neuroscience, 20*(8), 1122.

Cohen, R. A., Grieve, S., Hoth, K. F., Paul, R. H., Sweet, L., Tate, D., . . . Niaura, R. (2006). Early life stress and morphometry of the adult anterior cingulate cortex and caudate nuclei. *Biological Psychiatry, 59*(10), 975-982.

Colich, N. L., Williams, E. S., Ho, T. C., King, L. S., Humphreys, K. L., Price, A. N., . . . Gotlib, I. H. (2017). The association between early life stress and prefrontal cortex activation during implicit emotion regulation is moderated by sex in early adolescence. *Development and Psychopathology, 29*(5), 1851.

Comer, A. L., Jinadasa, T., Sriram, B., Phadke, R. A., Kretsge, L. N., Nguyen, T. P., . . . Cruz-Martin, A. (2020). Increased expression of schizophrenia-associated gene C4 leads to hypoconnectivity of prefrontal cortex and reduced social interaction. *PLoS Biology, 18*(1), e3000604.

Committee for the Update of the Guide for the Care and Use of Laboratory Animals, I. f. (2010). Guide for the care and use of laboratory animals (8th ed.). National Academies Press.

Corcoran, K. A., Donnan, M. D., Tronson, N. C., Guzman, Y. F., Gao, C., Jovasevic, V., . . . Radulovic, J. (2011). NMDA receptors in retrosplenial cortex are necessary for retrieval of recent and remote context fear memory. *Journal of Neuroscience, 31*(32), 11655-11659.

Cruz-Martin, A., El-Danaf, R. N., Osakada, F., Sriram, B., Dhande, O. S., Nguyen, P. L., . . . Huberman, A. D. (2014). A dedicated circuit links direction-selective retinal ganglion cells to the primary visual cortex. *Nature, 507*(7492), 358-361.

De Pisapia, N., & Braver, T. S. (2006). A model of dual control mechanisms through anterior cingulate and prefrontal cortex interactions. *Neurocomputing, 69*(10-12), 1322-1326.

DeNardo, L. A., Berns, D. S., DeLoach, K., & Luo, L. (2015). Connectivity of mouse somatosensory and prefrontal cortex examined with trans-synaptic tracing. *Nature Neuroscience, 18*(11), 1687-1697.

Deng, Y. Z., Lu, Y. C., Wu, W. W., Cheng, L., Zan, G. Y., Chai, J. R., . . . Liu, J. G. (2020). Anteromedial thalamic nucleus to anterior cingulate cortex inputs modulate histaminergic itch sensation. *Neuropharmacology, 168*, 108028.

Di Martino, A., Ross, K., Uddin, L. Q., Sklar, A. B., Castellanos, F. X., & Milham, M. P. (2009). Functional brain correlates of social and nonsocial processes in autism spectrum disorders: an activation likelihood estimation meta-analysis. *Biological Psychiatry, 65*(1), 63-74.

Drake, C. T., & Milner, T. A. (2002). Mu opioid receptors are in discrete hippocampal interneuron subpopulations. *Hippocampus*, *12*(2), 119-136.

Etkin, A., Egner, T., Peraza, D. M., Kandel, E. R., & Hirsch, J. (2006). Resolving emotional conflict: a role for the rostral anterior cingulate cortex in modulating activity in the amygdala. *Neuron, 51*(6), 871-882.

Feldman, R. (2012). Oxytocin and social affiliation in humans. *Hormones and Behavior, 61*(3), 380-391.

Ferezou, I., Cauli, B., Hill, E. L., Rossier, J., Hamel, E., & Lambolez, B. (2002). 5-HT3 receptors mediate serotonergic fast synaptic excitation of neocortical vasoactive intestinal peptide/cholecystokinin interneurons. *Journal of Neuroscience, 22*(17), 7389-7397.

Ferezou, I., Hill, E. L., Cauli, B., Gibelin, N., Kaneko, T., Rossier, J., & Lambolez, B. (2007). Extensive overlap of mu-opioid and nicotinic sensitivity in cortical interneurons. *Cerebral Cortex*, *17*(8), 1948-1957.

Fischer, L. F., Soto-Albors, R. M., Buck, F., & Harnett, M. T. (2020). Representation of visual landmarks in retrosplenial cortex. *Elife, 9*, e51458.

Fornito, A., & Bullmore, E. T. (2015). Connectomics: a new paradigm for understanding brain disease. *Neuropsychopharmacology, 25*(5), 733-748.

Frick, A., Howner, K., Fischer, H., Eskildsen, S. F., Kristiansson, M., & Furmark, T. (2013). Cortical thickness alterations in social anxiety disorder. *Neuroscience Letters, 536*, 52-55.

Frost, N. A., Haggart, A., & Sohal, V. S. (2021). Dynamic patterns of correlated activity in the prefrontal cortex encode information about social behavior. *PLoS Biology, 19*(5), e3001235.

Fu, Y., Tucciarone, J. M., Espinosa, J. S., Sheng, N., Darcy, D. P., Nicoll, R. A., ... & Stryker, M. P. (2014). A cortical circuit for gain control by behavioral state. *Cell*, *156*(6), 1139-1152.

Fuchs, P. N., Peng, Y. B., Boyette-Davis, J. A., & Uhelski, M. L. (2014). The anterior cingulate cortex and pain processing. *Fronteirs in Integrated Neuroscience, 8*(35).

Galarreta, M., & Hestrin, S. (1999). network of fast-spiking cells in the neocortex connected by electrical synapses. *Nature, 402*(6757), 72-75.

Garrett, M., Manavi, S., Roll, K., Ollerenshaw, D., Groblewski, P., Kiggins, J., . . . Williford, A. (2020). Experience shapes activity dynamics and stimulus coding of VIP inhibitory cells. *Elife, 9*, e50340.

Gehrig, W. J., & Knight, R. T. (2000). Prefrontal-cingulate interactions in action monitoring. *Nature Neuroscience, 3*(5), 516-520.

Ghosh, K. K., Burns, L. D., Cocker, E. D., Nimmerjahn, A., Ziv, Y., El Gamal, A., & Schnitzer, M. J. (2011). Miniaturized integration of a fluorescence microscope. *Nature Methods, 8*(10), 871-878.

Giovannucci, A., Friedrich, J., Gunn, P., Kalfon, J., Brown, B., Koay, S. A., . . . Pnevmatikakis, E. A. (2019). CaImAn an open source tool for scalable calcium imaging data analysis. *Elife, 8*, e38173.

Gompf, H. S., Mathai, C., Fuller, P. M., Wood, D. A., Pedersen, N. P., Saper, C. B., & Lu, J. (2010). Locus ceruleus and anterior cingulate cortex sustain wakefulness in a novel environment. *Journal of Neuroscience, 30*(43), 14543-14551.

Gonchar, Y., Wang, Q., & Burkhalter, A. H. (2008). Multiple distinct subtypes of GABAergic neurons in mouse visual cortex identified by triple immunostaining. *Frontiers in Neuroanatomy, 2*, 3.

Guido, W., Lu, S. M., Vaughan, J. W., Godwin, D. W., & Sherman, S. M. (1995). Receiver operating characteristic (ROC) analysis of neurons in the cat's lateral geniculate nucleus during tonic and burst response mode. *Visual Neuroscience*, *12*(4), 723-741.

Guo, B., Chen, J., Chen, Q., Ren, K., Feng, D., Mao, H., . . . Jia, F. (2019). nterior cingulate cortex dysfunction underlies social deficits in Shank3 mutant mice. *Nature Neuroscience, 22*(8), 1223-1234.

Hall, C., & Ballachey, E. L. (1932). A study of the rat's behavior in a field. A contribution to method in comparative psychology. *University of California Publications in Psychology*.

Harris, A. Z., Atsak, P., Bretton, Z. H., Holt, E. S., Alam, R., Morton, M. P., . . . Gordon, J. A. (2018). A novel method for chronic social defeat stress in female mice. *Neuropsychopharmacology, 43*(6), 1276-1283.

Harris, J. A., Mihalas, S., Hirokawa, K. E., Whitesell, J. D., Knox, J., Bernard, A., . . . Casal, L. (2018). The organization of intracortical connections by layer and cell class in the mouse brain. *BioRxiv*, 292961.

Harvard Medical School. (2007). *National Comorbidity Survey (NCS).* Retrieved May 2021, from https://www.hcp.med.harvard.edu/ncs/index.php

Hasselmo, M. E. (2006). The role of acetylcholine in learning and memory. *Current Opinion in Neurobiology, 16*(6), 710-716.

Hasselmo, M. E., & McGaughy, J. (2004). High acetylcholine levels set circuit dynamics for attention and encoding and low acetylcholine levels set dynamics for consolidation. *Progress in Brain Research, 145*, 207-231.

Haubensak, W., Kunwar, P. S., Cai, H., Ciocchi, S., Wall, N. R., Ponnusamy, R., . . . Fanselow, M. S. (2010). Genetic dissection of an amygdala microcircuit that gates conditioned fear. *Nature, 468*(7321), 270-276.

Heinrichs, M., von Dawans, B., & Domes, G. (2009). Oxytocin, vasopressin, and human social behavior. *Frontiers in Neuroendocrinology, 30*(4), 548-557.

Hill, J. M., Ades, A. M., McCune, S. K., Sahir, N., Moody, E. M., Abebe, D. T., . . . Brenneman, D. E. (2003). Vasoactive intestinal peptide in the brain of a mouse model for Down syndrome. *Experimental Neurology, 183*(1), 56-65.

Hill, J. M., Cuasay, K., & Abede, D. T. (2007). Vasoactive intestinal peptide antagonist treatment during mouse embryogenesis impairs social behavior and cognitive function of adult male offspring. *Experimental Neurology, 206*(1), 101-113.

Hodge, R. D., Bakken, T. E., Miller, J. A., Smith, K. A., Barkan, E. R., Graybuck, L. T., . . . Yao, Z. (2019). Conserved cell types with divergent features in human versus mouse cortex. *Nature, 573*(7772), 61-68.

Horii-Hayashi, N., Sasagawa, T., Matsunaga, W., Matsusue, Y., Azuma, C., & Nishi, M. (2013). Developmental Changes in Desensitisation of c-F os Expression Induced by Repeated Maternal Separation in Pre-Weaned Mice. *Journal of Neuroendocrinology, 25*(2), 158-167.

Jimenez, J. C., Su, K., Goldberg, A. R., Luna, V. M., Biane, J. S., Ordek, G., . . . Kheirbek, M. A. (2018). Anxiety cells in a hippocampal-hypothalamic circuit. *Neuron, 973*(3), 670-683.

Job, D. E., Whalley, H. C., McConnell, S., Glabus, M., Johnstone, E. C., & Lawrie, S. M. (2003). Voxel-based morphometry of grey matter densities in subjects at high risk of schizophrenia. *Schizophrenia Research, 64*(1), 1-13.

Johansen, J. P., Fields, H. L., & Manning, B. H. (2001). The affective component of pain in rodents: direct evidence for a contribution of the anterior cingulate cortex. *Proceedings of the National Academy of Sciences*, *98*(14), 8077-8082.

Jones, B. F., Groenewegen, H. J., & Witter, M. P. (2005). Intrinsic connections of the cingulate cortex in the rat suggest the existence of multiple functionally segregated networks. *Neuroscience, 133*(1), 193-207.

Kamigaki, T., & Dan, Y. (2017). Delay activity of specific prefrontal interneuron subtypes modulates memory-guided behavior. *Nature Neuroscience, 20*(6), 854.

Kampa, B. M., Letzkus, J. J., & Stuart, G. J. (2006). Cortical feed-forward networks for binding different streams of sensory information. *Nature Neuroscience, 9*(12), 1472-1473.

Karnani, M. M., Jackson, J., Ayzenshat, I., Sichani, A. H., Manoocheri, K., Kim, S., & Yuste, R. (2016). Opening holes in the blanket of inhibition: localized lateral disinhibition by VIP interneurons. *Journal of Neuroscience, 36*(12), 3471-3480.

Kasai, K., Yamasue, H., Gilbertson, M. W., Shenton, M. E., Rauch, S. L., & Pitman, R. K. (2008). Evidence for acquired pregenual anterior cingulate gray matter loss from a twin study of combat-related posttraumatic stress disorder. *Biological Psychiatry, 63*(6), 550-556.

Kawaguchi, Y., & Kubota, Y. (1997). GABAergic cell subtypes and their synaptic connections in rat frontal cortex. *Cerebral Cortex, 7*(6), 476-486.

Kawaguchi, Y., & Shindou, T. (1998). Noradrenergic excitation and inhibition of GABAergic cell types in rat frontal cortex. *Journal of Neuroscience, 18*(17), 6963-6976.

Ketchesin, K. D., Huang, N. S., & Seasholtz, A. F. (2017). Cell type-specific expression of corticotropin-releasing hormone-binding protein in GABAergic interneurons in the prefrontal cortex. *Frontiers in Neuroanatomy, 11*, 90.

Kim, S. S., Wang, H., Li, X. Y., Chen, T., Mercaldo, V., Descalzi, G., . . . Zhuo, M. (2011). Neurabin in the anterior cingulate cortex regulates anxiety-like behavior in adult mice. *Molecular Brain, 4*(1), 1-10.

Kingsbury, L., Huang, A., Raam, T., Letizia, S. Y., Wei, D., Hu, R. K., . . . Hong, W. (2020). Cortical representations of conspecific sex shape social behavior. *Neuron, 107*(5), 941-953.

Kitayama, N., Quinn, S., & Bremner, J. D. (2006). Smaller volume of anterior cingulate cortex in abuse-related posttraumatic stress disorder. *Journal of Affective Disorders, 90*(2-3), 171-174.

Kohara, K., Pignatelli, M., Rivest, A. J., Jung, H. Y., Kitamura, T., Suh, J., . . . Wickersham, I. R. (2014). Cell type–specific genetic and optogenetic tools reveal hippocampal CA2 circuits. *Nature Neuroscience, 17*(2), 269-279.

Koike, H., Ibi, D., Mizoguchi, H., Nagai, T., Nitta, A., Takuma, K., . . . Yamada, K. (2009). Behavioral abnormality and pharmacologic response in social isolation-reared mice. *Behavioural Brain Research, 202*(1), 114-121.

Krabbe, S., Paradiso, E., d'Aquin, S., Bitterman, Y., Cortin, J., Xu, C., . . . Grundemann, J. (2019). Adaptive disinhibitory gating by VIP interneurons permits associative learning. *Nature Neuroscience, 22*(11), 1-10.

Lee, S., Kruglikov, I., Huang, Z. J., Fishell, G., & Rudy, B. (2013). A disinhibitory circuit mediates motor integration in the somatosensory cortex. *Nature Neuroscience, 16*(11), 1662-1670.

Lein, E. S., Hawrylycz, M. J., Ao, N., Ayres, M., Bensinger, A., Bernard, A., . . . Jones, A. R. (2007). Genome-wide atlas of gene expression in the adult mouse brain. *Nature, 445*(7124), 168-176.

Leroy, F., de Solis, C. A., Boyle, L. M., Bock, T., Lofaro, O. M., Buss, E. W., ... & Siegelbaum, S. A. (2021). Enkephalin release from VIP interneurons in the hippocampal CA2/3a region mediates heterosynaptic plasticity and social memory. *Molecular Psychiatry*, 1-22.

Li, Y., Mathis, A., Grewe, B. F., Osterhout, J. A., Ahanonu, B., Schnitzer, M. J., . . . Dulac, C. (2017). Neuronal representation of social information in the medial amygdala of awake behaving mice. *Cell, 171*(5), 1176-1190.

Liang, B., Zhang, L., Barbera, G., Fang, W., Zhang, J., Chen, X., . . . Lin, D. T. (2018). Distinct and dynamic ON and OFF neural ensembles in the prefrontal cortex code social exploration. *Neuron, 100*(3), 700-714.

Liberti, W. A., Perkins, L. N., Leman, D. P., & Gardner, T. J. (2017). An open source, wireless capable miniature microscope system. *Journal of Neural Engineering, 14*(4), 045001.

Lim, M. A., Stack, C. M., Cuasay, K., Stone, M. M., McFarlane, H. G., Waschek, J. A., & Hill, J. M. (2008). Regardless of genotype, offspring of VIP-deficient female

mice exhibit developmental delays and deficits in social behavior. *International Journal of Developmental Neuroscience, 26*(5), 423-434.

Liu, N., Wang, Y., An, A. Y., Banker, C., Qian, Y. H., & O'Donnell, J. M. (2020). Single housing-induced effects on cognitive impairment and depression-like behavior in male and female mice involve neuroplasticity-related signaling. *European Journal of Neuroscience, 52*(1), 2694-2704.

Lopes-dos-Santos, V., Conde-Ocazionez, S., Nicolelis, M. A., Ribeiro, S. T., & Tort, A. B. (2011). Neuronal assembly detection and cell membership specification by principal component analysis. *PloS One*, *6*(6), e20996.

Marusak, H. A., Thomason, M. E., Peters, C., Zundel, C., Elrahal, F., & Rabinak, C. (2016). You say 'prefrontal cortex'and I say 'anterior cingulate': meta-analysis of spatial overlap in amygdala-to-prefrontal connectivity and internalizing symptomology. *Translational Psychiatry, 6*(11), e944.

Mathis, A., Mamidanna, P., Cury, K., Abe, T., Murthy, V. N., Mathis, M. W., & Bethge, M. (2018). DeepLabCut: markerless pose estimation of user-defined body parts with deep learning. *Nature Neuroscience, 21*(9), 1281-1289.

McCormick, D. A., & Prince, D. A. (1988). Noradrenergic modulation of firing pattern in guinea pig and cat thalamic neurons, in vitro. *Journal of Neurophysiology, 59*(3), 978-996.

Melzer, S., Newmark, E., Mizuno, G. O., Hyun, M., Philson, A. C., Quiroli, E., . . . Sabatini, B. L. (2020). Bombesin-like peptide recruits disinhibitory cortical circuits and enhances fear memories. *bioRXiv, 3724673*.

Milham, M. P., Banich, M. T., Webb, A., Barad, V., Cohen, N. J., Wszalek, T., & Kramer, A. F. (2001). The relative involvement of anterior cingulate and prefrontal cortex in attentional control depends on nature of conflict. *Cognitive Brain Research, 12*(3), 467-473.

Mossner, J. M., Batista-Brito, R., Pant, R., & Cardin, J. A. (2020). Developmental loss of MeCP2 from VIP interneurons impairs cortical function and behavior. *Elife, 9*, e55639.

Moy, S. S., Nadler, J. J., Perez, A., Barbaro, R. P., Johns, J. M., Magnuson, T. R., . . . Crawley, J. N. (2004). Sociability and preference for social novelty in five inbred strains: an approach to assess autistic-like behavior in mice. *Genes, Brain and Behavior, 3*(5), 287-302.

Murugan, M., Jang, H. J., Park, M., Miller, E. M., Cox, J., Taliaferro, J. P., ... & Witten, I. B. (2017). Combined social and spatial coding in a descending projection from the prefrontal cortex. *Cell*, *171*(7), 1663-1677.

Nath, T., Mathis, A., Chen, A. C., Patel, A., Bethge, M., & Mathis, M. W. (2019). Using DeepLabCut for 3D markerless pose estimation across species and behaviors. *Nature Protocols, 14*(7), 2152-2176.

Nelson, B. D., Bjorkquist, O. A., Olsen, E. K., & Herbener, E. S. (2015). Schizophrenia symptom and functional correlates of anterior cingulate cortex activation to emotion stimuli: An fMRI investigation. *Psychiatry Research: Neuroimaging, 234*(3), 285-291.

Nelson, K. B., Grether, J. K., Croen, L. A., Dambrosia, J. M., Dickens, B. F., Jelliffe, L. L., . . . Phillips, T. M. (2001). Neuropeptides and neurotrophins in neonatal blood of children with autism or mental retardation. *Annals of Neurology, 49*(5), 597-606.

Nitschke, J. B., Sarinopoulos, I., Oathes, D. J., Johnstone, T., Whalen, P. J., Davidson, R. J., & Kalin, N. H. (2009). Anticipatory activation in the amygdala and anterior cingulate in generalized anxiety disorder and prediction of treatment response. *American Journal of Psychiatry, 166*(3), 302-310.

Obermayer, J., Luchicchi, A., Heistek, T. S., de Kloet, S. F., Terra, H., Bruinsma, B., . . . Kroon, T. (2019). Prefrontal cortical ChAT-VIP interneurons provide local excitation by cholinergic synaptic transmission and control attention. *Nature Communications, 10*(1), 1-14.

Perlstein, W. M., Dixit, N. K., Carter, C. S., Noll, D. C., & Cohen, J. D. (2003). Prefrontal cortex dysfunction mediates deficits in working memory and prepotent responding in schizophrenia. *Biological Psychiatry, 53*(1), 25-38.

Perry, B. A., & Mitchell, A. S. (2019). Considering the Evidence for Anterior and Laterodorsal Thalamic Nuclei as Higher Order Relays to Cortex. *Frontiers in Molecular Neuroscience, 12*, 167.

Pfeffer, C. K., Xue, M., He, M., Huang, Z. J., & Scanziani, M. (2013). Inhibition of inhibition in visual cortex: the logic of connections between molecularly distinct interneurons. *Nature Neuroscience, 16*(8), 1068-1076.

Pi, H. J., Hangya, B., Kvitsiani, D., Sanders, J. I., Huang, Z. J., & Kepecs, A. (2013). Cortical interneurons that specialize in disinhibitory control. *Nature, 503*(7477), 521-524.

Pinto, L., & Dan, Y. (2015). Cell-type-specific activity in prefrontal cortex during goal-directed behavior. *Neuron, 87*(2), 437-450.

Poorthuis, R. B., Enke, L., & Letzkus, J. J. (2014). Cholinergic circuit modulation through differential recruitment of neocortical interneuron types during behaviour. *The Journal of Physiology, 592*(19), 4155-4164.

Porcelli, S., Van Der Wee, N., van der Werff, S., Aghajani, M., Glennon, J. C., van Heukelum, S., . . . Posadas, M. (2019). Social brain, social dysfunction and social withdrawal. *Neuroscience & Biobehavioral Reviews, 97*, 10-33.

Porter, J. T., Cauli, B., Tsuzuki, K., Lambolez, B., Rossier, J., & Audinat, E. (1999). Selective excitation of subtypes of neocortical interneurons by nicotinic receptors. *Journal of Neuroscience, 19*(13), 5228-5235.

Pouchelon, G., Bollman, Y., Fisher, E., Agba, C. K., Xu, Q., Ritola, K. D., . . . Fishell, G. (2020). The organization and developmental establishment ofcortical interneuron presynaptic circuits. *bioRxiv*.

Pronneke, A., Scheuer, B., Wagener, R. J., Mock, M., Witte, M., & Staiger, J. F. (2015). Characterizing VIP neurons in the barrel cortex of VIPcre/tdTomato mice reveals layer-specific differences. *Cerebral Cortex, 25*(12), 4854-4868.

Pronneke, A., Witte, M., Mock, M., & Staiger, J. F. (2020). Neuromodulation leads to a burst-tonic switch in a subset of VIP neurons in mouse primary somatosensory (barrel) cortex. *Cerebral Cortex, 30*(2), 488-504.

Qu, C., King, T., Okun, A., Lai, J., Fields, H. L., & Porreca, F. (2011). Lesion of the rostral anterior cingulate cortex eliminates the aversiveness of spontaneous neuropathic pain following partial or complete axotomy. *Pain*, *152*(7), 1641-1648.

Ramirez, S., Tonegawa, S., & Liu, X. (2014). Identification and optogenetic manipulation of memory engrams in the hippocampus. *Frontiers in Behavioral Neuroscience, 7*, 226.

Reijmers, L. G., Perkins, B. L., Matsuo, N., & Mayford, M. (2007). Localization of a stable neural correlate of associative memory. *Science, 317*(5842), 1230-1233.

Rudebeck, P. H., Buckley, M. J., Walton, M. E., & Rushworth, M. F. (2006). A role for the macaque anterior cingulate gyrus in social valuation. *Science, 313*(5791), 1310-1312.

Rudebeck, P. H., Putnam, P. T., Daniels, T. E., Yang, T., Mitz, A. R., Rhodes, S. E., & Murray, E. A. (2014). A role for primate subgenual cingulate cortex in sustaining autonomic arousal. *Proceedings of the National Academy of Sciences, 111*(14), 5391-5396.

Rudy, B., Fishell, G., Lee, S., & Hjerling-Leffler, J. (2011). Three groups of interneurons account for nearly 100% of neocortical GABAergic neurons. *Developmental Neurobiology, 71*(1), 45-61.

Russo, S. J., Murrough, J. W., Han, M. H., Charney, D. S., & Nestler, E. J. (2012). Neurobiology of resilience. *Nature Neuroscience, 15*(11), 1475-1484.

Sarter, M., & Bruno, J. P. (1997). Cognitive functions of cortical acetylcholine: toward a unifying hypothesis. *Brain Research Reviews, 23*(1-2), 28-46.

Scheinost, D., Holmes, S. E., DellaGioia, N., Schleifer, C., Matuskey, D., Abdallah, C. G., . . . Esterlis, I. (2018). Multimodal investigation of network level effects using intrinsic functional connectivity, anatomical covariance, and structure-to-function correlations in unmedicated major depressive disorder. *Neuropsychopharmacology, 43*(5), 1119-1127.

See, J. Z., Homma, N. Y., Atencio, C. A., Sohal, V. S., & Schreiner, C. E. (2021). Information diversity in individual auditory cortical neurons is associated with functionally distinct coordinated neuronal ensembles. *Scientfic Reports, 11*(1), 1-15.

Seibenhener, M. L., & Wooten, M. C. (2015). Use of the Open Field Maze to measure locomotor and anxiety-like behavior in mice. *JoVE (Journal of Visualized Experiments), 96*, e52434.

Shang, J., Fu, Y., Ren, Z., Zhang, T., Du, M., Gong, Q., . . . Zhang, W. (2014). The common traits of the ACC and PFC in anxiety disorders in the DSM-5: meta-analysis of voxel-based morphometry studies. *PloS One, 9*(3), e93432.

Shepherd, j. K., Grewal, S. S., Fletcher, A., Bill, D. J., & Dourish, C. T. (1994). Behavioural and pharmacological characterisation of the elevated “zero-maze” as an animal model of anxiety. *Psychopharmacology, 116*(1), 56-64.

Shibata, H. (1993). Efferent projections from the anterior thalamic nuclei to the cingulate cortex in the rat. *Journal of Comparative Neurology, 330*(4), 533-542.

Shibata, H. (1993). Efferent projections from the anterior thalamic nuclei to the cingulate cortex in the rat. *Journal of Comparative Neurology, 330*(4), 533-542.

Shibata, H., & Naito, J. (2005). Organization of anterior cingulate and frontal cortical projections to the anterior and laterodorsal thalamic nuclei in the rat. *Brain Research, 1059*(1), 93-103.

Shibata, H., Kondo, S., & Naito, J. (2004). Organization of retrosplenial cortical projections to the anterior cingulate, motor, and prefrontal cortices in the rat. *Neuroscience Research, 49*(1), 1-11.

Southwell, D. G., Seifikar, H., Malik, R., Lavi, K., Vogt, D., Rubenstein, J. L., & Sohal, V. S. (2020). Interneuron transplantation rescues social behavior deficits without restoring wild-type physiology in a mouse model of autism with excessive synaptic inhibition. *Journal of Neuroscience, 40*(11), 2215-2227.

Spellman, T., Rigotti, M., Ahmari, S. E., Fusi, S., Gogos, J. A., & Gordon, J. A. (2015). Hippocampal–prefrontal input supports spatial encoding in working memory. *Nature, 522*(7556), 309-314.

Sun, Q., Li, X., Ren, M., Zhao, M., Zhing, Q., Ren, Y., . . . Yuan, J. (2019). A whole-brain map of long-range inputs to GABAergic interneurons in the mouse medial prefrontal cortex. *Nature Neuroscience, 22*(8), 1357-1370.

Taniguchi, H., He, M., Wu, P., Kim, S., Paik, R., Sugino, K., . . . Lin, Y. (2011). A resource of Cre driver lines for genetic targeting of GABAergic neurons in cerebral cortex. *Neuron, 71*(6), 995-1013.

Tanimizu, T., Kenney, J. W., Okano, E., Kadoma, K., Frankland, P. W., & Kida, S. (2017). Functional connectivity of multiple brain regions required for the consolidation of social recognition memory. *Journal of Neuroscience, 37*(15), 4103-4116.

Tasic, B., Menon, V., Nguyen, T. N., Kim, T. K., Jarsky, T., Yao, Z., . . . Bertagnolli, D. (2016). Adult mouse cortical cell taxonomy revealed by single cell transcriptomics. *Nature Neuroscience, 19*(2), 335-346.

Tasic, B., Yao, Z., Graybuck, L. T., Smith, K. A., Nguyen, T. N., Bertagnolli, D., . . . Penn, O. (2018). Shared and distinct transcriptomic cell types across neocortical areas. *Nature, 563*(7729), 72-78.

Turi, G. F., Li, W. K., Chavlis, S., Pandi, I., O'Hare, J., Priestley, J. B., . . . Zhang, J. F. (2019). Vasoactive intestinal polypeptide-expressing interneurons in the hippocampus support goal-oriented spatial learning. *Neuron, 101*(6), 1150-1165.

Uematsu, A., Tan, B. Z., & Johansen, J. P. (2015). Projection specificity in heterogeneous locus coeruleus cell populations: implications for learning and memory. *Learning & Memory, 22*(9), 444-451.

Van der Werf, Y. D., Witter, M. P., Uylings, H. B., & Jolles, J. (2000). Neuropsychology of infarctions in the thalamus: a review. *Neuropsychologia, 38*(5), 613-627.

van Heukelum, S., Mars, R. B., Guthrie, M., Buitelaar, J. K., Beckmann, C. F., Tiesinga, P. H., . . . Havenith, M. N. (2020). Where is Cingulate Cortex? A Cross-Species View. *Trends in Neuroscience, 43*(5), 285-299.

Vann, S. D., Aggleton, J. P., & Maguire, E. A. (2009). What does the retrosplenial cortex do? *Nature Reviews Neuroscience, 10*(11), 792-802.

Venkatasubramanian, G., Jayakumar, P. N., Gangadhar, B. N., & Keshavan, M. S. (2008). Automated MRI parcellation study of regional volume and thickness of prefrontal cortex (PFC) in antipsychotic-naïve schizophrenia. *Acta Psychiatrica Scandinavica, 117*(6), 420-431.

Virtanen, P., Gommers, R., Oliphant, T. E., Haberland, M., Reddy, T., Cournapeau, D., . . . Mulbregt, P. (2020). SciPy 1.0: fundamental algorithms for scientific computing in Python. *Nature Methods, 17*(3), 261-272.

Voikar, V. A., Polus, A., Vasar, E., & Rauvala, H. (2005). Long-term individual housing in C57BL/6J and DBA/2 mice: assessment of behavioral consequences. *Genes, Brain and Behavior, 4*(4), 240-252.

Wall, N. R., De La Parra, M., Sorokin, J. M., Taniguchi, H., Huang, Z. J., & Callaway, E. M. (2016). Brain-Wide Maps of Synaptic Input to Cortical Interneurons. *Journal of Neuroscience, 36*(14), 4000-4009.

Wang, Q., Zheng, Y., & Ma, J. (2013). Cooperative dynamics in neuronal networks. *Chaos, Solitons & Fractals, 56*, 19-27.

Weible, A. P., Piscopo, D. M., Rothbart, M. K., Posner, M. I., & Neill, C. M. (2017). Rhythmic brain stimulation reduces anxiety-related behavior in a mouse model based on meditation training. *Proceedings of the National Academy of Sciences, 114*(10), 2532-2537.

Weible, A. P., Rowland, D. C., Monaghan, C. K., Wolfgang, N. T., & Kentros, C. G. (2012). Neural correlates of long-term object memory in the mouse anterior cingulate cortex. *Journal of Neuroscience, 32*(16), 5598-6008.

Weible, A. P., Rowland, D. C., Pang, R., & Kentros, C. (2009). Neural correlates of novel object and novel location recognition behavior in the mouse anterior cingulate cortex. *Journal of Neurophysiology, 102*(4), 2055-2068.

Wiithaus, H., Kaufmann, C., Bohner, G., Ozgurdal, S., Gudlowski, Y., Gallinat, J., . . . Juckel, G. (2009). Gray matter abnormalities in subjects at ultra-high risk for schizophrenia and first-episode schizophrenic patients compared to healthy controls. *Psychiatry Research: Neuroimaging, 173*(3), 163-169.

Womelsdorf et al., T., Ardid, S., Everling, S., & Valiante, T. A. (2014). Burst firing synchronizes prefrontal and anterior cingulate cortex during attentional control. *Current Biology, 24*(22), 2613-2621.

Xu, X., Roby, K. D., & Callaway, E. M. (2010). Immunochemical characterization of inhibitory mouse cortical neurons: three chemically distinct classes of inhibitory cells. *Journal of Comparative Neurology, 518*(3), 389-404.

Yizhar, O., Fenno, L. E., Prigge, M., Schneider, F., Davidson, T. J., O'shea, D. J., . . . Stehfest, K. (2011). Neocortical excitation/inhibition balance in information processing and social dysfunction. *Nature, 477*(7363), 171-178.

Zhang, L., Liang, B., Barbera, G., Hawes, S., Zhang, Y., Stump, K., ... & Lin, D. T. (2019). Miniscope GRIN lens system for calcium imaging of neuronal activity from deep brain structures in behaving animals. *Current Protocols in Neuroscience*, *86*(1), e56.

CURRICULUM VITAE